Performance Models for Flexural Damage in Reinforced Concrete Columns

Michael Berry

and

Marc Eberhard

Department of Civil & Environmental Engineering
University of Washington

Performance Models for Flexural Damage in Reinforced Concrete Columns

Michael Berry

and

Marc Eberhard

Department of Civil & Environmental Engineering
University of Washington

ABSTRACT

To implement performance-based earthquake engineering (PBEE), it is necessary to assess the probability of reaching multiple damage states in structural and nonstructural elements. To help with this assessment, the research presented in this report provides practical recommendations for estimating the likelihood that in a reinforced concrete column the concrete cover will have begun to spall or the longitudinal bars will have begun to buckle, based on the column's expected deformation demand.

Damage development in reinforced concrete columns is complex, involving three-dimensional material and geometrical nonlinearities in the concrete and reinforcing steel, as well as the interaction between the expansion of the concrete core and the restraint provided by the transverse reinforcement. Modeling such damage in detail challenges the most advanced and computationally demanding modeling strategies that are currently available. To develop recommendations that can be implemented easily in practice, this research relied on moment-curvature analysis and plastic-hinge analysis to predict trends in concrete compressive strain, plastic rotation, drift ratio, and displacement ductility at the onset of damage as functions of various key column properties (e.g., axial load ratio and aspect-ratio). The models were calibrated with existing experimental results from the UW-PEER reinforced concrete column performance database, which documents the performance of more than 450 columns.

The ratio of the observed displacement at bar buckling to the calculated displacement had a mean of 0.97 for spiral-reinforced concrete columns and 1.00 for rectangular-reinforced concrete columns. The corresponding coefficients of variation for these ratios were 25% and 26%, respectively.

ACKNOWLEDGMENTS

CONTENTS

LIST OF FIGURES

LIST OF TABLES

1 Introduction

1.1 PERFORMANCE-BASED EARTHQUAKE ENGINEERING

Current building codes and modern engineering practice address the issues of collapse prevention and life safety by requiring that the strengths of structural members exceed the nominal demands, but codes provide little indication of the actual state of a building after an earthquake. Even if a building or bridge is still standing after an earthquake, damage to structural and nonstructural members may require costly repairs. The indirect economic losses due to production interruption, loss of occupancy, and loss of data may even be costlier.

Performance-based earthquake engineering (PBEE) aims to improve structural engineering by providing engineers with the capability of designing structures to achieve a variety of performance levels. The impact of implementing PBEE goes beyond improving engineering practice as noted in the mission statement of the Pacific Earthquake Engineering Research Center (PEER):

> *…The approach is aimed at improving decision-making about seismic risk by making the choice of performance goals and the tradeoffs that they entail apparent to facility owners and society at large. The approach has gained worldwide attention in the past ten years with the realization that urban earthquakes in developed countries — Loma Prieta, Northridge, and Kobe — impose substantial economic and societal risks above and beyond potential loss of life and injuries. By providing quantitative tools for characterizing and managing these risks, performance-based earthquake engineering serves to address diverse economic and safety needs.* (http://peer.berkeley.edu)

To implement PBEE it is necessary to predict damage and assess the probability of reaching each damage state. Although damage to other elements can have economic and life-safety impacts, columns are often the most vulnerable elements in a structure. Excessive deformations in reinforced concrete columns can result in spalling of cover concrete, buckling of longitudinal reinforcement, reduction of flexural strength, shear failure, and eventually, structural collapse.

This research focuses on an important component of PBEE, the prediction of flexural damage in reinforced concrete columns. The following sections discuss the typical progression of flexural damage in reinforced concrete columns, as well as the objectives and scope of this report.

1.2 TYPICAL PROGRESSION OF FLEXURAL DAMAGE IN RC COLUMNS

Damage in reinforced concrete columns subjected to cyclic lateral deformations is controlled by a series of complex interactions. The typical progression of the development of flexural damage is reviewed here. Consider a column subjected to uniaxial compression:

- As the axial deformations on the column increase, the strains in the cover concrete increase until the cover concrete cracks and spalls (Bresler 1961).
- The loss of cross-sectional area imposes additional stresses on the remaining concrete core and longitudinal steel reinforcement (Bresler 1961).
- The longitudinal steel yields in compression and eventually begins to strain harden.
- Poisson's effect causes the concrete core to expand, which exerts pressure on the longitudinal and confining reinforcement.
- The confining reinforcement restrains the lateral deflection of the longitudinal reinforcement, and it confines the expanding core. The confining pressure is not uniform; it depends on the tensile and bending stiffness and strength of the confining reinforcement (Bresler and Gilbert 1961). Additionally, the tie stiffness will be a function of its strain, which in turn is affected by the axial deformation of the column and the ensuing core expansion (Pantazopoulou 1998). Bar buckling will also affect the strains in the ties.
- The increased axial strain and imposed lateral deformations (due to core expansion) lead to instability of the longitudinal bars (Bayrak and Sheikh 2001). When lateral ties are very stiff, the longitudinal reinforcing bars are very slender, and/or when the tie spacing is very large, longitudinal bar buckling can occur between two adjacent ties (Dhakal and Maekawa 2002). In other situations, bar buckling can occur over several tie spacings.

The progression of damage is even more complicated if, in addition to compression, the column is subjected to lateral deformations.

- Not all bars will have the same strain due to the strain gradient across the cross section.
- The moment gradient along the length of the column will create a strain gradient in the longitudinal direction.

  Cyclic loading adds further complexity.
- Bar buckling is affected by the maximum tension strain and the tension strain growth (associated with cyclic inelastic deformations) in the longitudinal reinforcement (Moyer and Kowalsky 2001).
- The load history and cycling affect damage progression and, specifically, bar buckling (Kunnath et al. 1997).
- The effect of cycling on the constitutive properties of the concrete and steel, is significant. Gomes and Appleton (1997), Monti and Nuti (1992), and Rodriguez et al. (1999) all identified the importance of cycling on modeling the nonlinear stress-strain response of reinforcing bars. A complete model would need to account for the effects of cycling and load history.

1.3   OBJECTIVE

To quantitatively implement PBEE for reinforced concrete columns, it is necessary to predict the likelihood of reaching important damage states at particular levels of column deformation. The objective of this research was to develop practical tools to estimate the deformations at the onset of concrete spalling and bar buckling, given a column geometry, reinforcement and axial load.

This report focuses first on concrete cover spalling (Fig. 1.1a), because it represents the first flexural damage state in which there are marginal safety implications and where there may be a possible short-term loss of function. In addition, the cost to repair concrete spalling could be significant. Buckling of the longitudinal bars (Fig. 1.1b) was a second area of interest, because this level of damage represents the first damage state in which safety implications are significant, partial replacement may be required, and a temporary loss of function may occur.

3
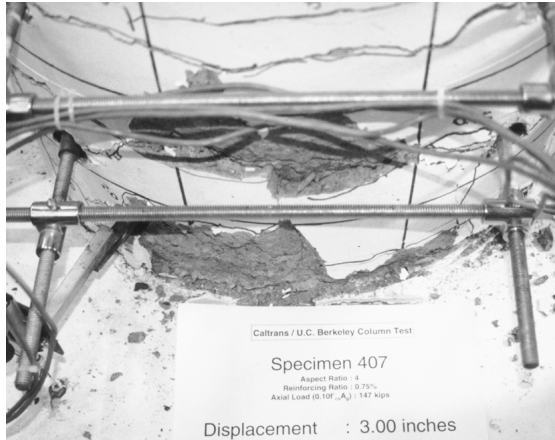
Figure 1.1 (a) Cover Spalling, and   (b) Longitudinal Bar Buckling (Lehman 2003)

1.4   SCOPE

This report is organized in the following manner. The column data used in this research are presented in Chapter 2. Chapter 3 reviews plastic-hinge analysis and discusses the expected influences of key column properties (e.g., axial load ratio, longitudinal reinforcement ratio) on the flexural response of reinforced concrete columns. Then, Chapters 4 and 5 discuss the expected and observed trends in the deformation at the onset of longitudinal bar buckling and concrete cover spalling as functions of various key column properties. In Chapter 6, equations to predict damage are developed from regression analyses, and the accuracies of these equations are assessed. Next, Chapter 7 introduces simple design equations and fragility curves suitable for engineering practice. Finally, Chapter 8 provides conclusions.

2 Column Data

In this chapter, the column data that were used to evaluate the accuracies of the proposed damage models are discussed. The UW-PEER structural performance database is discussed first. Then, the column tests used in this research are identified, and the key deformation measures used in this research are defined.

2.1 UW-PEER DATABASE

A database containing the results of cyclic lateral-load tests on reinforced concrete columns was assembled at the University of Washington with the support of the National Science Foundation through the Pacific Earthquake Engineering Research Center (PEER). The database is available on the World Wide Web at *http://www.ce.washington.edu/~peera1*. The database allows researchers around the world to evaluate uncertainties in performance estimates for reinforced concrete columns, considering uncertainties in analytical procedures, and in material and geometric properties.

The database contains the results of 253 tests of rectangular columns and 163 tests of spiral-reinforced columns. For each column test, the database provides the column geometry; material, reinforcement, and loading properties; test results; and a reference. The test results include the digital force-displacement history and the maximum recorded tip deflections before the onset of the particular damage states, Δ_{damage}. Parrish (2001) describes the database in greater detail.

In addition, 48 more rectangular columns and 3 more spiral-reinforced columns were included in this study. These additional columns are not yet included in the UW-PEER database, because only the digital force-displacement envelopes are included in the test results instead of the full force-displacement history.

2.2   DAMAGE DISPLACEMENTS

To implement performance-based earthquake engineering for reinforced concrete columns, it is necessary to estimate deformations at the onset of particular damage states. The focus of this research is on predicting longitudinal bar buckling and concrete cover spalling in flexure-dominant reinforced concrete columns. Therefore, to be included in the analysis, the column tests needed to meet the following screening criteria:

- Flexure-critical column, as defined by Camarillo (2003)
- An aspect ratio of 1.95 or greater
- Longitudinal reinforcement not spliced

Table 2.1 provides the number of rectangular and spiral-reinforced column tests that met the screening criteria, and in which the tip displacements at the onset of longitudinal bar buckling and concrete cover spalling were reported. In addition, Table 2.1 provides the number of tests in which the displacements at 20% reduction in flexural capacity were calculated with the procedure described in Camarillo 2003. Appendix A provides a complete list of the tests that were included in this research.

Table 2.1 Number of Tests for Which Damage Displacement Was Available

	Bar Buckling	Cover Spalling	20% Reduction
Rectangular Columns	62	102	162
Spiral-Reinforced Columns	42	40	58

2.3   MEASURES OF COLUMN DEFORMATION

The column data were used in this research to study the influences of key column properties on the deformations at the onset of bar buckling and concrete cover spalling, and to evaluate the accuracy of the proposed damage models.

Deformations can be expressed as global deformation measures, such as displacement ductility and drift ratio, or local deformation measures, such as plastic rotation, θ_{p_damage} and compressive strain, ε_{damage}.

Usually, only the tip displacements at particular damage states were reported by researchers. For a given tip displacement, the following procedures were used to calculate the drift ratio, displacement ductility, plastic rotation, and compressive strain at the onset of a particular damage state.

The drift ratio at the onset of a particular damage state was defined as $\dfrac{\Delta_{damage}}{L}$, where Δ_{damage} is the maximum reported tip deflection before the onset of a particular damage state, and L is the distance from the column base to the point of contraflexure.

The displacement ductility at the onset of a particular damage state was defined as, $\dfrac{\Delta_{damage}}{\Delta_y}$, where Δ_y is the yield displacement. In this research, Δ_y was defined as follows:

$$\Delta_y = \frac{F_{0.004}\Delta_{firstyield}}{F_{firstyield}} \tag{Eq. 2.1}$$

where:

- $F_{firstyield}$ is the effective force at first yield, which was obtained by dividing the moment at first yield by the effective length. The moment at first yield was calculated with moment-curvature analysis, by assuming that the extreme tensile reinforcement had yielded or the concrete had reached a compressive strain of 0.002, whichever came first. In this moment-curvature analysis, the Mander et al. (1988) constitutive model was used to model the concrete, and the ACI (2002) steel constitutive model was used to model the response of the longitudinal reinforcement. If $F_{firstyield}$ (calculated with the procedure above) was larger than the maximum measured effective force, $F_{firstyield}$ was taken as 95% of the maximum measured effective force.

- $\Delta_{firstyield}$ is the displacement corresponding to $F_{firstyield}$ on the measured force-displacement envelope.

- $F_{0.004}$ is the effective force at a given strain of 0.004 (defined in a similar manner as $F_{firstyield}$).

7

This procedure is illustrated in Figure 2.1 (Camarillo 2003).
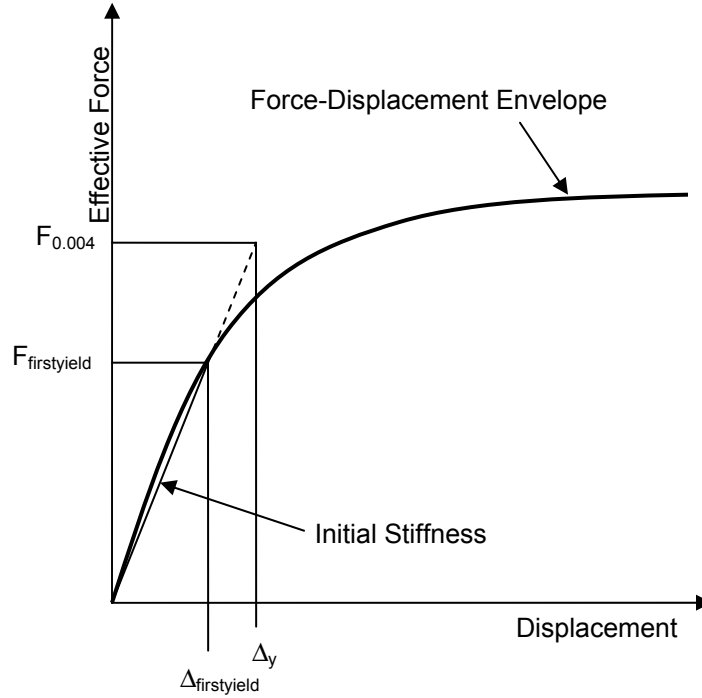
Figure 2.1 Yield Displacement (Camarillo 2003)

According to plastic-hinge analysis (Chapter 3), the displacement at the onset of a particular damage state can be approximated with Equation 3.4. It follows from this equation that given the maximum recorded displacement a particular damage state, the nominal plastic rotation can be calculated with Equation 2.2. The word "nominal" is used in order to stress that these plastic rotations are not the measured values; they are estimated with plastic-hinge analysis.

$$\theta_{p\_damage} = \left(\phi_{damage} - \phi_y\right)L_p = \frac{\Delta_{damage} - \Delta_y}{L - \dfrac{L_p}{2}} \qquad\text{(Eq. 2.2)}$$

Equation 2.2 was used in this research to approximate the plastic rotation at the particular damage states. In this approximation, the plastic-hinge length was calculated with the equation proposed by Priestley et al. (1996), and Δ_y was calculated with the procedure described previously.

Given the tip displacement at a damage state, the nominal column curvature at the damage state, ϕ_{damage}, can be approximated using the following equation.

$$\phi_{damage} = \frac{\Delta_{damage} - \Delta_y}{L_p \left(L - \frac{L_p}{2} \right)} + \phi_y$$ (Eq. 2.3)

where, ϕ_y is the yield curvature. Once ϕ_{damage} is obtained with Equation 2.3, the nominal strain at the particular damage state, ε_{damage}, can be obtained from the results of moment-curvature analysis.

Equation 2.3 was used in this research to approximate the curvature at each damage state. In this research, ϕ_y was calculated with moment-curvature analysis by assuming that the extreme tensile reinforcement had yielded, and L_p was calculated with the equation proposed by Priestley et al. (1996). The moment-curvature analysis used to calculate the nominal strains and the yield curvatures used the Mander et al. (1988) constitutive model to model the concrete, and the modified Burns and Seiss (Park and Paulay 1975) steel constitutive model to model the response of the longitudinal reinforcement.

It should be noted that the Priestley et al. (1996) plastic-hinge length model was derived from measured experimental data at failure. Therefore, it is likely that the plastic-hinge length calculated with this equation would be larger than a more reasonable estimate of plastic-hinge length at intermediate damage states (e.g., spalling). Consequently, it is likely that the nominal plastic rotations at intermediate damage states overestimate the true values, and the nominal compressive strains underestimate the true values.

The calculated deformation measures at the onset of bar buckling, concrete cover spalling, and 20% reduction in flexural capacity are provided in Appendix A. The references for the individual column tests can be found at the UW-PEER column database website (*http://www.ce.washington.edu/~peera1*).

3 Trends Expected From Plastic-Hinge Analysis

The methodology used to develop the proposed damage models relies heavily on the assumption that plastic-hinge analysis adequately captures key deformation characteristics of reinforced concrete columns. This chapter describes the plastic-hinge method and discusses the expected influence of key column characteristics on the flexural response of reinforced concrete columns.

3.1 INTRODUCTION TO PLASTIC-HINGE ANALYSIS

Plastic-hinge analysis assumes that the post-yield displacement, Δ, of a reinforced concrete member can be decomposed into two parts, the response up to the yield displacement, Δ_y, and the plastic deformation, Δ_p.

$$\Delta = \Delta_y + \Delta_P \tag{Eq. 3.1}$$

where $\Delta > \Delta_y$.

The plastic deformation is assumed to result from the rigid body rotation of the member around a plastic hinge near the base of the column. For simplicity, the curvature in the plastic-hinge is assumed to be constant ($\phi_p = \phi - \phi_y$) over an equivalent plastic-hinge length, L_p, as shown in Figure 3.1. With this assumption, the plastic rotation can be expressed with the following equation:

$$\theta_p = \int_0^{Lp} \phi_p \, dx = \phi_p L_p \tag{Eq. 3.2}$$

This plastic rotation primarily accounts for the rotation due to the nonlinear curvature distribution near the base of the column. In addition, the rotation due to slip of the longitudinal reinforcement and the influence of shear are often also included in the plastic rotation. In such cases, the length of the plastic region is increased (Priestley and Park, 1987). Several models are

available to estimate the plastic-hinge length as a function of column properties. These models are discussed in greater detail in Section 3.3.
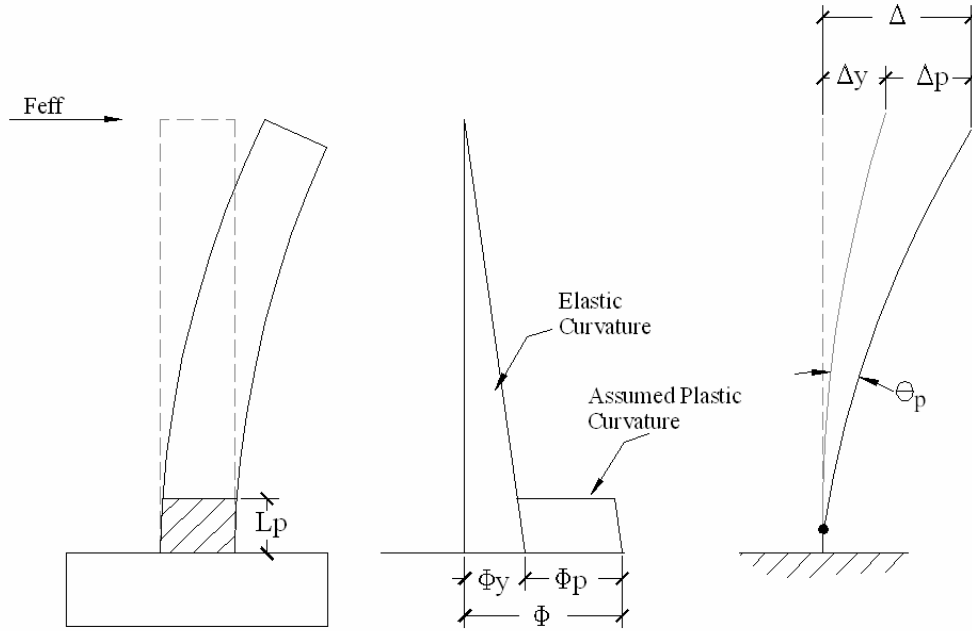
Figure 3.1 Plastic-Hinge Analysis

Using Equation 3.2 and assuming that the plastic rotation is concentrated at the center of the plastic hinge, the displacement due to the rotation of the hinge can be represented with the following equation:

$$\Delta_P = \theta_p \left(L - L_p / 2 \right) = \left(\phi - \phi_y \right) L_p \left(L - L_p / 2 \right) \tag{Eq. 3.3}$$

It follows that the resulting total tip deflection is

$$\Delta = \Delta_y + \left(\phi - \phi_y \right) L_p \left(L - L_p / 2 \right) \tag{Eq. 3.4}$$

If it is assumed that $\dfrac{L_p}{2} << L$, the displacement can be approximated as

$$\Delta = \Delta_y + \theta_p L \tag{Eq. 3.5}$$

Equation 3.5 was used to estimate local column deformation measures, such as strain, curvature and plastic rotation, from reported tip deflections, as described in subsequent sections. This equation also provided a mechanism to estimate the influences of key column properties on flexural deformation.

12

3.2   PLASTIC-HINGE LENGTHS

Several models have been proposed to estimate the plastic-hinge length based on the column properties. Previous research (e.g., Priestley et al. 1996; Mattock 1967) suggests that the plastic-hinge length is proportional to the column length, L, column depth, D, and the longitudinal reinforcement properties, as in the following equation:

$$L_p = \alpha L + \beta D + \xi f_y d_b \qquad\qquad\qquad\qquad\qquad \text{(Eq. 3.6)}$$

where D is the column depth, and f_y and d_b are the yield stress and bar diameter of the tension reinforcement, respectively.

The column length is included in Equation 3.6 to account for the moment gradient along the length of the cantilever, and the column depth is included to account for the influence of shear on the size of the plastic region. The properties of the longitudinal bars are included to account for additional rotation at the plastic-hinge resulting from strain penetration of the longitudinal reinforcement into the supporting element.

Priestley and Mattock both used this form of equation and calibrated it with experimental results to obtain values of α, β, and ξ. Mattock (1967) proposed an equation to calculate the plastic-hinge length in beams, in which $\alpha = \dfrac{1}{20}$, $\beta = \dfrac{1}{2}$ and $\xi = 0$. Priestley et al. (1998) proposed an equation to calculate the plastic-hinge length in columns, in which $\alpha = 0.08$, $\beta = 0$, and $\xi = 0.022$ (f_y in MPa) with an upper limit on L_p of $0.044 f_y d_b$.

The general form of the plastic-hinge equation (Eq. 3.6) will be used in this research to represent the length of plastic hinges, and ultimately, to study the expected influence of column properties on flexural response and column damage.

The flexural response of a reinforced concrete column is influenced by its geometry, reinforcement, and loading, so it is important for proposed damage models to consider these influences. In the following sections, the plastic-hinge theory presented in Section 3.1 and the general plastic-hinge length equation (Eq. 3.6) will be used to estimate the influences of key column properties on the strain, plastic curvature, plastic rotation, drift ratio, and displacement ductility at particular damage states.

3.3   EXPECTED TRENDS FOR MAXIMUM COMPRESSIVE STRAIN

The modeling strategy proposed in this report is based on the assumption that damage is controlled by the maximum compressive strain, ε_{damage}. This critical compressive strain is affected by the column axial load, loading history, geometry, and reinforcement properties. The particular effects of these properties on the critical compressive strain depend on the particular damage state. For example, the buckling strain for longitudinal reinforcement will be influenced by the effectiveness of the transverse reinforcement and longitudinal bar size. On the other hand, the critical strain for cover spalling is unlikely to depend on the amount of transverse reinforcement.

In the following sections, equations for estimating deformation measures will be formulated as functions of this maximum compressive strain. The discussion on how particular properties affect the critical strain, and ultimately the deformation measures, at two damage states will be presented in Chapters 4 and 5.

3.4   EXPECTED TRENDS IN PLASTIC CURVATURE

The plastic curvature at a particular damage state can be linked to the maximum compressive strain at that damage state through moment-curvature analysis. This relationship is a function of the column axial load, longitudinal reinforcement ratio, ρ_l, and the ratio of steel yield stress to concrete compressive strength $\dfrac{f_y}{f'_c}$. The following paragraphs provide a simple means of approximating this relationship.

The normalized curvature of a column cross section is defined as follows:

$$\phi_{norm} = \frac{D}{C} = \frac{\phi_n D}{\varepsilon_n} \tag{Eq. 3.7}$$

where ϕ_n is the nominal curvature associated with a given compressive strain, ε_n.

A typical rectangular column cross section under flexural loading is shown in Figure 3.2. In this cross section, the steel is assumed to behave elasto-plastically, and the Whitney stress block is assumed to adequately model the concrete compressive stresses (ACI-318 2002). By enforcing equilibrium conditions on the cross section, the normalized curvature at a given compressive strain can be approximated with the following equation:

14

$$\frac{\phi_n D}{\varepsilon_n} = \frac{0.85 f_c' \beta_1 BD}{P + A_s f_s - A_s' f_s'}$$
(Eq. 3.8)

where f_c' is the concrete compressive strength; β_1 is a Whitney stress constant ranging from 0.65 to 0.85 depending on concrete compressive strength; A_s' and f_s' are the compressive steel area and stress, respectively; A_s and f_s are the tension steel area and stress, respectively; and P is the axial load. The directions for the positive axial load and steel stresses are shown in Figure 3.2.
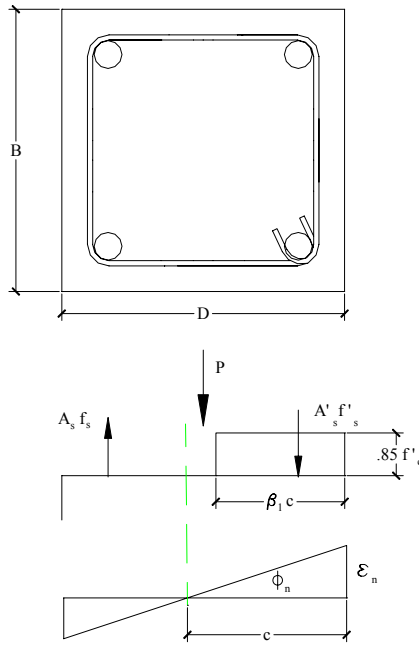
Figure 3.2 Typical Column Cross Section under Flexural Loading

Equation 3.8 can be simplified to the following equation:

$$\frac{\phi_n D}{\varepsilon_n} = \frac{0.85 \beta_1}{\dfrac{P}{A_g f_c'} + \eta \omega}$$
(Eq. 3.9)

where $A_g = BD$, $\omega = \rho_l \left(\dfrac{f_y}{f_c'} \right)$, and η ranges from -1 to 1 depending on the location of the neutral axis. η can be approximated as follows:

$$\eta = A_0 \omega^{A_1} \left(1 - \frac{P}{A_g f_c'} \right)$$
(Eq. 3.10)

15

where A_0 and A_1 are constants, equal to -0.0675 and -0.75 respectively for a compressive strain of 0.004. Equation 3.9 provides an approximate, simple link between curvature and compressive strain.

As shown in Figure 3.1, the plastic curvature is the difference between the total curvature and the yield curvature. Priestley et al. (1996) proposed that the yield curvature can be approximated as a function of the column depth and the yield strain of the tension reinforcement.

$$\phi_y = \lambda \frac{\varepsilon_y}{D} \tag{Eq. 3.11}$$

where $\lambda = 2.45$ for spiral-reinforced columns and 2.14 for rectangular reinforced columns. Using this approximation for the yield curvature, the definition of plastic curvature $(\phi_n - \phi_y)$, and Equation 3.9, the normalized plastic curvature can be approximated with the following equation:

$$\frac{\phi_{pn}D}{\varepsilon_n} = \frac{\phi_n D}{\varepsilon_n} - \frac{\phi_y D}{\varepsilon_n} = \frac{0.85\beta_1}{\dfrac{P}{A_g f_c'} + \eta\omega} - \lambda\frac{\varepsilon_y}{\varepsilon_n} \tag{Eq. 3.12}$$

By substituting Equation 3.10 into Equation 3.12, combining constants, and simplifying, the following equation is obtained

$$\frac{\phi_{pn}D}{\varepsilon_n} = \frac{C_0}{\dfrac{P}{A_g f_c'} + C_1\omega^{C_2+1}\left(1 - \dfrac{P}{A_g f_c'}\right)} - \lambda\frac{\varepsilon_y}{\varepsilon_n} \tag{Eq. 3.13}$$

Equation 3.13 was calibrated using 288 flexure dominant columns from the UW-PEER database (Chapter 2). The coefficient of variation of the ratio of calculated curvature (from moment-curvature analysis for a strain of 0.004) to predicted curvature (from Eq. 3.13) was minimized. C_0, C_1, and C_2 were determined to be 0.43, 0.105, and 0.18, respectively. This form of equation approximated the normalized plastic curvature with a coefficient of variation of 16%.

Equation 3.13 can be simplified by setting $\omega^{C_2+1}\left(1 - \dfrac{P}{A_g f_c'}\right) = 1$ and neglecting the effect

of $\lambda\dfrac{\varepsilon_y}{\varepsilon_n}$. The following equation can be used to approximate the normalized plastic curvature.

$$\frac{\phi_{p\_n}D}{\varepsilon_n} = \frac{G_0}{1 + G_1 \dfrac{P}{A_g f_c'}} = G_0\left(1 + G_1\frac{P}{A_g f_c'}\right)^{-1} \tag{Eq. 3.14}$$

This equation was also calibrated using the database by minimizing the coefficient of variation of the ratio of calculated curvature (from moment-curvature analysis) to predicted curvature (from Eq. 3.14) for the 288 flexure dominant column in the database. G_0 and G_1 were determined to be 5.3 and 9.4, respectively. This form of equation estimated the plastic curvature with a coefficient of variation of 18%.

The normalized plastic curvature (from moment-curvature analysis) for a compressive strain of $\varepsilon_n = 0.004$ is plotted as a function of the axial load ratio in Figure 3.3 for the 288 flexure-dominant columns in the database. Equation 3.14 is shown as a dashed line in this figure. This plot demonstrates that, for a given strain and column cross section, the normalized plastic curvature decreases with an increase in axial load, and levels off at a value around one.
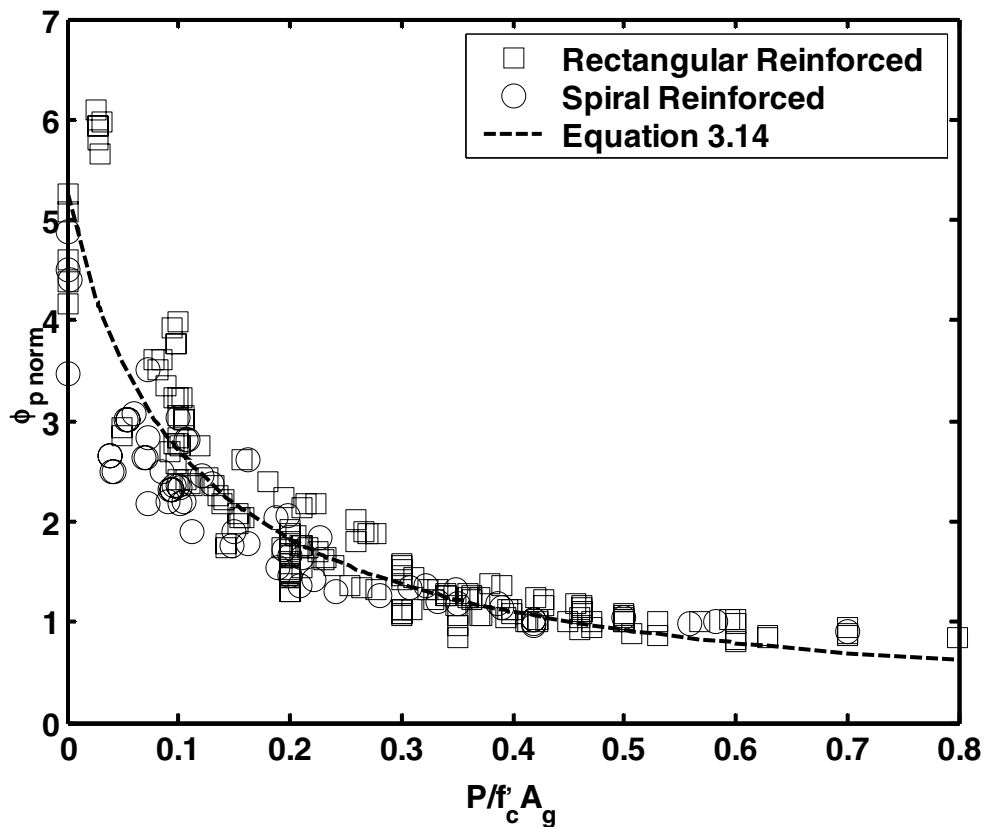
Figure 3.3 Normalized Plastic Curvature vs. Axial Load Ratio

Simplifying Equation 3.13 to Equation 3.14 resulted in only a slight increase in the coefficient of variation. For simplicity and because the additional calculations in Equation 3.13 do not provide a significant increase in accuracy, Equation 3.14 will be used to estimate the normalized plastic curvature.

Equation 3.14 can be used to calculate the plastic curvature as a function of maximum compressive strain and axial-load ratio. Assuming that the neutral axis depth is independent of the level of deformation, this equation can be used to express the plastic curvature at the onset of a particular damage state as a function of axial load and critical compressive strain, ε_{damage}.

$$\phi_{p\_damage} = \phi_{damage} - \phi_y \cong C_0 \left(\frac{\varepsilon_{damage}}{D} \right) \left(1 + C_1 \frac{P}{A_g f'_c} \right)^{-1} \qquad \text{(Eq. 3.15)}$$

3.5   EXPECTED TRENDS IN PLASTIC ROTATION

The plastic rotation in a reinforced concrete column at a damage state, θ_{p_damage}, can be represented with the Equation 3.16.

$$\theta_{p\_damage} = \phi_{p\_damage} L_p = (\phi_{damage} - \phi_y) L_p \qquad \text{(Eq. 3.16)}$$

By substituting the expression for plastic-hinge length, given by Equation 3.6, into Equation 3.16 the plastic rotation can be expressed as

$$\theta_{p\_damage} = \phi_{p\_damage} (\alpha L + \beta D + \xi f_y d_b) \qquad \text{(Eq. 3.17)}$$

By substituting Equation 3.14 into Equation 3.17, the plastic rotation can be represented with Equation 3.18.

$$\theta_{p\_damage} = C_0 \frac{1}{D} (\varepsilon_{damage}) \left(1 + C_1 \frac{P}{A_g f'_c} \right)^{-1} (\alpha L + \beta D + \xi f_y d_b) \qquad \text{(Eq. 3.18)}$$

Rearranging this equation, the plastic rotation becomes

$$\theta_{p\_damage} = \frac{C_0}{\beta} (\varepsilon_{damage}) \left(1 + C_1 \frac{P}{A_g f'_c} \right)^{-1} \left(1 + \alpha\beta \frac{L}{D} + \xi\beta \frac{f_y d_b}{D} \right) \qquad \text{(Eq. 3.19)}$$

For a given column cross section and critical strain, the plastic rotation is expected to decrease with an increase in axial load. Conversely, the plastic rotation will increase with an increase in aspect ratio, $\dfrac{L}{D}$, and the normalized bar diameter multiplied by the steel yield stress, $\dfrac{d_b f_y}{D}$.

3.6   EXPECTED TRENDS IN DRIFT RATIO

The drift ratio at the onset of a particular damage state is defined as the maximum recorded tip deflection before the onset of a particular damage state, Δ_{damage}, divided by the distance from the column base to the point of contraflexure, L. If it is assumed that $\dfrac{L_p}{2} << L$, the drift ratio at the onset of a particular damage state can be represented as

$$\frac{\Delta_{damage}}{L} \cong \frac{\Delta_y}{L} + \theta_p \qquad\qquad\qquad\qquad \text{(Eq. 3.20)}$$

By substituting the equation for plastic rotation (Eq. 3.19) into Equation 3.20, the drift ratio at the onset of a particular damage state can be represented with the following equation:

$$\frac{\Delta_{damage}}{L} \cong \frac{\Delta_y}{L} + \frac{C_0}{\beta}\left(\varepsilon_{damage}\right)\left(1+C_1\frac{P}{A_g f'_c}\right)^{-1}\left(1+\alpha\beta\frac{L}{D}+\xi\beta\frac{f_y d_b}{D}\right) \qquad \text{(Eq. 3.21)}$$

The yield displacement can be approximated as

$$\Delta_y \cong \frac{\phi_y L^2}{3} \qquad\qquad\qquad\qquad \text{(Eq. 3.22)}$$

By substituting in Priestley's equation for yield curvature (Eq. 3.11) and this representation of yield displacement into Equation 3.21, the drift ratio at the onset of a particular damage state can be represented as

$$\frac{\Delta_{damage}}{L} \cong \frac{\lambda}{3E_s}f_y\frac{L}{D} + \frac{C_0}{\beta}\left(\varepsilon_{damage}\right)\left(1+C_1\frac{P}{A_g f'_c}\right)^{-1}\left(1+\alpha\beta\frac{L}{D}+\xi\beta\frac{f_y d_b}{D}\right) \text{(Eq. 3.23)}$$

where E_s is the elastic modulus of the tension reinforcement.

This equation can be used to study the influence of key column properties on the drift ratio at select damage states. For a given column cross section and critical compressive strain, the drift ratio will decrease with an increase in axial load. In contrast, the drift ratio will increase with an increase in aspect ratio, tension yield stress, and normalized bar diameter.

3.7 DISPLACEMENT DUCTILITY

Displacement ductility is defined as the ratio of damage displacement to yield displacement, Δ_y.

Therefore, again assuming $\dfrac{L_p}{2} \ll L$, displacement ductility, μ_Δ, can be expressed as

$$\mu_\Delta = \frac{\Delta_{damage}}{\Delta_y} = 1 + \frac{\theta_p L}{\Delta_y} \qquad \text{(Eq. 3.24)}$$

By substituting the equation for plastic rotation (Eq. 3.19) into this equation, the displacement ductility at the onset of a particular damage state can be represented with the following:

$$\frac{\Delta_{damage}}{\Delta_y} = 1 + \frac{\dfrac{C_0}{\beta}\left(\varepsilon_{damage}\right)\left(1 + C_1 \dfrac{P}{A_g f'_c}\right)^{-1}\left(1 + \alpha\beta\dfrac{L}{D} + \xi\beta\dfrac{f_y d_b}{D}\right)L}{\Delta_y} \qquad \text{(Eq. 3.25)}$$

Substituting in the equations for yield displacement (Eq. 3.22) and yield curvature (Eq. 3.11) and simplifying

$$\frac{\Delta_{damage}}{\Delta_y} = 1 + 3\frac{C_0 E_s}{\beta\lambda}\left(\frac{\varepsilon_{damage}}{f_y}\right)\left(1 + C_0 \frac{P}{A_g f'_c}\right)^{-1}\left(\frac{1}{L/D} + \alpha\beta + \xi\beta\frac{1}{L/D}\frac{f_y d_b}{D}\right) \text{(Eq. 3.26)}$$

This equation can be used to study the influence of key column properties on displacement ductility at a particular damage state. Displacement ductility is expected to decrease with an increase in aspect ratio and axial load. In contrast, displacement ductility will increase with an increase in $\dfrac{f_y d_b}{D}$. The effect of tension yield stress is unclear because it appears in both a numerator and denominator in this equation.

3.8 SUMMARY

Plastic-hinge analysis provides a useful tool to estimate the effects of key column characteristics on the flexural response and the deformations at various damage states of flexure dominant reinforced concrete columns. By using this tool, the effects of key column characteristics on plastic rotation, drift ratio, and displacement ductility were studied. Table 3.1 provides a summary of the study.

Table 3.1 Influence of Key Column Characteristics on Deformation Measures

	P/A_gf_c	w (Low Axial Load)	L/D	d_bf_y/D	f_y
Plastic Rotation	⬇	⬇	⬆	⬆	⬆
Drift Ratio	⬇	⬇	⬆	⬆	⬆
Displacement Ductility	⬇	⬇	⬇	—	—

4 Onset of Longitudinal Bar Buckling

Buckling of longitudinal bars in reinforced concrete members will be investigated in this chapter. The behavior controlling the onset of this damage state was discussed in Chapter 1. In this chapter, previous modeling approaches will be reviewed and assessed. In addition, this chapter evaluates the influences of key column properties on compressive strain, plastic rotation, drift ratio, and displacement ductility at the onset of bar buckling.

4.1 MODELING STRATEGIES

Numerous models have been proposed to model the bar buckling phenomenon, but few accurately account for all significant aspects controlling this damage state. A complete model would account for the effectiveness of the transverse reinforcement in confining the longitudinal reinforcement, the concrete core expansion, the number of spaces over which the bar buckles, the effects of cycling, and the effects of load history.

Euler's buckling theory for slender members has been utilized by numerous researchers to study the likelihood of longitudinal bar buckling in reinforced concrete columns (Bresler and Gilbert 1961; Scribner 1986). Euler's buckling equation is as follows:

$$P_{cr} = \frac{\pi E_b I_b}{L_b{}^2}$$

(Eq. 4.1)

where E_b, I_b, and L_b are the instantaneous modulus of elasticity, second moment of inertia, and assumed buckling length of the longitudinal reinforcement. L_b will vary depending on the assumed end conditions, and depending on the number of tie spaces over which the bar buckles.

The instantaneous modulus of elasticity, included in Equation 4.1, is not the elastic modulus (E_s=29,000 ksi). Bresler and Gilbert (1961) and Scribner (1986) both used the tangent modulus theory to estimate this instantaneous modulus, while Papia and Russo (1989), among others, used the double modulus theory to estimate it. Both these methods assume sufficient

detailing to ensure redistribution of stresses from the bar to surrounding concrete when passing through the yield plateau to the strain-hardening portion of the stress-strain curve (Henry 1998).

According to Equation 4.1, the assumed buckling length, *L*, is one of the parameters that governs the buckling load. When lateral ties are very stiff, longitudinal reinforcing bars are very slender, and/or the tie spacing is very large, longitudinal bar buckling can occur between two adjacent ties (Dhakal and Maekawa 2002). In other situations, bar buckling can occur over several tie spacings, in which case, the effects of tie stiffness on buckling length must be considered.

Estimating the confinement stiffness is difficult because the stiffness depends on both the tensile and flexural responses of the confinement. Bresler and Gilbert (1961) proposed a strain-independent method to estimate the tie stiffness for rectangular reinforced concrete members. However, the actual tie stiffness is a function of its strain, which in turn is affected by the axial deformation of the column and the ensuing core expansion. Pantazopoulou (1998) addresses this effect and provides a method to estimate the tie stiffness based on its strain.

Buckling over several tie spacings was investigated in early research by Bresler and Gilbert (1961). Their research focused on developing design requirements for confining reinforcement in order to prevent bar buckling. They assumed a buckled length of 2 tie spacings and determined the transverse reinforcement necessary to prevent buckling at the intermediate tie. Scribner (1986) used a similar approach but assumed a buckled length of 3 tie spacings.

Other researchers have taken a more general approach and have left the buckling length a variable in their model formulation. Pantazopoulou (1998) and Henry (1998) both developed expressions for P_{cr} as functions of longitudinal bar properties, as well as the effective stiffness (*k*) and spacing (*S*) of the transverse reinforcement.

By enforcing mechanical equilibrium of the buckled shape (Fig. 4.1), Pantazopoulou's expression for critical load is as follows.

$$P_{cr} = \frac{4\pi\ I_b E_b}{L_b{}^2} + \beta L^2\ \frac{k}{S}$$ (Eq. 4.2)

where $\beta = \dfrac{\pi^2 + 4}{16\pi^2} = 0.0875$.
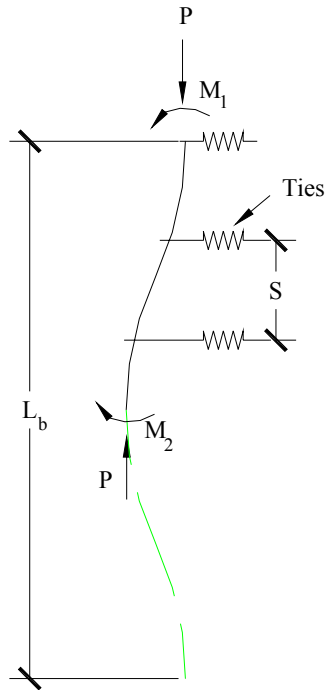
Figure 4.1 Buckled Bar Segment

Henry developed a similar model, but used the dynamic vibration approach to develop the following expression for the buckling load.

$$P_{cr} = \frac{4\pi\, I_b E_b}{L_b{}^2} + \frac{3L^2 k}{4\pi^2 S} \qquad\qquad \text{(Eq. 4.3)}$$

In these equations, the buckling length is taken as integral multiples of the tie spacing, and the minimum buckling load is calculated. Dhakal and Maekawa (2002) proposed a more complex method to estimate the potential buckling length as a function of geometrical and mechanical properties of the transverse and longitudinal reinforcement.

Several researchers have modeled the effects of cycling and load history on bar buckling. For example, Moyer and Kowalsky (2001) proposed a model based on the maximum tensile strain and the tensile strain growth (associated with cyclic inelastic deformations) of the longitudinal reinforcement prior to buckling. Their model still requires a critical compressive buckling model, but it takes into consideration the effects of tensile strain.

These buckling models ignore aspects of the damage state that could affect the deformations at the onset of bar buckling. With the exception of the model proposed by Pantazopoulou (1998), the effect of concrete core expansion on tie stiffness is ignored. In addition, these models ignore the geometric effect of the imposed deformation (due to core

25

expansion) on bar instability. Also, with the exception of Moyer and Kowalsky (2001), the effect of cycling and load history on the bar buckling phenomenon is ignored. And finally, the effect of cycling on material constitutive models is ignored by all models.

Because of the complexity of modeling this damage state with traditional analytical models, the proposed modeling approach will be based on theoretically expected trends in the deformation measures at the onset of bar buckling.

4.2   TRENDS IN COMPRESSIVE STRAIN

The critical compressive strain at which bars buckle will be influenced by numerous column properties. In this section, the effects of key column properties on the buckling strain are investigated.

A pilot study was performed in order to investigate the potential of using detailed buckling models (e.g., Pantazopoulou 1998). It was determined that simple models (e.g., Euler buckling) provided as much accuracy as the more complex models. Therefore, for the purpose of this study, Euler's buckling equation will be used to investigate the influences of column properties on the buckling strain, ε_{bb}. It is understood that many aspects controlling the onset of bar buckling (e.g., core expansion, cycling) are not accounted for with this form of equation, but Euler's buckling theory does capture the basic mechanics of buckling in compression members.

According to linear-elastic buckling theory, the buckling strain can be approximated as follows:

$$\varepsilon_{bb} = \frac{f_{cr}}{E_s} = \frac{P_{cr}}{A_b E_s} = \frac{\pi^2}{(L_b / r)^2} \qquad \text{(Eq. 4.4)}$$

where r is the radius of gyration of the longitudinal bar, L_b is the buckled length, and E_s is the elastic modulus of steel.

Since the radius of gyration for a circular cross section can be calculated as $r = d_b / 4$, the critical elastic buckling strain can be expressed as

$$\varepsilon_{bb} = \frac{\pi^2}{16(L_b / d_b)^2} \qquad \text{(Eq. 4.5)}$$

The buckling length, L_b, can be expressed as a multiple of n and S, where n varies depending on assumed end conditions and depending on the number of tie spacings over which

the bar buckles, and S is the spacing of the transverse reinforcement. Substituting this representation of L into Equation 4.5, the buckling strain can be expressed as

$$\varepsilon_{bb} = \frac{\pi^2}{16(n\,S/d_b)^2} \qquad\qquad (Eq.\ 4.6)$$

Equation 4.6 can be used to estimate the influence of key column properties on the buckling strain.

The expected influences of key column characteristics are compared with experimental data by plotting the nominal buckling strains (calculated with the procedure described in Section 2.3 using the plastic-hinge length proposed by Priestley et al. 1996) versus key column properties for columns in the UW-PEER database. In order to isolate the effect of each key column property, the database was arranged into families in which all columns in a family had similar properties except for the property being studied. These families are represented as lines in Figures 4.2 and 4.3. It should be noted that the families do not take into consideration the load history of each column. It should also be noted that the vertical axes for the two figures differ by a factor of 2.
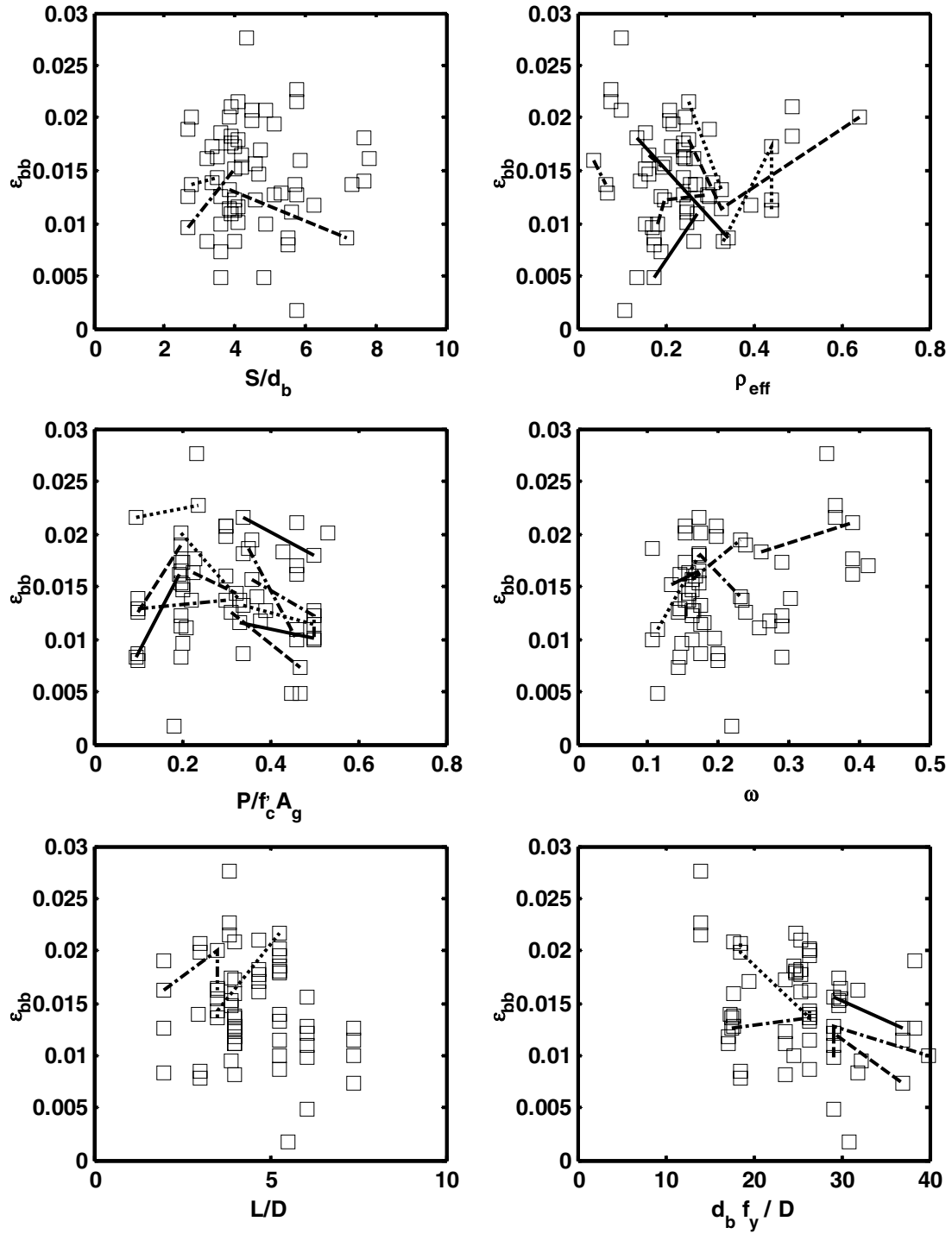
Figure 4.2 Trends in Nominal Compressive Strain at Bar Buckling, Rectangular Columns
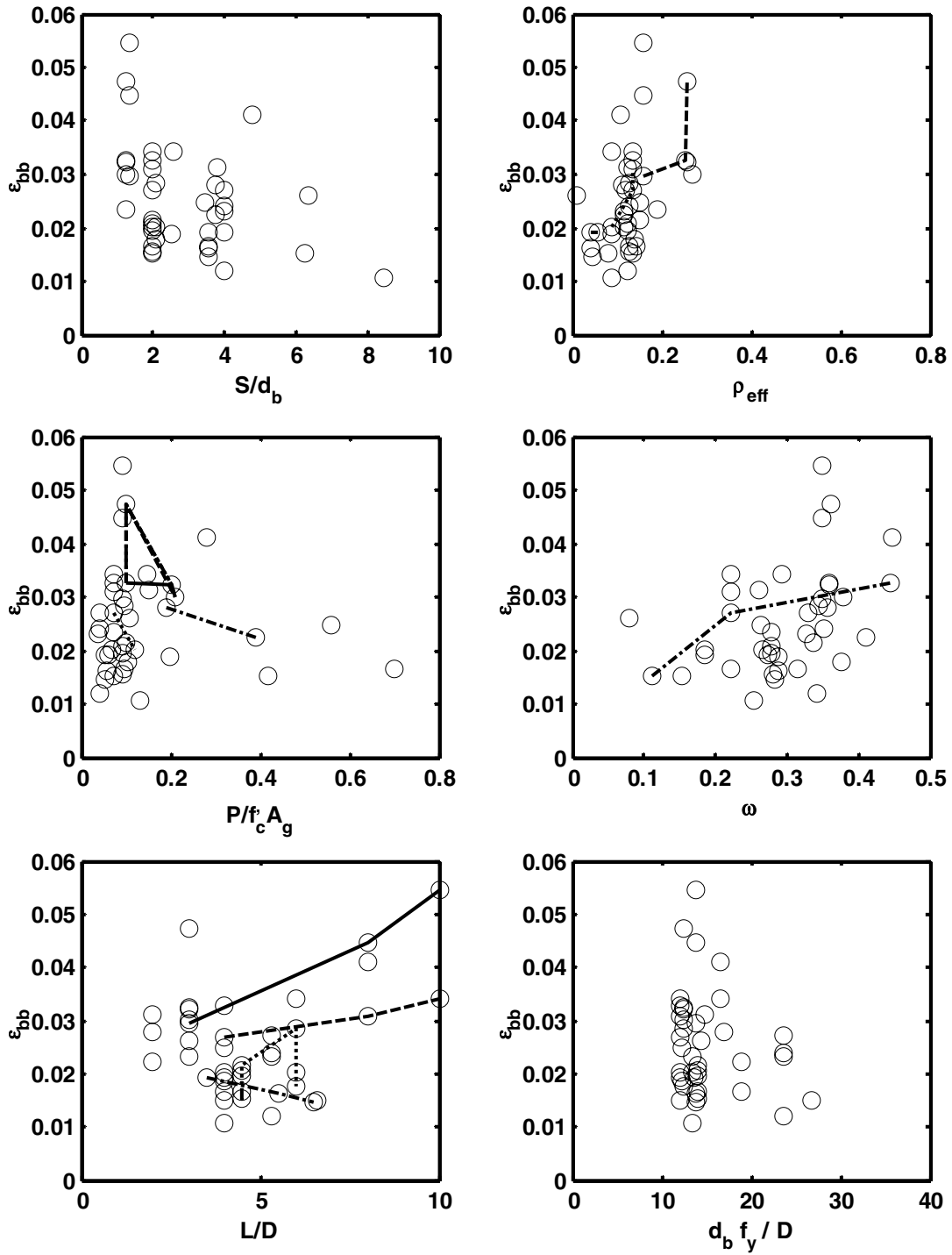
Figure 4.3 Trends in Nominal Compressive Strain at Bar Buckling, Spiral Columns

The following trends can be observed in Figures 4.2 and 4.3.

- Overall, the buckling strain decreases with an increase in S/d_b (as expected) for the spiral-reinforced columns. However, the expected influence is not observed in the overall trend in rectangular data or in the three rectangular families.

- The buckling strain is expected to increase with an increase in the effective confinement ratio. Pantazopoulou (1998) stated, "Visible buckling in adequately detailed columns has been reported to occur at strains 5–10 times as large as the yield strain, suggesting that stability of longitudinal reinforcement is a function of the confinement, i.e., the degree of effectiveness of tie arrangement." The effective confinement ratio, $\rho_{eff} = \dfrac{\rho_s f_{ys}}{f_c'}$, is commonly used to measure tie effectiveness, where ρ_s, f_{ys}, and f_c' are the volumetric transverse reinforcement ratio, yield stress of transverse reinforcement, and concrete compressive strength respectively. The expected trend is observed in the data from the column database (overall trends in rectangular and spiral data, four of seven rectangular families and both spiral families).

- According to Equation 4.6, the axial-load ratio should not affect the buckling strain, but there is a slight trend in the data. The nominal buckling strain decreases slightly with an increase in axial load for eight of twelve rectangular families and the three spiral families. This trend may be attributed to the plastic-hinge length used to calculate nominal buckling strains. Previous researchers have suggested that the plastic-hinge length should increase with an increase in axial load; the plastic-hinge length used in this study (Priestley et al. 1996) does not take into consideration axial load.

- No trend is expected in strain as a function of $\omega = \rho_l \dfrac{f_y}{f_c'}$ (where ρ_l is the longitudinal reinforcement ratio). A slight trend is observed in the data; the buckling strain increases with an increase in ω for both rectangular families and the one spiral family.

- The aspect ratio is not expected to affect the buckling strain, and no trend is observed in the column data.

- The ratio $\dfrac{d_b f_y}{D}$ is not expected to influence the buckling strain. However, the buckling strain decreases with an increase in $\dfrac{d_b f_y}{D}$ for 4 of 5 rectangular families. Three rectangular tests from the same test series (Wehbe et al. 1998) stand out as having the highest nominal buckling strains and the lowest values of $\dfrac{d_b f_y}{D}$. These columns also had the lowest normalized plastic-hinge lengths, $\dfrac{L_p}{D}$. These columns may stand out due to an inadequacy in the plastic-hinge length model (Priestley et al. 1996) used in the calculation of the buckling strain (Section 2.3). These columns suggest that the Priestley model may underestimate the effects of bar slip on plastic-hinge length at small values of $\dfrac{d_b f_y}{D}$.

It should be noted that the nominal buckling strains in Figures 4.2 and 4.3 are affected by the assumed plastic-hinge length; therefore the observed trends in all of theses plots might differ if another plastic-hinge model were used. In addition, there is a significant amount of scatter in the data. The coefficient of variation of the nominal buckling strain is 34% for rectangular columns and 40% for spiral-reinforced columns.

Table 4.1 summarizes the expected and observed influences of the key column properties on the buckling strain. The large arrows indicate a strong trend, while the small arrows indicate a slight trend.

Table 4.1 Influence of Key Column Properties on Buckling Strain

	S/db	r_{eff}	P/Agfc	w	L/D	$d_b f_y/D$
Expected	⬇	⬆	—	—	—	—
Observed (Rectangular)	—	↑	↓	↑	—	⬇
Observed (Spiral)	⬇	⬆	↓	↑	—	—

4.3 TRENDS IN PLASTIC ROTATION

The influences of key column properties on plastic rotation at the onset of bar buckling are investigated in this section. The expected trends for this damage state will be compared with the observed trends from the column database.

If bar buckling is assumed to be controlled by the buckling strain, and plastic-hinge analysis is assumed to adequately capture key column deformation characteristics, Equation 4.7 (Similar to Eq. 3.19) can be used to estimate the plastic rotation at the onset of bar buckling.

$$\theta_{p\_bb} = \frac{C_0}{\beta}\left(\varepsilon_{bb}\right)\left(1 + C_1\frac{P}{A_g f'_c}\right)^{-1}\left(1 + \alpha\beta\frac{L}{D} + \xi\beta\frac{f_y d_b}{D}\right) \qquad (\text{Eq. 4.7})$$

By using the study of trends in buckling strain (Section 4.3, Table 4.1) and Equation 4.7, the expected influences of key column characteristics on plastic rotation at bar buckling can be determined.

The observed trends are studied by plotting the plastic rotation at the onset of bar buckling (calculated with the procedure described in Section 2.3 using the plastic-hinge length proposed by Priestley et al. 1996) versus key column properties for columns in the column database (Figs 4.4 and 4.5). The lines in the figures represent families in which all column properties are similar except for the parameter being studied.

Figure 4.4 Trends in Nominal Plastic Rotation at Bar Buckling, Rectangular Columns
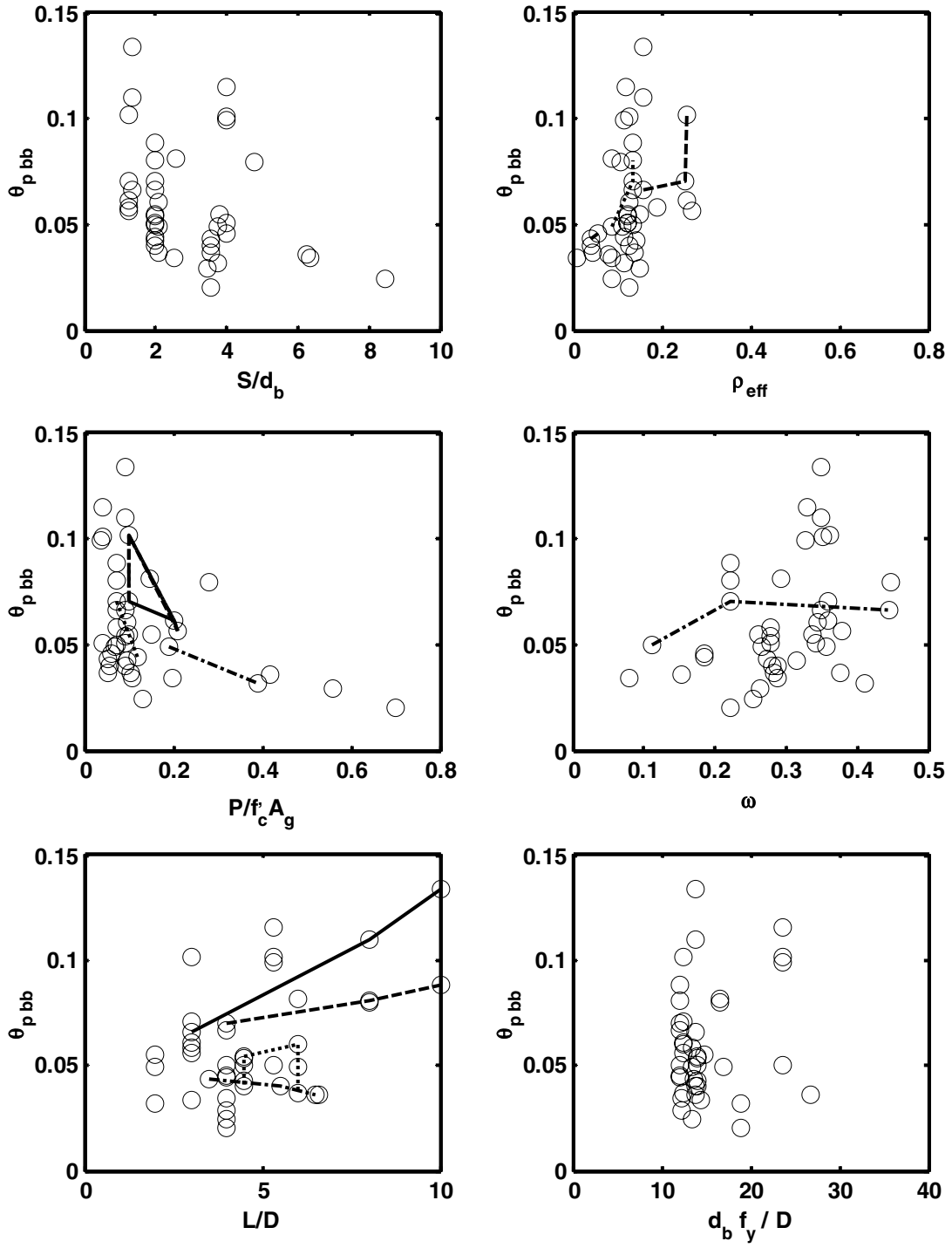
Figure 4.5 Trends in Nominal Plastic Rotation at Bar Buckling, Spiral Columns

The following discussion compares the expected influences with the observed trends in the data from the UW-PEER database.

- Overall, the plastic rotation at the onset of bar buckling decreases with an increase in S/d_b for both the rectangular and spiral data, as expected.

- The expected influence of effective confinement ratio on the plastic rotation at the onset of bar buckling (an increase in plastic rotation with an increase in effective confinement ratio) is observed in the data from the column database (five of seven rectangular families, the three spiral families, and the overall trends in the rectangular and spiral data).

- As expected, the plastic rotation at the onset of bar buckling decreases with an increase in axial load ratio (all twelve rectangular families, all six spiral families, and the overall trends in rectangular and spiral data).

- According to Chapter 3 (Table 3.1), the plastic rotation at a given strain should decrease with an increase in ω for columns with low axial load. It is difficult to tell if the expected trend is evident in the column data because the figure includes columns with low, moderate and high axial loads. However, the plastic rotation increases with an increase in ω for four of five rectangular families and the overall trend in the spiral data.

- The plastic rotation at the onset of bar buckling is expected to increase with an increase in aspect ratio. The expected trend can be observed in the spiral data (the overall trend and two of four spiral families), but the overall trend in the rectangular data suggests the opposite effect of aspect ratio.

- The expected trend in plastic rotation as a function of $\dfrac{d_b f_y}{D}$ (an increase in plastic rotation with an increase in $\dfrac{d_b f_y}{D}$) is not evident in the observed data.

It should be noted that the nominal plastic rotations at the onset of bar buckling in Figures 4.4 and 4.5 are slightly affected by the assumed plastic-hinge length; therefore the observed trends in all of theses plots might differ if another plastic-hinge model were used.

Table 4.2 summarizes the influence of key column properties on plastic rotation at the onset of bar buckling.

Table 4.2 Influence of Key Column Properties on Plastic Rotation at Bar Buckling

	S/db	r_{eff}	P/Agfc	w	L/D	$d_b f_y$/D
Expected	↓	↑	↓	↓ (Low Axial Load)	↑	↑
Observed (Rectangular)	↓	↑	↓	↑	—	—
Observed (Spiral)	↓	↑	↓	↑	↑	—

4.4   TRENDS IN DRIFT RATIO

In this section, the effects of key column characteristics on the drift ratio at the onset of bar buckling will be investigated. The expected influence of the column properties will be compared to observed influences in the UW-PEER database.

If plastic-hinge analysis is assumed to capture key column deformation characteristics, Equation 4.8 (Section 3.6) can be used to express the drift ratio at the onset of bar buckling.

$$\frac{\Delta_{bb}}{L} = \frac{\Delta_y}{L} + \theta_{p\_bb} \tag{Eq. 4.8}$$

By assuming $\Delta_y = \dfrac{\phi_y L^2}{3}$ (Eq. 3.22) and substituting in Priestley's equation for yield curvature (Eq. 3.11), the drift ratio at the onset of bar buckling can be expressed as follows.

$$\frac{\Delta_{bb}}{L} = \frac{\lambda}{3E_s} f_y \frac{L}{D} + \theta_{p\_bb} \tag{Eq. 4.9}$$

From Equation 4.9, the expected influences of key column characteristics on the drift ratio at the onset of bar buckling should be the same as those expected in plastic rotation, because the drift ratio is merely a summation of $\dfrac{\Delta_y}{L}$ (a function of *L/D,* with the same trend as in plastic rotation) and plastic rotation.

The results of Section 4.2 (Table 4.2) will be used to estimate the influence of key column properties on the drift ratio at the onset of bar buckling. The drift ratio at the onset of bar buckling is expected to increase with an increase in $\dfrac{d_b f_y}{D}$, ρ_{eff}, and L/D; and decrease with an increase in S/d_b, axial load ratio, and ω.

36

These expected influences will be compared to the observed trends in the column database. The drift ratio at the onset of bar buckling has been plotted versus the various column properties in Figures 4.6 and 4.7. Again, the solid lines represent families in which all column properties are similar except the study parameter.
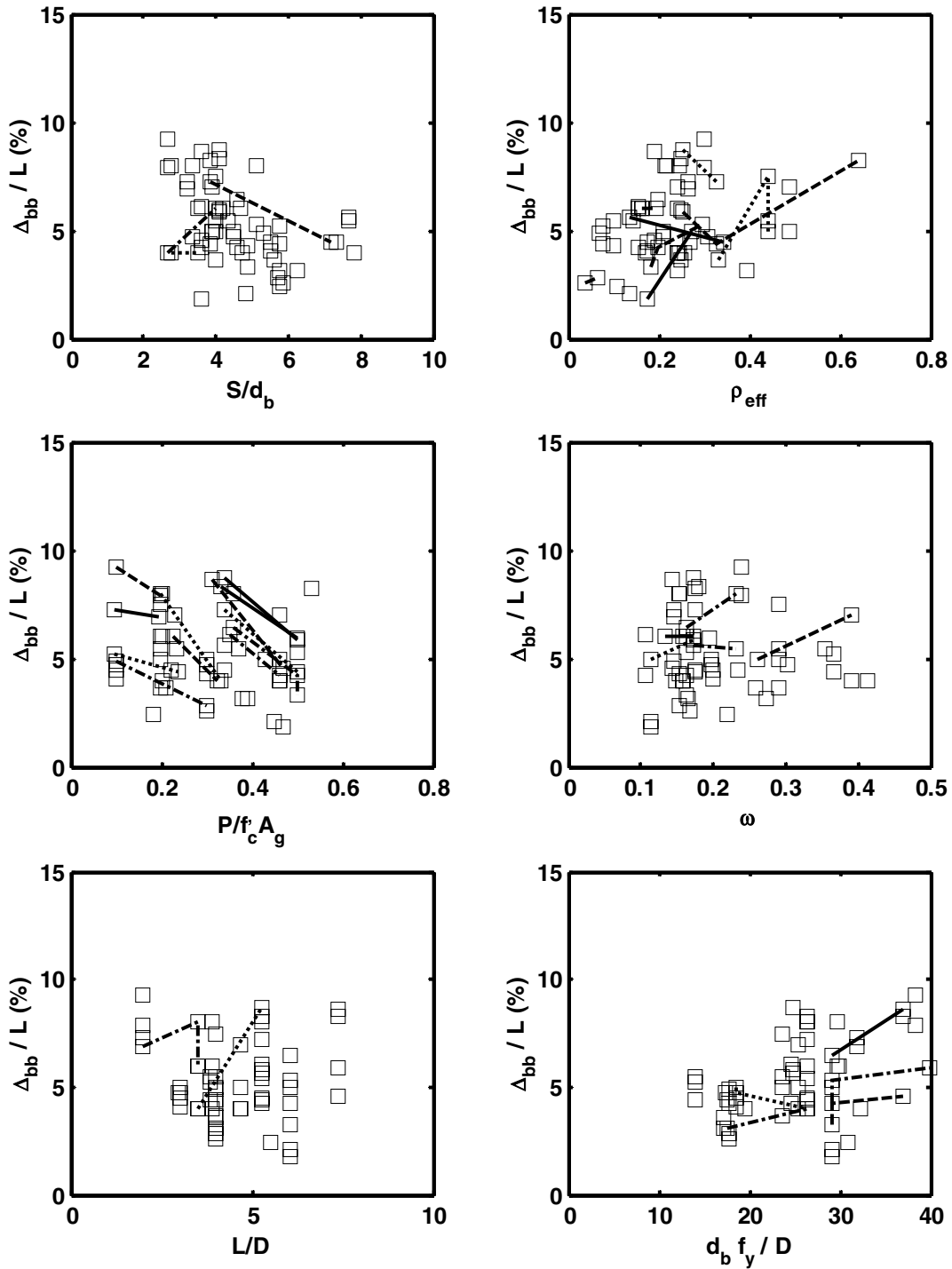
Figure 4.6 Trends in Drift Ratio at Bar Buckling, Rectangular Columns
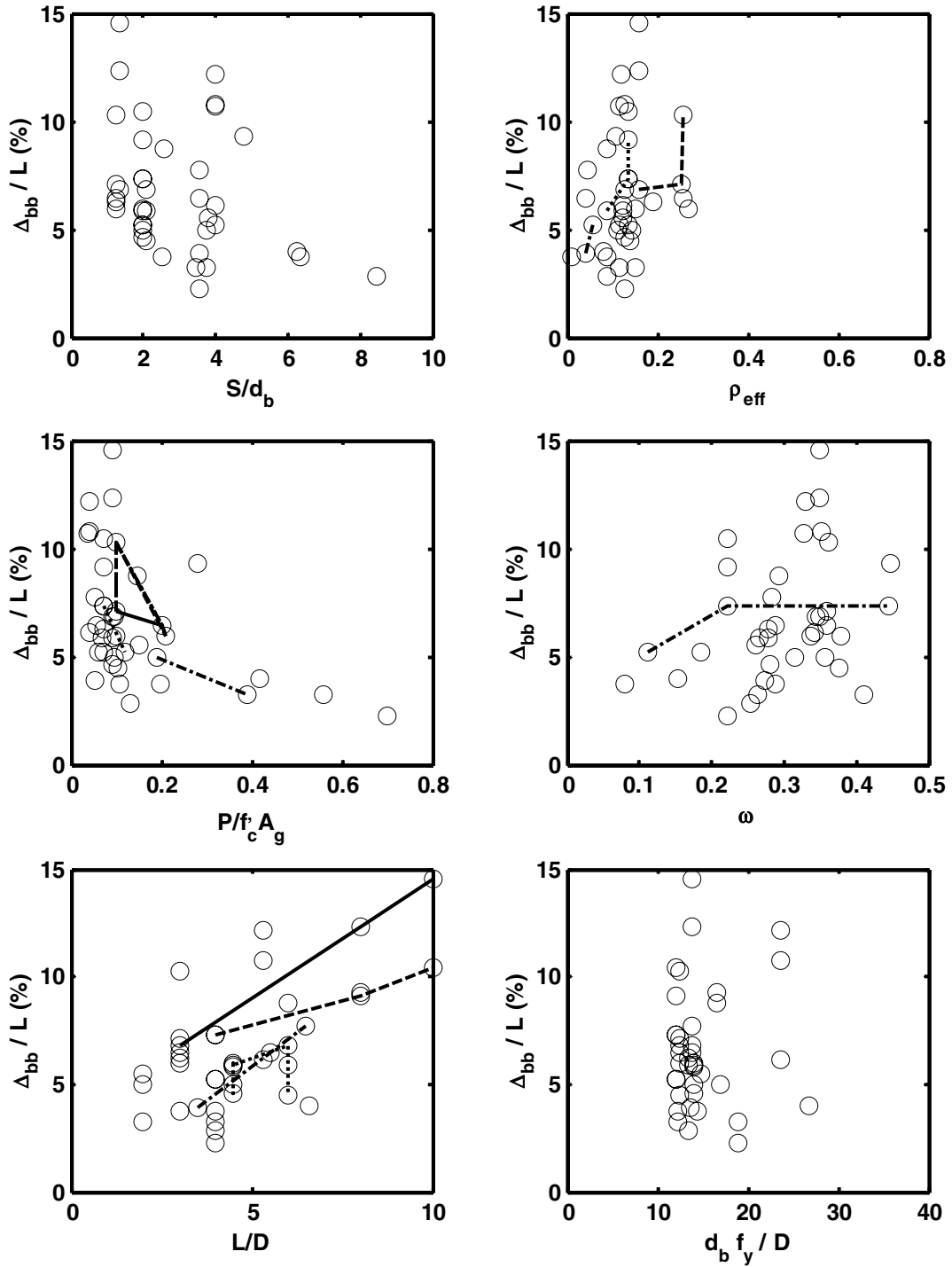
Figure 4.7 Trends in Drift Ratio at Bar Buckling, Spiral Columns

The observed trends are discussed below.

- As expected, the drift ratio at the onset of bar buckling decreases with an increase in S/d_b (overall trends in rectangular and spiral data).

- The expected influence of effective confinement ratio on drift ratio at the onset of bar buckling (an increase in drift ratio with an increase in effective confinement ratio) is observed in the column data (the overall spiral and rectangular data, five of seven rectangular families, and the three spiral families).

- As expected, the drift ratio at the onset of bar buckling decreases with an increase in axial load ratio (the overall trends in rectangular and spiral data, all 12 rectangular families, and all six spiral families).

- From Chapter 3 (Table 3.1), the drift ratio at the onset of bar buckling is expected to decrease with an increase in ω for columns with low axial load. The opposite trend can be observed in the rectangular data (three of four rectangular families) and spiral data (overall trend).

- The expected influence of aspect ratio on the drift ratio at the onset of bar buckling (an increase in drift ratio with an increase in aspect ratio) can be observed in the spiral data (the overall trend and two of four spiral families). The opposite trend can be observed in the rectangular data (overall trend).

- The expected influence of $\dfrac{d_b f_y}{D}$ on drift ratio (an increase in drift ratio with an increase in $\dfrac{d_b f_y}{D}$) can be observed in the rectangular data (four of five rectangular families).

Table 4.3 summarizes the influences of key column characteristics on the drift ratio at the onset of bar buckling.

Table 4.3 Influence of Key Column Properties on Drift Ratio at Bar Buckling

	S/db	r_{eff}	P/Agfc	w	L/D	$d_b f_y/D$
Expected	⬇	⬆	⬇	⬇ (Low Axial Load)	⬆	⬆
Observed (Rectangular)	⬇	⬆	⬇	⬆	⬇	⬆
Observed (Spiral)	⬇	⬆	⬇	⬆	⬆	—

4.5 TRENDS IN DISPLACEMENT DUCTILITY

In this section, the influence of key column characteristics on displacement ductility at the onset of bar buckling are studied.

If bar buckling is assumed to be controlled by the buckling strain, and plastic-hinge analysis is assumed to adequately capture key column deformation characteristics, Equation 4.10 (Section 1.7) can be used to represent the displacement ductility at the onset of bar buckling.

$$\frac{\Delta_{bb}}{\Delta_y} = 1 + 3\frac{C_0 E_s}{\beta\lambda}\left(\frac{\varepsilon_{bb}}{f_y}\right)\left(1 + C_0\frac{P}{A_g f'_c}\right)^{-1}\left(\frac{1}{L/D} + \alpha\beta + \xi\beta\frac{1}{L/D}\frac{d_b f_y}{D}\right) \quad \text{(Eq. 4.10)}$$

By using the results of the study on buckling strain trends (Section 4.3) and Equation 4.10, the influence of key column properties on the displacement ductility at the onset of bar buckling can be estimated.

The expected influences are compared to experimental results by plotting the displacement ductility at the onset of bar buckling versus the key column characteristics (Figs. 4.8 and 4.9). To isolate the effect of the study parameter, the database was assembled into families, in which all column properties are similar except the study parameter. The families are represented by lines in the figures.
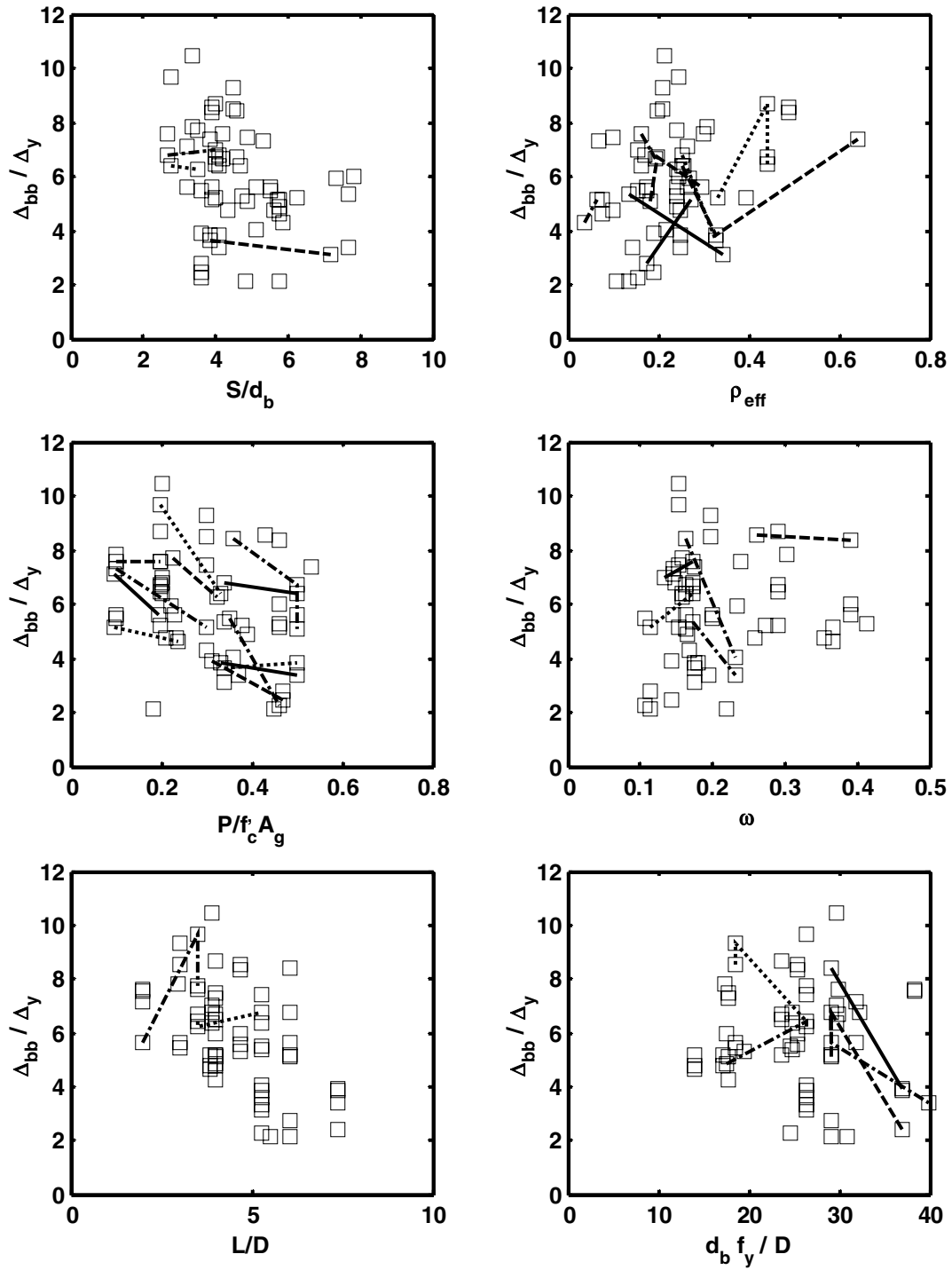
Figure 4.8 Trends in Displacement Ductility at Bar Buckling, Rectangular Columns
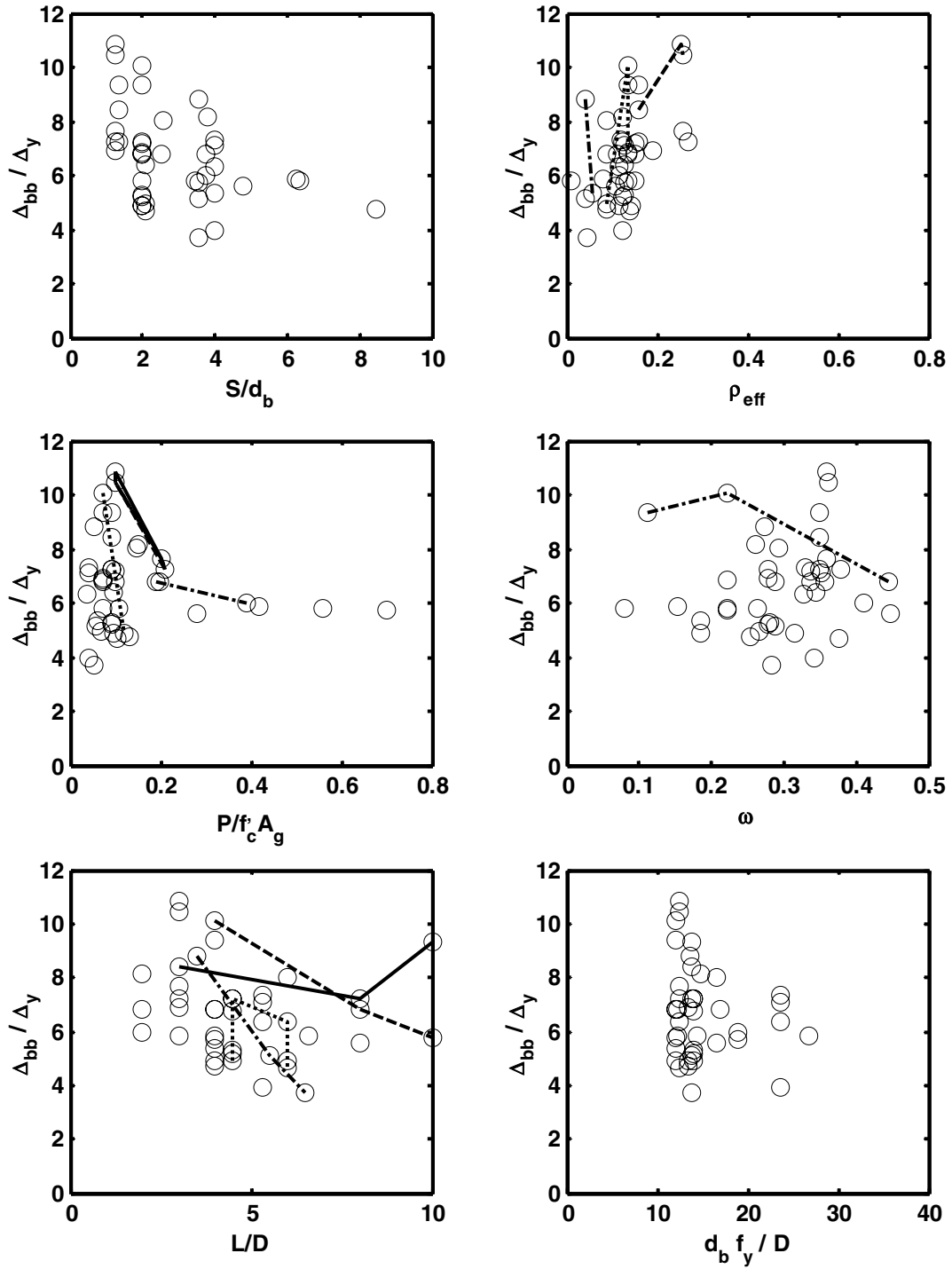
Figure 4.9 Trends in Displacement Ductility at Bar Buckling, Spiral Columns

The expected influences are now compared to the trends in the data from the column database.

- As expected, the displacement ductility at the onset of bar buckling decreases with an increase in S/d_b (overall trends in rectangular and spiral data).

- The expected influence of effective confinement ratio on displacement ductility at the onset of bar buckling (an increase in displacement ductility with an increase in effective confinement ratio) is observed in the experimental data (the overall trends in rectangular and spiral data, four of seven rectangular families, and two of three spiral families).

- The data in the database strongly suggest that an increase in axial load ratio decreases the displacement ductility at the onset of bar buckling (ten of twelve rectangular families and all six spiral families). This trend was expected.

- No trends are observed in displacement ductility at the onset of bar buckling as a function of ω.

- As expected, the displacement ductility at the onset of bar buckling decreases with an increase in aspect ratio for the spiral data (three of four families) and the rectangular data (overall trend).

- Contrary to what is expected, the displacement ductility at the onset of bar buckling decreases with an increase in $\dfrac{d_b f_y}{D}$ for the rectangular data (four of five rectangular families).

Table 4.4 summarizes the expected and observed influences of key column characteristics on the displacement ductility at the onset of bar buckling.

Table 4.4 Influence of Key Column Properties on Displacement Ductility at Bar Buckling

	S/db	r $_{eff}$	P/Agfc	w	L/D	$d_b f_y /D$
Expected	⬇	⬆	⬇	⬇ (Low Axial Load)	⬇	⬆
Observed (Rectangular)	⬇	⬆	⬇	—	⬇	⬇
Observed (Spiral)	⬇	⬆	⬇	—	⬇	—

4.6   SUMMARY

Because of the complexity controlling the onset of this damage state, bar buckling in reinforced concrete members is difficult to model using traditional analytical modeling strategies. The proposed modeling strategy (Chapter 6) is based on theoretically expected trends in critical compressive strain, plastic rotation, drift ratio, and displacement ductility at the onset of bar buckling as functions of key column properties. The expected and observed trends in these deformation measures were studied, and Table 4.5 provides a summary of the results of this investigation. The following can be observed from Table 4.5.

- The buckling strain is expected to decrease with an increase in S/d_b, and increase with an increase in ρ_{eff}. The expected influence of S/d_b can be observed in the spiral data, and the expected influence of ρ_{eff} can be observed in both the spiral and rectangular data.

- The plastic rotation, drift ratio, and displacement ductility at the onset of bar buckling are expected to increase with an increase in ρ_{eff}, and decrease with an increase in S/d_b and $P/A_g f_c'$. Each of these trends can be observed in both the spiral-reinforced and rectangular-reinforced column data. Two key trends in drift ratio at bar buckling are shown in Figures 4.10 and 4.11 for both the rectangular- and spiral-reinforced column data.

It should be noted that similar trends can be observed in the columns from the UW-PEER database at 20% reduction in flexural capacity. The trend plots at 20% reduction in flexural capacity are provided in Appendix B. The tip displacements at 20% reduction in flexural capacity were calculated with the procedure described in Camarillo 2003.
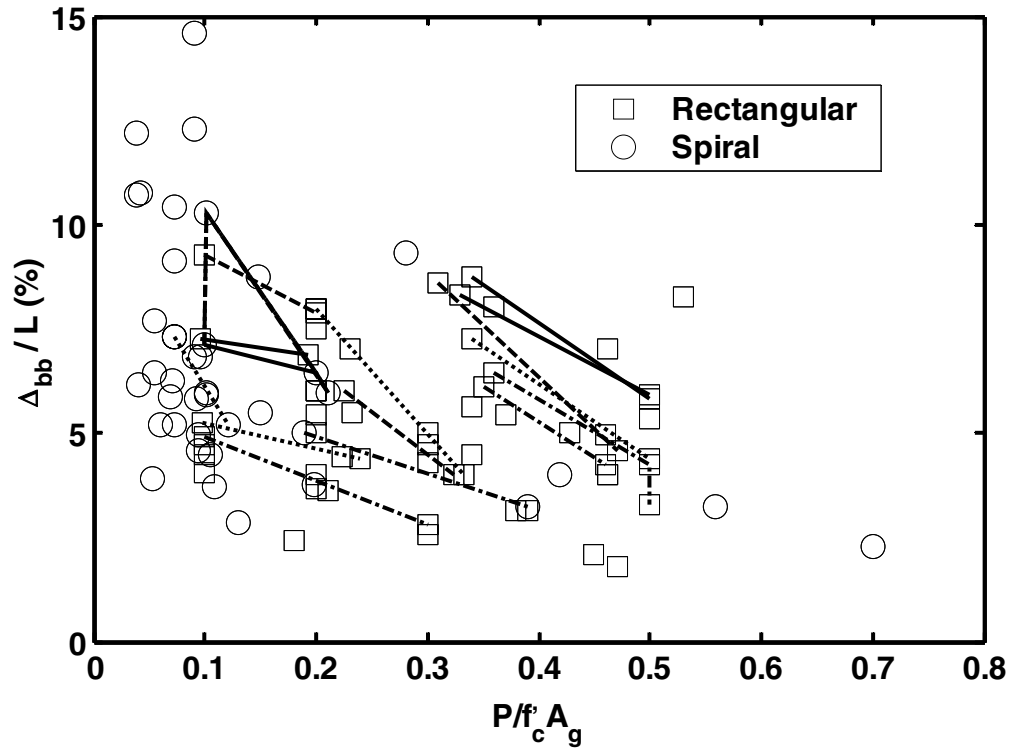
Figure 4.10 Drift Ratio at Bar Buckling vs. $P/f'_c A_g$
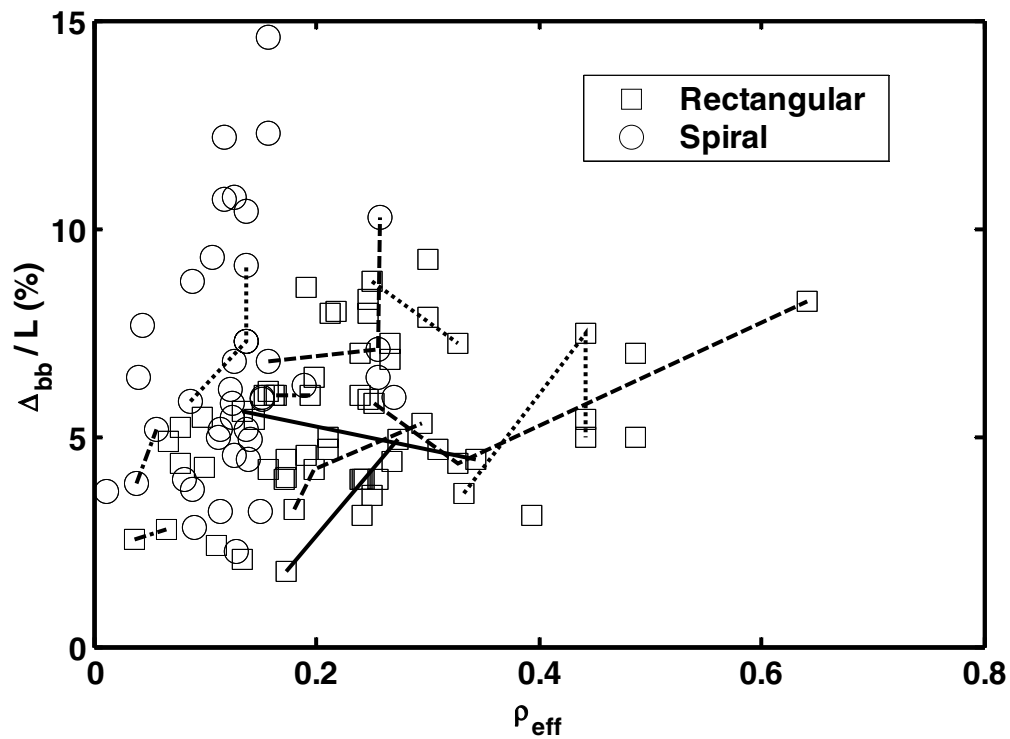
Figure 4.11 Drift Ratio at Bar Buckling vs. r_{eff}

- The expected influences ω on the deformation measures at the onset of bar buckling and the trends observed in the column data are on no account similar. The expected trends

45

may not be observed in the data, because the data include columns with moderate and high axial loads, and ω is only expected to influence columns with low axial loads.

- The aspect ratio influences the deformation measures at the onset of bar buckling in spiral-reinforced columns. An increase in aspect ratio is expected to increase the drift ratio and plastic rotation at the onset of bar buckling, and decrease the displacement ductility. These trends can be observed in the spiral data. Only the trend in displacement ductility can be observed in the rectangular data.

- The effect of $\dfrac{d_b f_y}{D}$ on the deformations at the onset of bar buckling is unclear.

Table 4.5 Influence of Key Column Properties on Deformation Measures at Bar Buckling

		S/db	r_{eff}	P/Agfc	w	L/D	$d_b f_y/D$
ε_{bb}	Expected	↓	↑	—	—	—	—
	Observed (Rectangular)	—	↑	↓	↑	—	↓
	Observed (Spiral)	↓	↑	↓	↑	—	—
θ_{p_bb}	Expected	↓	↑	↓	↓ (Low Axial)	↑	↑
	Observed (Rectangular)	↓	↑	↓	↑	—	—
	Observed (Spiral)	↓	↑	↓	↑	↑	—
$\dfrac{\Delta_{bb}}{L}$	Expected	↓	↑	↓	↓ (Low Axial)	↑	↑
	Observed (Rectangular)	↓	↑	↓	↑	↓	↑
	Observed (Spiral)	↓	↑	↓	↑	↑	—
$\dfrac{\Delta_{bb}}{\Delta_y}$	Expected	↓	↑	↓	↓ (Low Axial)	↓	↑
	Observed (Rectangular)	↓	↑	↓	—	↓	↓
	Observed (Spiral)	↓	↑	↓	—	↓	—

5　Onset of Concrete Spalling

The influence of key column characteristics on compressive strain, plastic rotation, drift ratio, and displacement ductility at the onset of concrete spalling will be studied in the following sections.

5.1　TRENDS IN COMPRESSIVE STRAIN

In order to determine the influences of key column characteristics on the compressive spalling strain (ε_{spall}), the nominal spalling strain (calculated with the procedure described in Section 2.3 and the plastic-hinge model proposed by Priestley et al. 1996) is plotted versus various column properties. The lines in Figures 5.1 and 5.2 represent families in which all column properties are similar except the property being studied. It should be noted that the families do not take into consideration the load histories of the column tests. It should also be noted that the vertical axes for the two figures differ by a factor of 2.
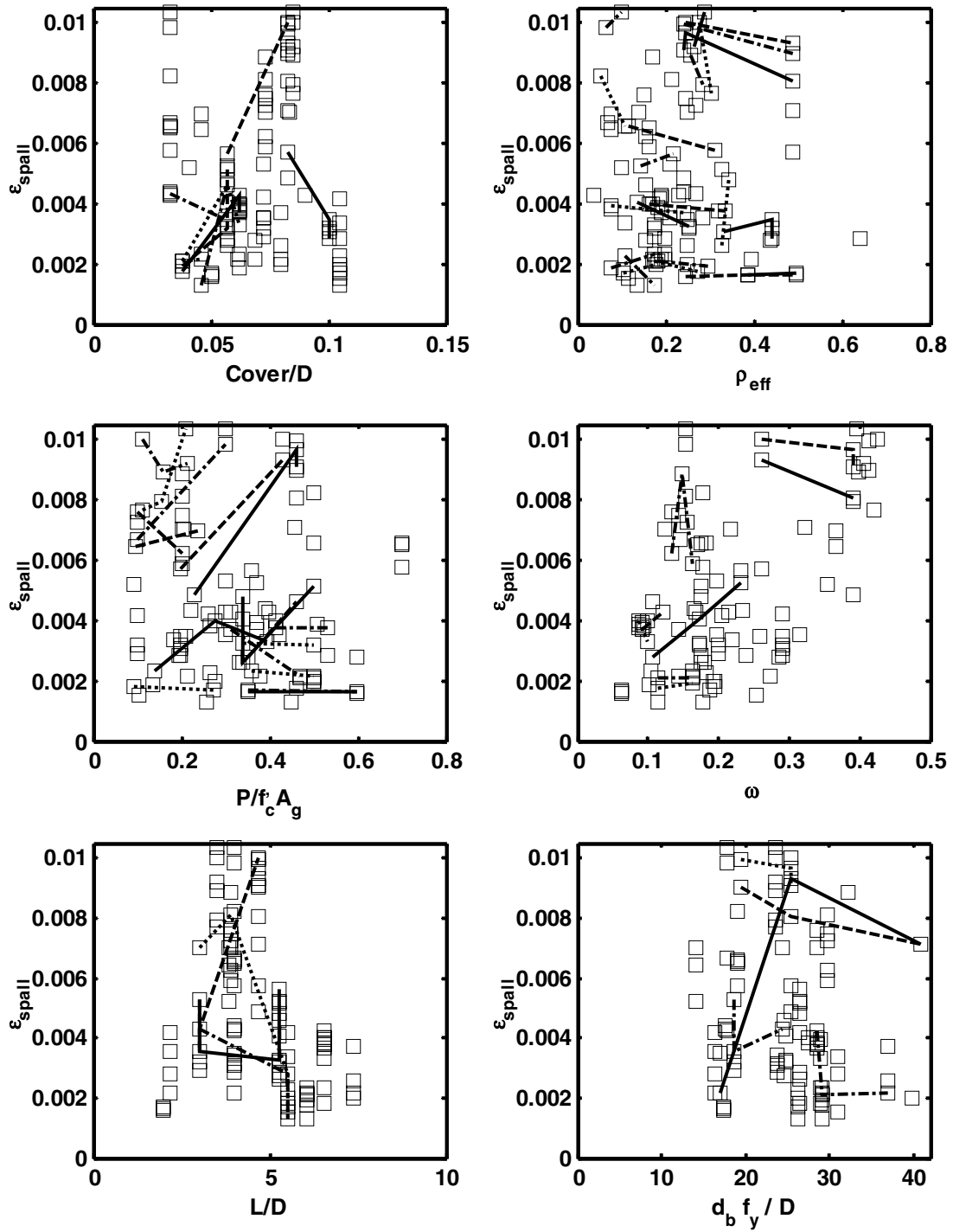
Figure 5.1 Trends in Nominal Compressive Strain at Cover Spalling, Rectangular Columns
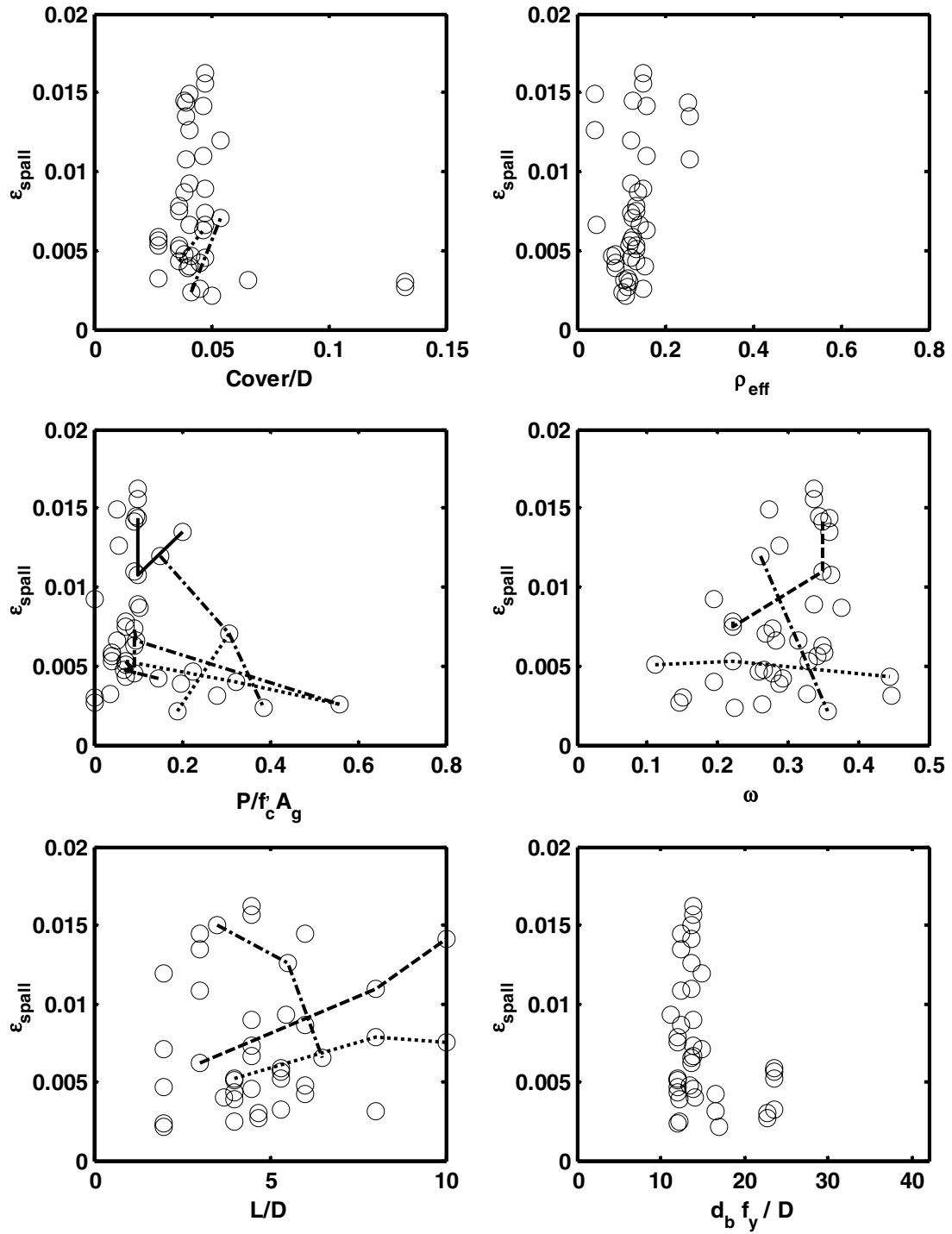
Figure 5.2 Trends in Nominal Compressive Strain at Cover Spalling, Spiral Columns

There is significant scatter in the data, and few trends can be observed. The coefficient of variation of critical spalling strain is 55% for rectangular columns and 56% for spiral columns. The following trends can be observed.

- The critical spalling strain increases with an increase in normalized clear cover (ratio of clear cover to column depth) for five of eight rectangular families and both spiral families.
- The critical spalling strain decreases with an increase in axial load ratio for the spiral-reinforced data (four of six spiral families and the overall trend in spiral data).

It should be noted that the observed trends in the data might be affected by the plastic-hinge model used in the calculation of the nominal spalling strain.

Table 5.1 summarizes observed influences of the key column properties on the critical spalling strain. The large arrows indicate a strong trend, while the small arrows indicate a slight trend.

Table 5.1 Influence of Key Column Properties on Critical Spalling Strain

	Cover/D	r_{eff}	P/Agfc	w	L/D	d_bf_y/D
Expected	—	—	—	—	—	—
Observed (Rectangular)	↑	—	—	—	—	—
Observed (Spiral)	↑	—	⬇	—	—	—

5.2   TRENDS IN PLASTIC ROTATION

The influence of key column properties on the plastic rotation at the onset of concrete spalling will be investigated in this section.

If the following assumptions are made, Equation 5.1 (from Equation 3.18) can be used to estimate the plastic rotation at the onset of concrete spalling.

- Spalling is controlled by the maximum compressive strain.
- Spalling occurs after the column has reached its yield displacement.
- Plastic-hinge analysis adequately captures key column deformation characteristics.

$$\theta_{p\_spall} = \frac{C_0}{\beta}\left(\varepsilon_{spall}\right)\left(1 + C_1\frac{P}{A_g f'_c}\right)^{-1}\left(1 + \alpha\beta\frac{L}{D} + \xi\beta\frac{f_y d_b}{D}\right)$$
(Eq. 5.1)

According to Equation 5.1, for a given strain, the plastic rotation at the onset of concrete spalling is expected to increase with an increase in aspect ratio and $\dfrac{f_y d_b}{D}$, and decrease with an increase in axial load ratio. In addition, if the critical spalling strain is assumed to be influenced by the normalized clear cover (as observed in Section 5.1), the plastic rotation at the onset of bar buckling should increase with an increase in normalized clear cover.

The expected and observed influences of key column properties on plastic rotation at the onset of concrete spalling are compared in the following paragraphs. The normalized plastic rotation at the onset of cover spalling (from the procedure described in Section 2.3 and using the plastic-hinge model proposed by Priestley et al. 1996) are plotted versus the key column properties for the columns from the database. In order to isolate the effect of a column property, the database was assembled into families in which all column properties are similar except the property being studied. These families are represented by lines in Figures 5.3 and 5.4.
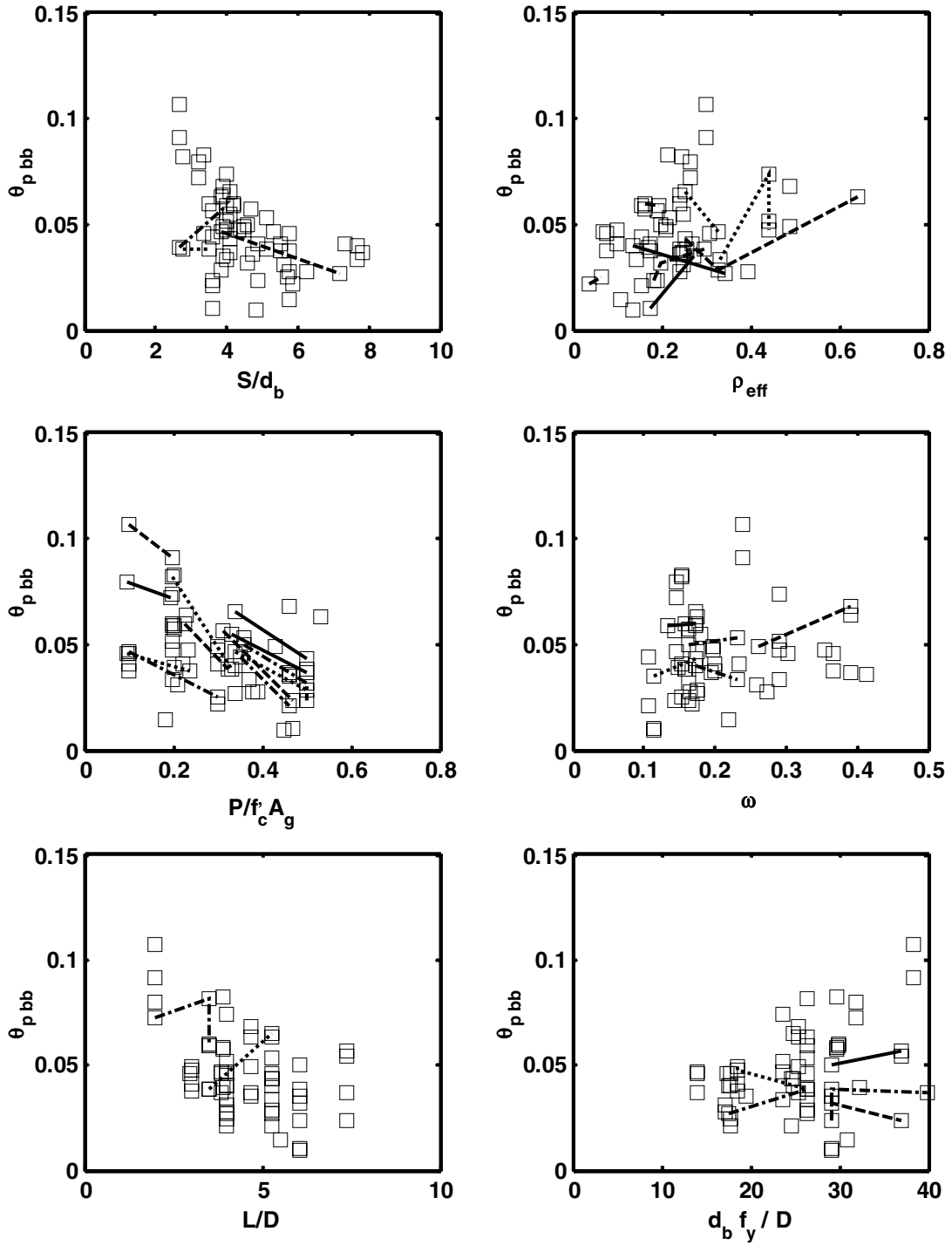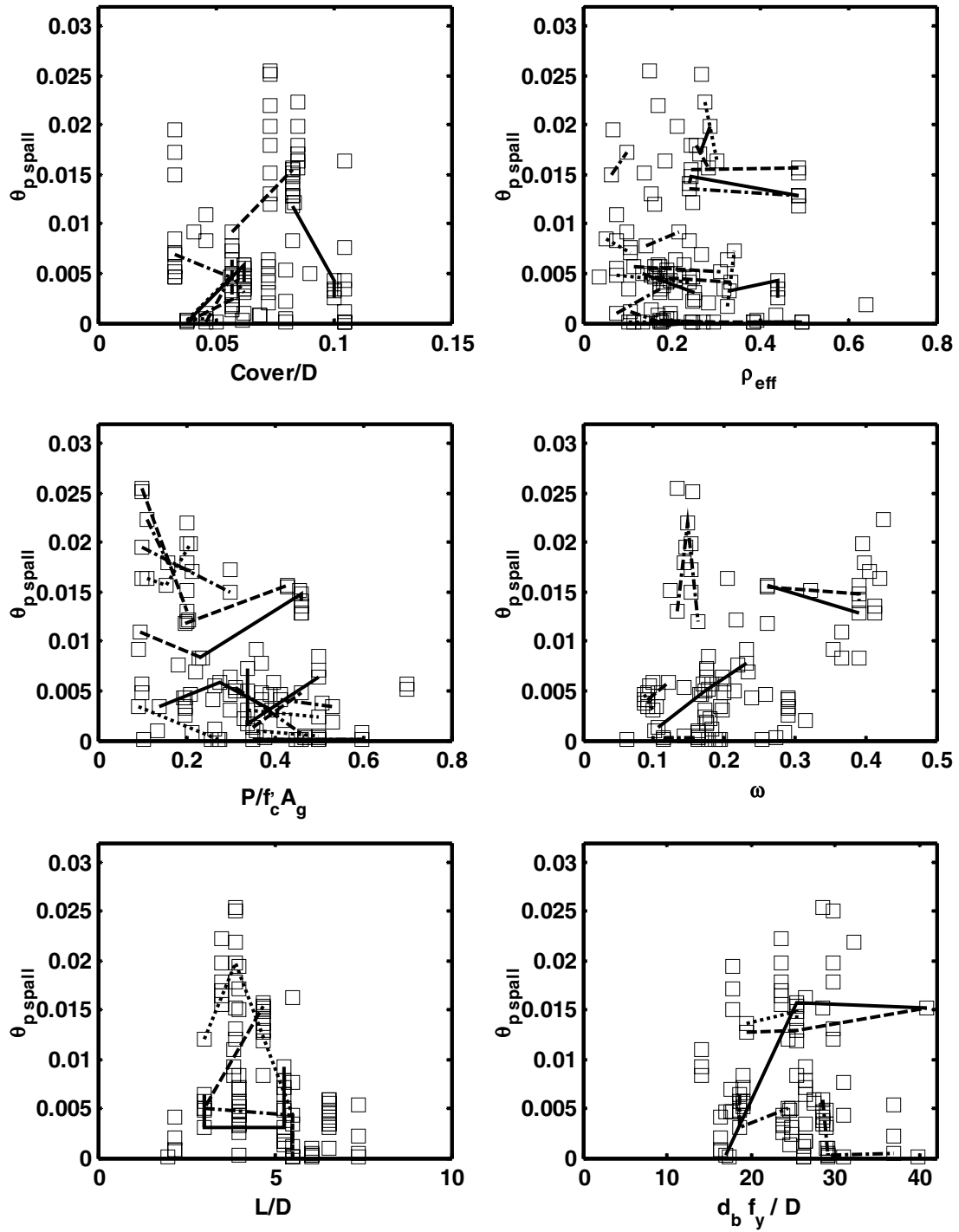
Figure 5.3 Trends in Nominal Plastic Rotation at Cover Spalling, Rectangular Columns
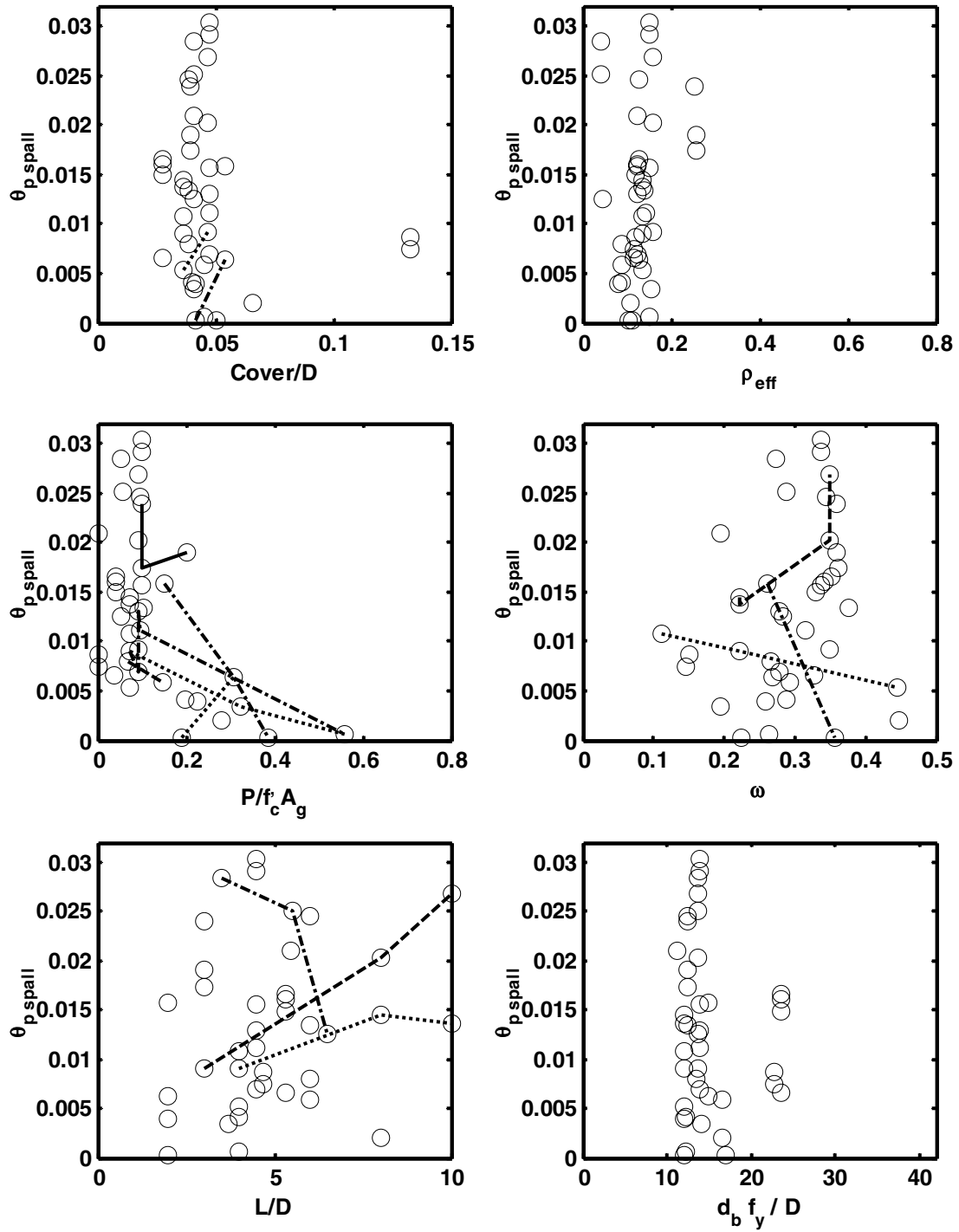
Figure 5.4 Trends in Nominal Plastic Rotation at Cover Spalling, Spiral Columns

53

Again, there is significant scatter in the data, and few trends can be observed. The coefficient of variation of the plastic rotation at the onset of concrete spalling is 92% for rectangular columns and 65% for spiral columns. It should be noted that for several rectangular columns, the cover concrete spalled prior to reaching the yield displacement. In these cases, the plastic rotation is set to zero.

The following discusses the trends that can be observed in the data:

- The plastic rotation at the onset of bar buckling increases with an increase in normalized clear cover for five of eight rectangular families and both of the spiral families. This trend is expected only if the spalling strain is assumed to be controlled by the normalized clear cover (observed in Section 5.1).
- As expected, the plastic rotation at the onset of concrete spalling decreases with an increase in axial load ratio for both the rectangular and spiral columns (nine of fifteen rectangular families and five of six spiral families).

Table 5.2 summarizes the influence of key column properties on plastic rotation at the onset of bar buckling.

Table 5.2 Influence of Key Column Properties on Plastic Rotation at Cover Spalling

	Cover/D	r_{eff}	P/Agfc	w	L/D	d_bf_y/D
Expected	—	—	↓	↓ (Low Axial)	↑	↑
Observed (Rectangular)	↑	—	↓	—	—	—
Observed (Spiral)	↑	—	↓	—	—	—

5.3   TRENDS IN DRIFT RATIO

If concrete spalling is assumed to be controlled by the critical compressive strain, and plastic-hinge analysis is assumed to adequately capture key column deformation characteristics, Equation 5.2 (from Equation 3.20) can be used to estimate the drift ratio at the onset of concrete cover spalling.

$$\frac{\Delta_{spall}}{L} = \frac{\Delta_y}{L} + \theta_{p\_spall}$$
(Eq. 5.2)

By substituting in Priestley's equation (1996) for yield curvature (Eq. 3.11), the drift ratio can be approximated as follows.

$$\frac{\Delta_{spall}}{L} = \frac{\lambda}{3E_s} f_y \frac{L}{D} + \theta_{p\_spall}$$ (Eq. 5.3)

The influences of key column properties on the drift ratio at the onset of cover spalling should be similar to those expected in plastic rotation because drift ratio is merely the summation of the yield displacement (assumed to vary only with $\frac{L}{D}$) and the plastic rotation.

From Equation 5.3 and Table 5.2, the drift ratio at the onset of concrete spalling is expected to increase with an increase in $\frac{L}{D}$, $\frac{f_y d_b}{D}$, and $\frac{Cover}{D}$; and decrease with an increase in axial load ratio and ω. The expected influences will be compared in the column data by plotting the drift ratio at the onset of spalling versus the key column properties (Figs. 5.5 and 5.6).
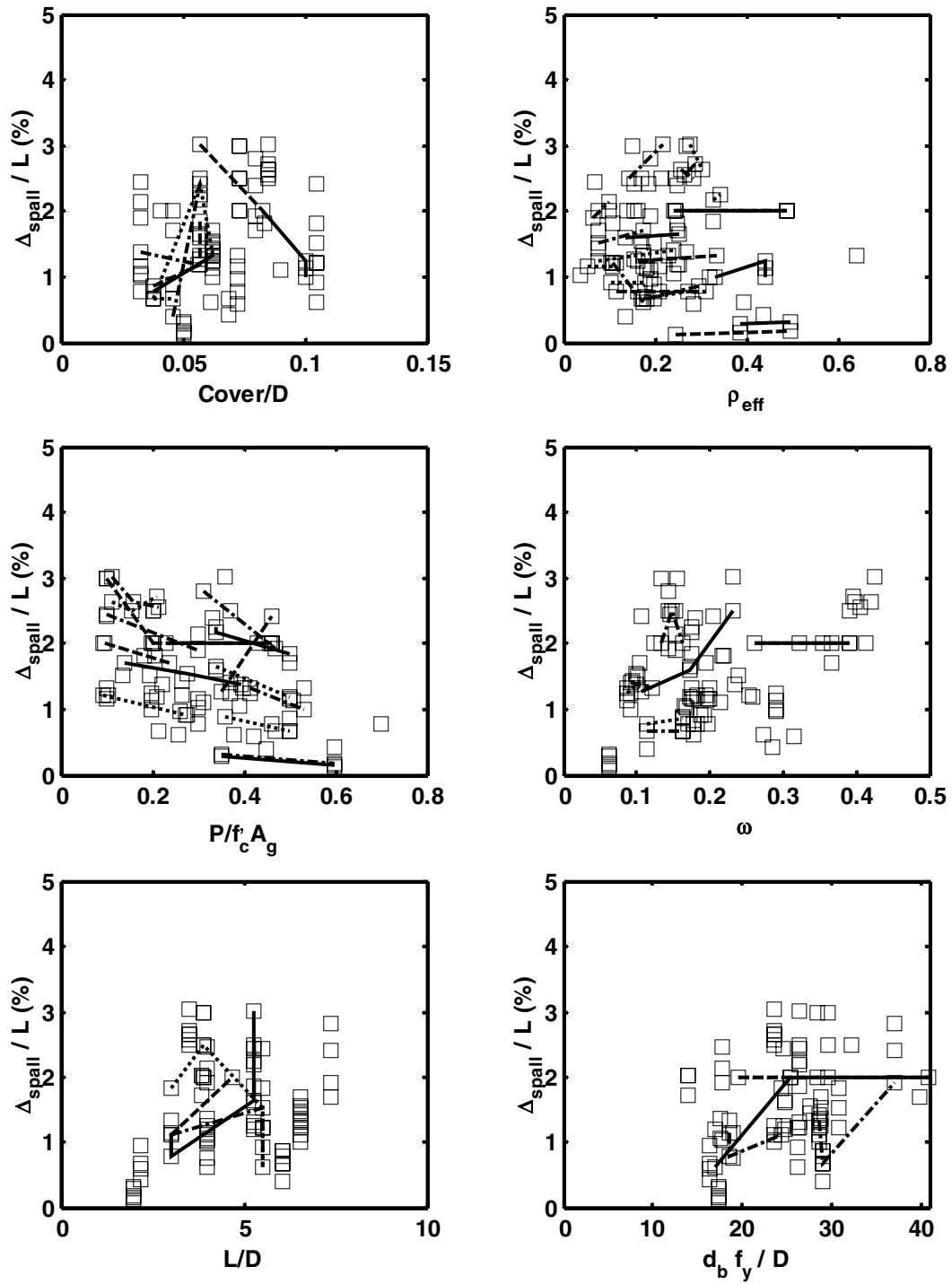
Figure 5.5 Trends in Drift Ratio at Cover Spalling, Rectangular Columns

56
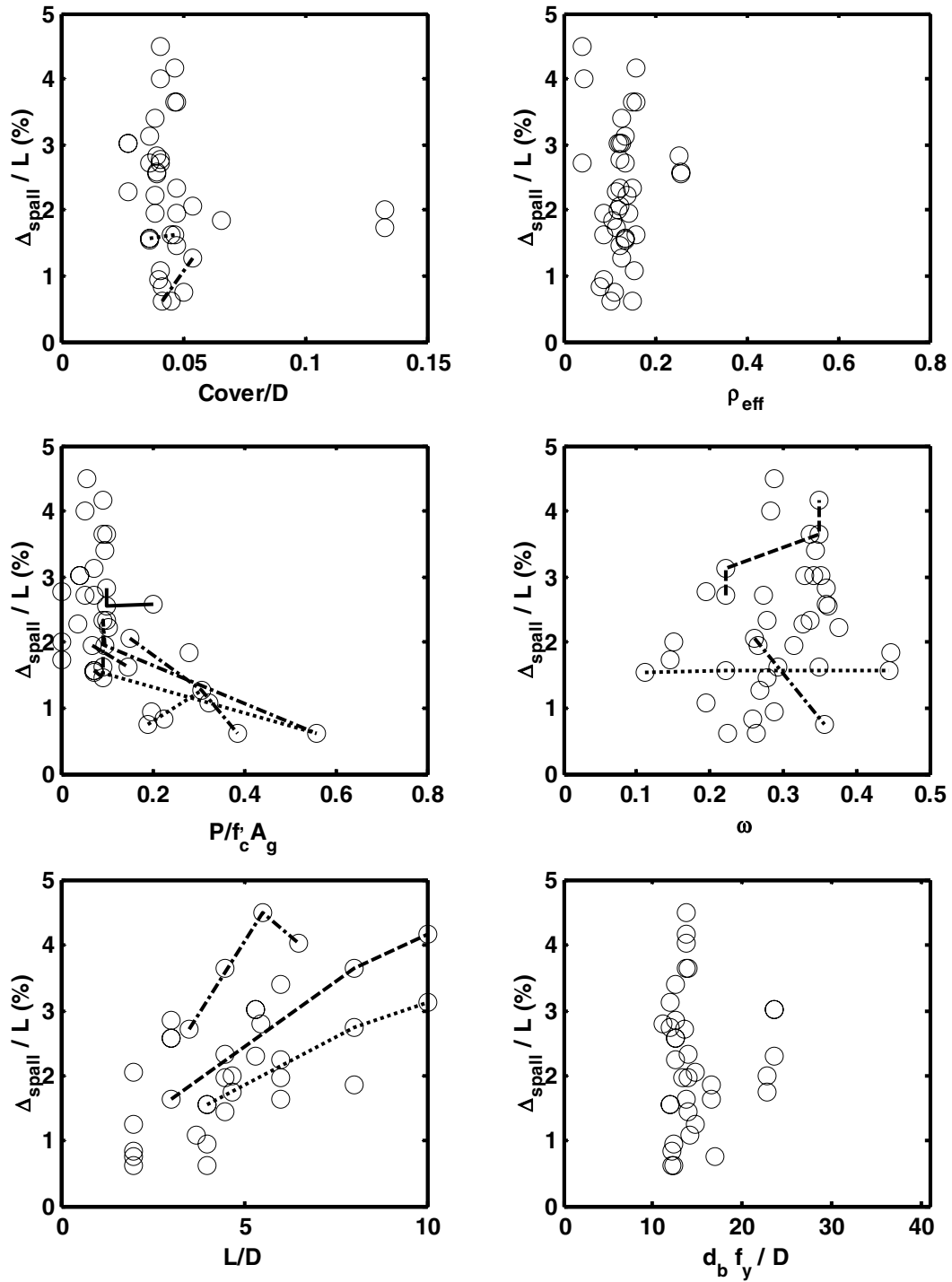
Figure 5.6 Trends in Drift Ratio at Cover Spalling, Spiral-Reinforced Columns

Again, few trends can be observed in the column data.

- The drift ratio at the onset of concrete spalling increases with an increase in normalized clear cover (five of eight rectangular families and both of the spiral families). Again, this can be expected if the critical spalling strain is assumed to be controlled by normalized clear cover (as observed in Section 5.1).

- As expected, the drift ratio at the onset of bar buckling decreases with an increase in axial load ratio for both the rectangular (15 of 17 families and the overall trend) and spiral data (5 of 6 spiral families and the overall trend).

- As expected, the drift ratio at the onset of bar buckling increases with an increase in aspect ratio (three of four rectangular families and two of three spiral families).

Table 5.3 summarizes this study of the influences of key column characteristics on the drift ratio at the onset of concrete spalling.

Table 5.3 Influence of Key Column Properties on Drift Ratio at Cover Spalling

	Cover/D	r_{eff}	P/Agfc	w	L/D	$d_b f_y/D$
Expected	—	—	↓	↓ (Low Axial)	↑	↑
Observed (Rectangular)	↑	—	↓	—	↑	—
Observed (Spiral)	↑	—	↓	—	↑	—

5.4   TRENDS IN DISPLACEMENT DUCTILITY

The influence of key column deformation characteristics on the displacement ductility at the onset of concrete spalling will be investigated in this section.

If plastic-hinge analysis is assumed to capture key column deformation characteristics, the displacement ductility can be approximated with Equation 5.4 (from Eq. 3.26).

$$\frac{\Delta_{spall}}{\Delta_y} = 1 + 3 \frac{C_0 E_s}{\beta \lambda} \left(\frac{\varepsilon_{spall}}{f_y} \right) \left(1 + C_0 \frac{P}{A_g f'_c} \right)^{-1} \left(\frac{1}{L/D} + \alpha\beta + \xi\beta \frac{1}{L/D} \frac{f_y d_b}{D} \right) \qquad \text{(Eq. 5.4)}$$

From Equation 5.4, the displacement ductility at the onset of spalling is expected to increase with an increase in $\dfrac{f_y d_b}{D}$, and decrease with an increase in axial load ratio, aspect ratio, and ω.

The expected influences are now compared to the trends in the data from the column database by plotting the displacement ductility at the onset of cover spalling versus the key column characteristics (Figs. 5.7 and 5.8).
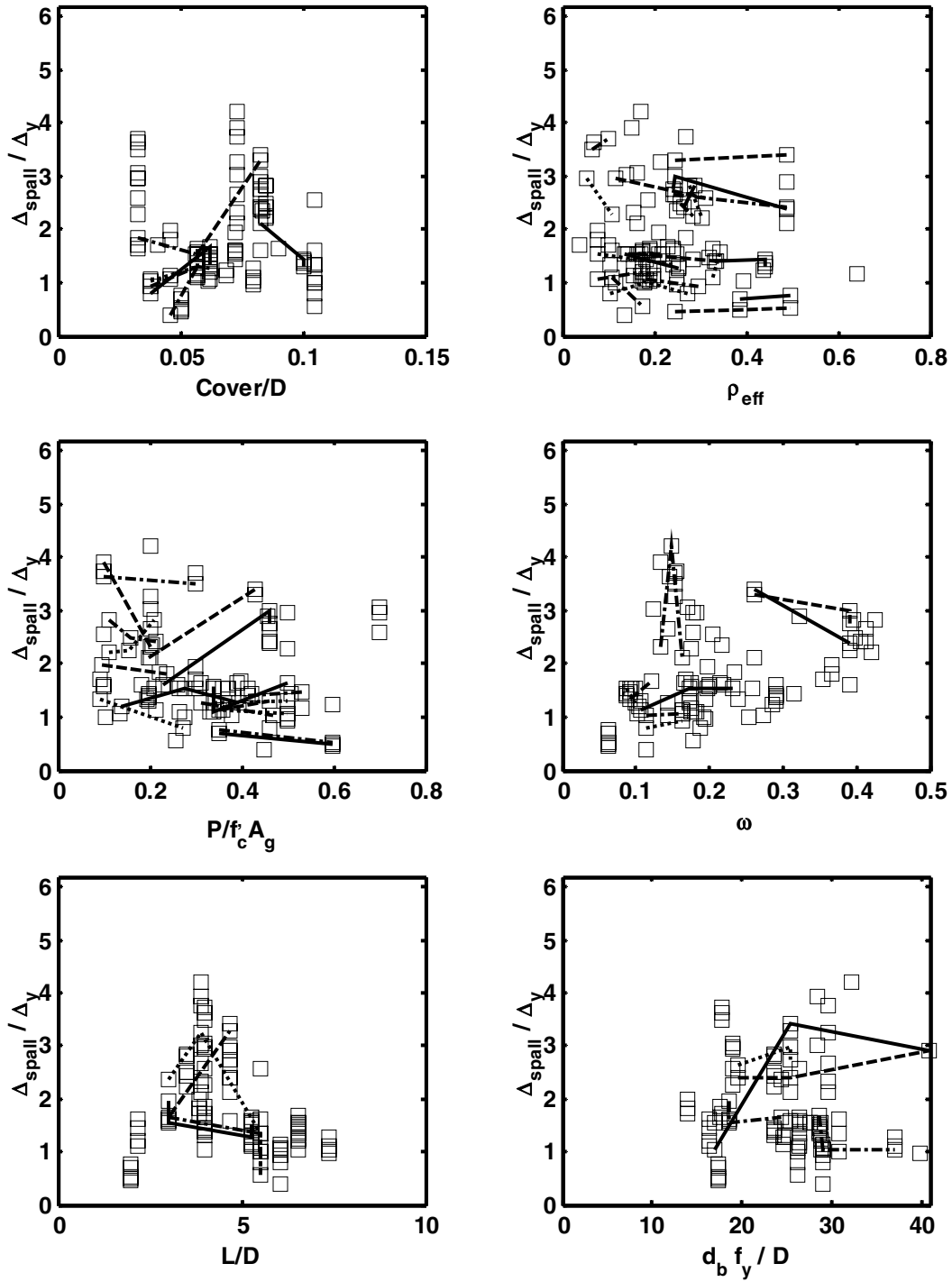
Figure 5.7 Trends in Displacement Ductility at Cover Spalling, Rectangular Columns

60
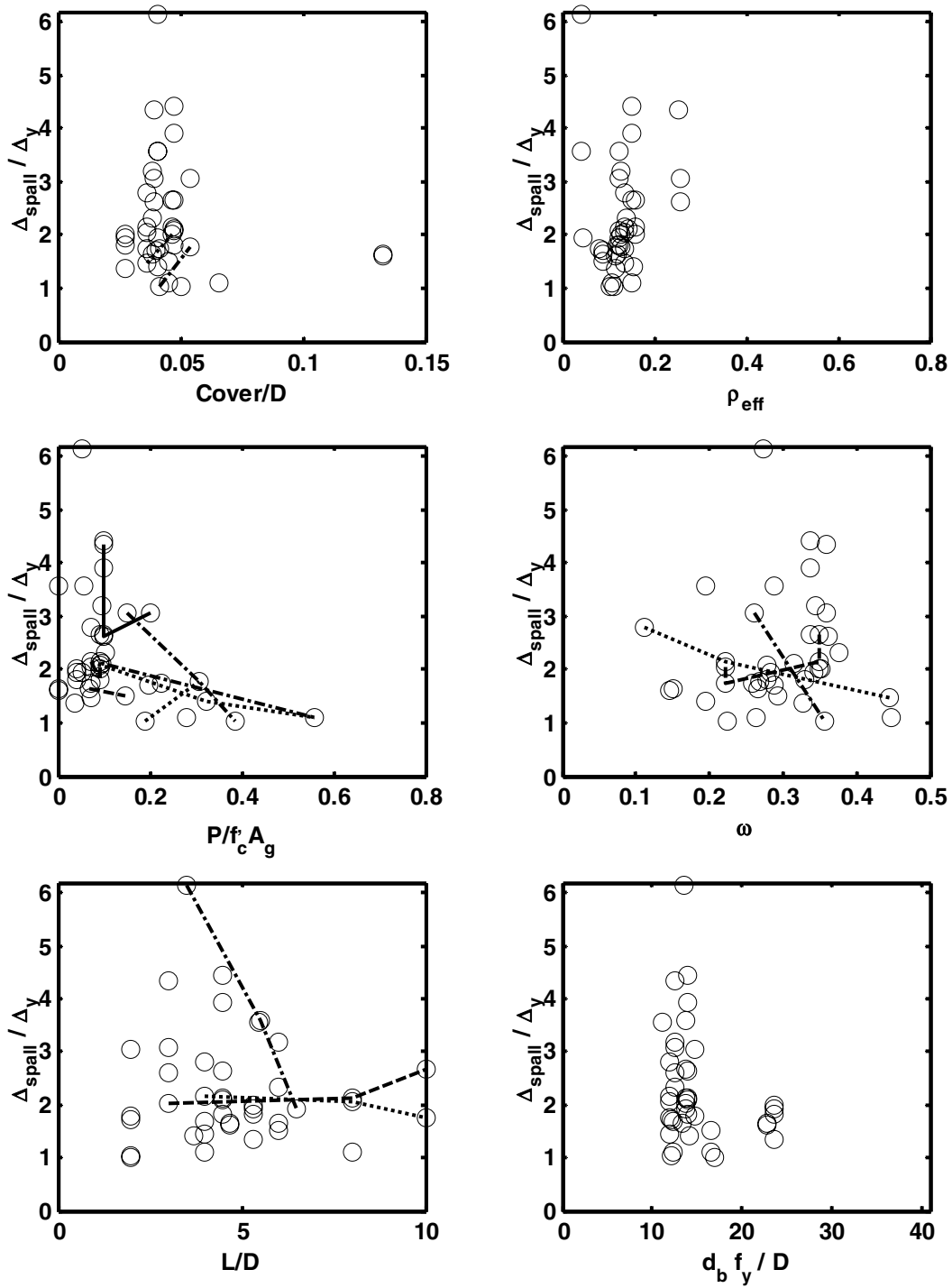
Figure 5.8 Trends in Displacement Ductility at Cover Spalling, Spiral-Reinforced Columns

61

Again, few trends can be observed in the column data. The trends that can be observed in Figures 5.7 and 5.8 are discussed below.

- The displacement ductility at the onset of cover spalling increases with an increase in normalized clear cover for five of eight rectangular families and both of the spiral families.

- The expected influence of axial load ratio on displacement ductility (a decrease in displacement ductility with an increase in axial load ratio) is not clear in the rectangular data. However, the trend is observed in the spiral data (four of six spiral families and the overall trend).

Table 5.4 summarizes the expected and observed influences of key column characteristics on the displacement ductility at the onset of bar buckling.

Table 5.4 Influence of Key Column Properties on Displacement Ductility at Cover Spalling

	Cover/D	r_{eff}	P/Agfc	w	L/D	$d_b f_y/D$
Expected	—	—	↓	↓ (Low Axial)	↑	↑
Observed (Rectangular)	↑	—	—	—	—	—
Observed (Spiral)	↑	—	↓	—	—	—

5.5   SUMMARY

The modeling strategy proposed in Chapter 6 is based on the theoretically expected trends in deformation measures at the onset of particular damage states. This chapter has studied the influences of key column properties on the compressive strain, plastic rotation, drift ratio, and displacement ductility at the onset of cover spalling. Table 5.5 summarizes the results of this study of cover spalling. The following can be concluded from this study:

- Few trends can be observed in the column deformations at the onset of cover spalling, and there was significant scatter in the cover spalling deformations.

- Plastic rotation is a poor measure of the deformation at cover spalling, because cover spalling often occurs at a displacement less than or near to the yield displacement.

- As expected, the drift ratio at the onset of cover spalling decreases with an increase in axial load ratio, $\dfrac{P}{A_g f_c'}$, and increases with an increase in aspect ratio, L/D.

- In addition, each deformation measure at the onset of cover spalling slightly increased with an increase in normalized clear cover.

Table 5.5 Influence of Key Column Properties on Deformation Measures at Spalling

		Cover/D	r_{eff}	P/Agfc	w	L/D	$d_b f_y$/D
ε_{spall}	Expected	—	—	—	—	—	—
	Observed (Rectangular)	↑	—	—	—	—	—
	Observed (Spiral)	↑	—	↓	—	—	—
θ_{p_spall}	Expected	—	—	↓	↓ (Low Axial)	↑	↑
	Observed (Rectangular)	↑	—	↓	—	—	—
	Observed (Spiral)	↑	—	↓	—	—	—
$\dfrac{\Delta_{spall}}{L}$	Expected	—	—	↓	↓ (Low Axial)	↑	↑
	Observed (Rectangular)	↑	—	↓	—	↑	—
	Observed (Spiral)	↑	—	↓	—	↑	—
$\dfrac{\Delta_{spall}}{\Delta_y}$	Expected	—	—	↓	↓ (Low Axial)	↑	↑
	Observed (Rectangular)	↑	—	—	—	—	—
	Observed (Spiral)	↑	—	↓	—	—	—

6 Regression Analysis

In order to implement performance-based earthquake engineering in reinforced concrete structures, it is necessary to quantitatively predict the deformations in reinforced concrete members at the onset of particular damage states. The focus of this chapter is to develop equations that predict the deformations at the onset of longitudinal bar buckling and concrete cover spalling in reinforced concrete columns as functions of key column properties.

In this chapter, a general form of equation is chosen to estimate the deformations at the onset of the damage states. A regression analysis is performed using this general equation and the UW-PEER database. Then, the results of this analysis are reviewed and the accuracies of the proposed models are assessed.

6.1 PROCEDURE

6.1.1 Regression Equations

A general equation was chosen to estimate the deformations at the onset of bar buckling and concrete spalling as functions of key column properties. The general form of the regression equations for one, two, and three column properties are as follows:

$$DD = A\left(1 + B\, prop1^{C}\right) \tag{Eq. 6.1}$$

$$DD = A\left(1 + B\, prop1^{C}\right)\left(1 + D\, prop2^{E}\right) \tag{Eq. 6.2}$$

$$DD = A\left(1 + B\, prop1^{C}\right)\left(1 + D\, prop2^{E}\right)\left(1 + F\, prop3^{G}\right) \tag{Eq. 6.3}$$

where DD is the deformation measure at the onset of bar buckling or concrete spalling, $A\text{-}G$ are all unknown constants, and *prop1-3* are the key column properties being studied.

The general regression equations are similar to the deformation measure equations based on plastic-hinge analysis developed in Chapter 3. For example, Equation 6.3 is similar to Equation 3.18. It should be noted that the equations based on plastic-hinge analysis (e.g., Eq.

3.18) were used in a pilot regression analysis, and it was determined that the increase in complexity did not entail a significant increase in accuracy.

6.1.2 Model Calibration

The UW-PEER database was used to calibrate Equations 6.1, 6.2, and 6.3 to estimate the deformations at the onset of bar buckling and concrete spalling. The values of the unknown constants (*A-G*) were determined such that (1) the mean value of the ratios of the measured damage displacement (from the column database) to the calculated damage displacement was equal to 1.0, and (2) the coefficient of variation (COV) of the ratios was minimized.

The calculated damage displacement in this procedure refers to the tip displacement associated with a particular deformation measure calculated with Equations 6.1, 6.2, and 6.3. For example, if the regression equations are used to estimate ε_{damage}, the calculated damage displacement would be computed by substituting in the curvature (from moment-curvature analysis) corresponding to the calculated strain into Equation 3.4.

The MATLAB function, *fmincon*, was used to perform the constrained nonlinear optimization. The function *fmincon* finds the constrained minimum of a scalar function of several variables starting at an initial estimate by using the sequential quadratic programming (SQP) method (MATLAB 2000).

6.1.3 Regression Analysis

A comprehensive study was performed using the general, nonlinear regression equations described above and the key column properties identified in Chapters 4 (for bar buckling) and 5 (for spalling).

For both damage states and each deformation measure (ε_{damage}, θ_{p_damage} , $\dfrac{\Delta_{damage}}{L}$,

$\dfrac{\Delta_{damage}}{\Delta_y}$), Equation 6.1 was calibrated as a function of each key column property. Then, Equation 6.2 was calibrated for every combination of two column properties. Finally, Equation 6.3 was calibrated for every combination of three column properties.

The resulting equations are presented and evaluated in the following sections.

6.2   LONGITUDINAL BAR BUCKLING

The expected and observed influences of the following key column properties on the deformations at the onset of bar buckling were studied in Chapter 4. In this chapter, equations are developed to estimate the maximum compressive strain, plastic rotation, drift ratio, and displacement ductility at the onset of bar buckling as functions of these key column properties. Regression analyses (as described in Section 1.1.3) were performed using the following key column properties:

$$S/d_b, \quad \rho_{eff} = \rho_s \frac{f_{ys}}{f'_c}, \quad \frac{P}{A_g f'_c}, \quad \omega = \rho_l \frac{f_y}{f'_c}, \quad \frac{L}{D}, \quad \frac{d_b f_y}{D}$$

where S is the tie spacing, d_b is the diameter of the longitudinal reinforcing bar, ρ_s is the volumetric transverse reinforcement ratio, f_{ys} is the yield stress of the transverse reinforcement, f'_c is the concrete compressive strength, P is the axial load, A_g is the gross area of the cross section, ρ_l is the longitudinal reinforcement ratio, f_y is the yield stress of the longitudinal reinforcement, and L and D are the column length and depth, respectively.

For each deformation measure, the most accurate equations developed in this analysis are provided in tabular form in Appendix C. In these tables, the four equations that yield the lowest COVs of $\dfrac{\Delta_{bb}}{\Delta_{calc}}$ are listed in ascending order for one, two, and three column properties.

In the following sections, the results of these analyses are presented for maximum nominal strain, plastic rotation, drift ratio, and displacement ductility at the onset of bar buckling. The effectiveness of the models is evaluated by comparing the resulting COVs of $\dfrac{\Delta_{bb}}{\Delta_{calc}}$ to the COVs

of $\dfrac{\Delta_{bb}}{\Delta_{mean\_DD}}$ (Δ_{mean_DD} is the tip displacement associated with the mean value of the deformation measure being studied).

6.2.1 *Critical Compressive Strain*

Table 6.1 summarizes the statistics of the critical nominal buckling strains (calculated with the procedure described in Section 2.3, and the plastic-hinge model proposed by Priestley et al. 1996) from the column database.

Table 6.1 Statistics of Buckling Strain

	Statistics	Rectangular	Spiral
e_{bb}	n	62	42
	min	0.0018	0.0107
	max	0.0275	0.0546
	mean	0.0144	0.0253
	COV	0.3415	0.3799
D_{BB}/D_{mean_e}	min	0.3158	0.4924
	max	1.6883	1.7727
	mean	1.0574	0.9884
	COV	0.2668	0.2862

The mean value of the nominal buckling strains for the rectangular columns was 0.0144, whereas the mean value in the spiral columns was significantly higher at 0.0253. The coefficients of variation of the rectangular and spiral strains were 34% and 38%, respectively.

$\dfrac{\Delta_{bb}}{\Delta_{mean\_\varepsilon}}$ is the ratio of the observed displacement (from the column database) to the displacement associated with the mean strain (this displacement is calculated by finding the curvature associated with the mean strain and substituting this curvature into Eq. 3.4). The mean value of $\dfrac{\Delta_{bb}}{\Delta_{mean\_\varepsilon}}$ was 1.06 for rectangular columns and 0.99 for spiral-reinforced columns. The COVs for rectangular and spiral columns were 27% and 29% respectively.

The equations that were developed to estimate the buckling strains (as a result of the regression analysis) will now be discussed. The following can be observed in Tables C.1 to C.6:

- Little accuracy was gained by including the influences of key column properties in the estimation of buckling strain in rectangular reinforced columns. For example, when the mean buckling strain in the rectangular data (0.0144) was used to calculate the displacement at the onset of bar buckling, the resulting COV of $\dfrac{\Delta_{bb}}{\Delta_{mean\_\varepsilon}}$ was 27%. In

68

comparison, the COV of $\dfrac{\Delta_{bb}}{\Delta_{calc}}$ only improved to 26% when three column properties were used in the estimation.

- When two column properties (L/D and ρ_{eff}, or L/D and S/db) were used in the estimation of the buckling strain in spiral-reinforced columns, the COVs of $\dfrac{\Delta_{bb}}{\Delta_{calc}}$ reduced from 29% (using the mean strain, 0.025) to approximately 20%. The influences of the effective confinement ratio and S/db on the critical spalling strain predicted with the above equations are consistent with our study in Chapter 4. However, L/D was not expected to influence the buckling strain. This influence of L/D could be a result of the plastic-hinge model used in the calculation of the buckling strains (Chapter 2). Little is gained by including a third property in the estimation.

6.2.2 Plastic Rotation

The statistics of the observed plastic rotations (calculated with procedure in Section 2.3 and the plastic-hinge model proposed by Priestley et al. 1996) at the onset of bar buckling are summarized in Table 6.2.

Table 6.2 Statistics of Plastic Rotation at Bar Buckling

	Statistics	Rectangular	Spiral
θ_{p_bb}	n	62	42
	min	0.0098	0.0206
	max	0.1072	0.1343
	mean	0.046	0.0597
	COV	0.422	0.4423
$D_{spall}/D_{mean\_q\,p}$	min	0.3834	0.3898
	max	1.9828	1.9822
	mean	1.0581	0.9967
	COV	0.3231	0.3616

The mean value of the plastic rotations at the onset of bar buckling was 0.046 for the rectangular columns and 0.06 for the spiral-reinforced columns. The COVs of the plastic rotations were 42% and 44% for the rectangular and spiral-reinforced columns, respectively.

The ratios of the measured displacements to the displacements associated with the mean plastic rotations ($\dfrac{\Delta_{bb}}{\Delta_{mean\_\theta p}}$) had a mean value of 1.06 for rectangular columns with a COV of 32%. The ratios had a mean value of 1.0 for spiral-reinforced columns with a COV of 36%.

The equations that were developed to estimate the plastic rotation at the onset of bar buckling will now be discussed. The following can be observed in Tables C.7 – C.12.

- By including three column properties ($d_b f_y/D$, ρ_{eff}, $P/A_g f_c'$) in the estimation of plastic rotation at the onset of bar buckling in rectangular columns, the COV of $\dfrac{\Delta_{bb}}{\Delta_{calc}}$ was improved from 32% (using the mean value of the plastic rotation) to 24%. The influences of $d_b f_y/D$, ρ_{eff}, and $P/A_g f_c'$ predicted with the regression equations are consistent with Chapter 4 (i.e., plastic rotation at the onset of bar buckling increases with an increase in $d_b f_y/D$ and ρ_{eff}, and decreases with an increase in $P/A_g f_c'$).

- When three column properties were used in the estimation of the plastic rotation at the onset of bar buckling in spiral columns, a significant improvement in the COV of $\dfrac{\Delta_{bb}}{\Delta_{calc}}$ was obtained. The COV of $\dfrac{\Delta_{bb}}{\Delta_{calc}}$ was reduced from 36% (using the mean value of the plastic rotation) to 20% using three column properties (L/D, ρ_{eff}, $P/A_g f_c'$). Again, the trends predicted by this regression equation are consistent with those expected in Chapter 4.

6.2.3   Drift Ratio

The following table summarizes the statistics of the drift ratios at the onset of bar buckling for the rectangular and spiral-reinforced columns in the database.

Table 6.3 Statistics of Drift Ratio at Bar Buckling

	Statistics	Rectangular	Spiral
D_{bb}/L (%)	n	62	42
	min	1.8079	2.2687
	max	9.252	14.5833
	mean	5.3421	6.5509
	COV	0.3328	0.4289
D_{BB}/D_{mean_DR}	min	0.3384	0.3463
	max	1.7319	2.2262
	mean	1.00	1.00
	COV	0.3328	0.4205

The mean values of $\dfrac{\Delta_{bb}}{L}$ are 5.34% and 6.55% for rectangular and spiral columns, respectively. The COV of $\dfrac{\Delta_{bb}}{L}$ was 33% for rectangular columns and 42% for spiral columns.

Mean values of $\dfrac{\Delta_{bb}}{\Delta_{mean\_DR}}$ were 1.0 for both spiral and rectangular columns, and the COVs of

$\dfrac{\Delta_{bb}}{\Delta_{mean\_DR}}$ were the same as for $\dfrac{\Delta_{bb}}{L}$.

The results of the regression analysis will now be discussed. The equations that estimate the drift ratio at the onset of bar buckling as functions of 1, 2, and 3 column properties are provided in Tables C.13 – C.18.

- By including three column properties (ρ_{eff}, $P/A_g f'_c$, and $d_b f_y/D$) in the estimation of the drift ratio at the onset of bar buckling in rectangular columns, a 25% COV of $\dfrac{\Delta_{bb}}{\Delta_{calc}}$ was obtained. This is a significant improvement over the 33% COV of $\dfrac{\Delta_{bb}}{\Delta_{mean}}$. The influences of the column properties, predicted with this regression equation, are consistent with Chapter 4. It should be noted that similar results were obtained if S/db and ω are used in place of $d_b f_y/D$.

- When three column properties (L/D, ρ_{eff}, and $P/A_g f'_c$) were used in the estimation of the drift ratio at the onset of bar buckling in spiral-reinforced columns, the resulting COV of $\dfrac{\Delta_{bb}}{\Delta_{calc}}$ was 23%. This COV is significantly smaller than the COV of $\dfrac{\Delta_{bb}}{\Delta_{mean\_DR}}$ (42%).

A similar COV was obtained by using S/db in place of ρ_{eff} (COV = 23.8%). The effects

of L/D, ρ_{eff}, S/db, and $P/A_g f_c'$ on $\dfrac{\Delta_{bb}}{L}$ predicted with the regression equations

discussed above are all consistent with the expected trends in Chapter 4.

6.2.4 Displacement Ductility

The statistics of displacement ductility at the onset of bar buckling are summarized in   Table 6.4.

Table 6.4 Statistics of Displacement Ductility at Bar Buckling

	Statistics	Rectangular	Spiral
	n	62	42
	min	2.1227	3.7101
D_{bb}/D_y	max	10.4574	10.8679
	mean	5.8582	6.7026
	COV	0.3295	0.2547
	min	0.3623	0.5535
D_{BB}/D_{mean_m}	max	1.7851	1.6215
	mean	1	1
	COV	0.3295	0.2547

The mean value of $\dfrac{\Delta_{bb}}{\Delta_y}$ was 5.86 for rectangular columns with a COV of 33%. The

mean value was 6.70 for spiral-reinforced columns with a COV of 26%. The mean value of

$\dfrac{\Delta_{bb}}{\Delta_{mean\_\mu}}$ was 1.0 for both spiral and rectangular columns, and the COVs of $\dfrac{\Delta_{bb}}{\Delta_{mean\_\mu}}$ were the

same as for $\dfrac{\Delta_{bb}}{\Delta_y}$.

The equations developed in the regression analysis to estimate $\dfrac{\Delta_{calc}}{\Delta_y}$ are presented in

Tables C.18–C.24. The following can be observed in these tables.

- Little accuracy can be gained by including more than one column property in the estimation of displacement ductility at the onset of bar buckling for rectangular and spiral-reinforced columns. By including the influences of L/D or S/db in the estimate of $\dfrac{\Delta_{calc}}{\Delta_y}$ in rectangular columns, a COV of approximately 30% was obtained for $\dfrac{\Delta_{bb}}{\Delta_{calc}}$.

72

When S/db or ρ_{eff} was included in the estimate of $\dfrac{\Delta_{calc}}{\Delta_y}$ in spiral columns, a COV of

approximately 22% was obtained for $\dfrac{\Delta_{bb}}{\Delta_{calc}}$. Again the influences of these key column

properties are consistent with the trends expected in Chapter 4.

6.2.5 Summary

The results of the regression analysis are summarized in Table 6.5 for both spiral- and rectangular-reinforced columns.

Table 6.5 Summary of Regression Results for Bar Buckling

Deformation Demand	Column Type	Statistics of D_{BB}/D_{mean_DD}		# of Properties	Properties Used in Estimation of DD			Statistics of D_{BB}/D_{calc}	
		mean	CoV					mean	CoV
ε_{bb}	Rectangular	1.06	26.7%	0	Mean e_{bb}			1.06	26.7%
	Spiral	0.99	28.6%	2	L/D	r_{eff} S/d_b		1.00	~21.0%
θ_{p_bb}	Rectangular	1.06	32.3%	3	$d_b f_y/D$	r_{eff}	P/Agfc	1.00	24.4%
	Spiral	1.00	36.2%	3	L/D	r_{eff}	P/Agfc	1.00	20.1%
$\dfrac{\Delta_{bb}}{L}$	Rectangular	1.00	33.3%	3	$d_b f_y/D$ S/db w	r_{eff}	P/Agfc	1.00	~25%
	Spiral	1.00	42.1%	3	L/D	r_{eff} S/d_b	P/Agfc	1.00	~23%
$\dfrac{\Delta_{bb}}{\Delta_y}$	Rectangular	1.00	33.0%	1	L/D or S/db			1.00	~30%
	Spiral	1.00	25.5%	1	S/db or r_{eff}			1.00	~22%

6.3   COVER SPALLING

In Chapter 5, the influences of the following key column properties on the deformations at the onset of cover spalling were studied.

$$S/d_b, \quad \rho_{eff} = \rho_s \frac{f_{ys}}{f'_c}, \quad \frac{P}{A_g f'_c}, \quad \omega = \rho_l \frac{f_y}{f'_c}, \quad \frac{L}{D}, \quad \frac{d_b f_y}{D}$$

where *Cover* is the clear cover dimension.

These column properties were used in the regression analysis (described in Section 6.1) to develop equations to estimate the maximum compressive strain, plastic rotation, drift ratio and displacement ductility at the onset of cover spalling. These equations are provided, in table form, in Appendix D for rectangular- and spiral-reinforced columns.

The effectiveness of these equations to estimate the deformations at the onset of cover spalling are evaluated by comparing the COVs of $\dfrac{\Delta_{bb}}{\Delta_{calc}}$ to the COVs of $\dfrac{\Delta_{bb}}{\Delta_{mean\_DD}}$. In addition, the estimated influences of the key column properties on the deformations at the onset of cover spalling (predicted with the regression equations) are compared to the expected influences in Chapter 5.

6.3.1 Compressive Strain

Table 6.6 summarizes the statistics of the critical nominal spalling strains for the column from the database (calculated with the procedure described in Section 2.3 and the plastic-hinge model proposed by Priestley et al. 1996).

Table 6.6 Statistics of Critical Spalling Strain

	Statistics	Rectangular	Spiral
	n	102	40
	min	0.001	0.002
e_{spall}	max	0.010	0.016
	mean	0.005	0.008
	COV	0.551	0.563
	min	0.250	0.501
D_{spall}/D_{mean_e}	max	1.891	1.820
	mean	0.984	1.009
	COV	0.418	0.381

The mean strain values at the onset of cover spalling were 0.005 for rectangular columns and 0.008 for the spiral-reinforced columns. The COV of the rectangular strains was 55% for the rectangular columns and 56% for the spiral-reinforced columns.

The mean value of $\dfrac{\Delta_{spall}}{\Delta_{mean\_\varepsilon}}$ (where, $\Delta_{mean\_\varepsilon}$, is the calculated tip displacement associated with the mean strain value) is 0.98 for rectangular columns and 1.01 for spiral-reinforced columns. The COV of this ratio is 42% for rectangular columns and 38% for spiral-reinforced columns.

74

The four best regression equations that estimate the critical spalling strain as functions 1, 2, and 3 column properties are provided in Tables D.1–D.6. The following can be observed in these tables.

- When the mean strain was used to estimate the displacement at the onset of spalling, the COV of the ratios of measured to calculated displacement was 42% for rectangular columns. By including the influences of two column properties in the estimation of critical spalling strain (L/D and ω), a COV of 36% was obtained for $\dfrac{\Delta_{spall}}{\Delta_{calc}}$. L/D and ω were not expected to influence the maximum compressive strain at concrete spalling (Chapter 5).

- The COV of $\dfrac{\Delta_{spall}}{\Delta_{mean\_\varepsilon}}$ was 38% for spiral-reinforced columns. When two column properties (ω and $\dfrac{d_b f_y}{D}$) were used in the estimation of critical spalling strain, the COV of $\dfrac{\Delta_{spall}}{\Delta_{calc}}$ was reduced to 31%. Again, the influences of ω and $\dfrac{d_b f_y}{D}$ were not expected (Chapter 5).

6.3.2   Plastic Rotation

Table 6.7 summarizes the statistics of the plastic rotations at the onset of spalling for columns from the database (calculated with the procedure described in Chapter 2.3 and by using the plastic-hinge model proposed by Priestley et al. 1996).

Table 6.7 Statistics of Plastic Rotation at Spalling

	Statistics	Rectangular	Spiral
θ_{p_spall}	n	102	40
	min	0.000	0.000
	max	0.025	0.030
	mean	0.007	0.013
	COV	0.929	0.650
$D_{spall}/D_{mean\_q\,p}$	min	0.146	0.344
	max	2.155	1.833
	mean	0.988	1.003
	COV	0.448	0.391

The mean value of the nominal plastic rotations at the onset of spalling was 0.007 for rectangular columns and 0.013 for rectangular columns. The COVs of the plastic rotations were 93% and 65% for the rectangular and spiral-reinforced columns, respectively.

The mean value of $\dfrac{\Delta_{spall}}{\Delta_{mean\_\vartheta p}}$ was 0.98 for the rectangular columns and 1.00 for the spiral columns. The COVs of this ratio were 49% and 39% for rectangular and spiral columns, respectively.

The equations developed in the regression analysis to estimate the plastic rotation at the onset of cover spalling are provided in Tables D.7 – D.12. The following can be observed in these tables.

- By including three column properties (L/D, $\dfrac{P}{A_g f_c'}$, and ω) in the estimation of the plastic rotation at the onset of concrete spalling in rectangular columns, a COV of 34% was obtained for $\dfrac{\Delta_{spall}}{\Delta_{calc}}$. This is significantly better than the COV obtained by using the mean value of the plastic rotation (45%). Similar results were obtained when ρ_{eff}, $\dfrac{d_b f_y}{D}$, or $\dfrac{Cover}{D}$ were used in the estimate instead of ω.

- When two column properties ($\dfrac{P}{A_g f_c'}$ and ω, or $\dfrac{P}{A_g f_c'}$ and $\dfrac{Cover}{D}$) were used in the estimation of the ϑ_{p_spall} in spiral-reinforced columns, a COV of ~30% was obtained for $\dfrac{\Delta_{spall}}{\Delta_{calc}}$. This is significantly better than the COV obtained by using the mean value of the

plastic rotation (39%). The effects of axial load and $\dfrac{Cover}{D}$ are consistent with Chapter 5

(i.e., plastic rotation increases with an increase in $\dfrac{Cover}{D}$ and decreases with an increase

in axial load). The expected influence of ω varies depending on axial load, so it is

difficult to tell if the trend predicted with the regression equation is consistent with the

expected trend.

6.3.3   Drift Ratio

Table 6.8 summarizes the statistics of the measured drift ratios at the onset of cover spalling for

the rectangular and spiral-reinforced columns in the database.

Table 6.8 Statistics of Drift Ratio at Spalling

	Statistics	Rectangular	Spiral
D_{spall}/L (%)	n	102	40
	min	0.133	0.609
	max	3.036	4.514
	mean	1.532	2.295
	COV	0.476	0.442
D_{spall}/D_{mean_DR}	min	0.087	0.266
	max	1.982	1.967
	mean	1.000	1.000
	COV	0.476	0.442

The mean value of the drift ratios at the onset of spalling was 1.53% for rectangular

columns and 2.30% for spiral-reinforced columns. The COV of $\dfrac{\Delta_{spall}}{\Delta_{mean}}$ was 48% for rectangular

columns and 44% for spiral-reinforced columns.

The equations that were developed in the regression analysis to estimate the drift ratio at

the onset of cover spalling as functions of 1, 2, and 3 column properties are provided in Tables

D.13–D.18. The following discussion summarizes key equations found in these tables.

- By including two column properties (L/D and $\dfrac{P}{A_g f_c'}$) in the estimation of the drift ratio at

  the onset of concrete spalling, the COV of $\dfrac{\Delta_{spall}}{\Delta_{calc}}$ was 36% for rectangular columns and

  32% for spiral-reinforced columns. These COVs are significantly better than the COVs

  obtained by using the mean value of the drift ratios (48% for rectangular and 44% for

spiral). The influences of L/D and $\dfrac{P}{A_g f_c'}$ on $\dfrac{\Delta_{spall}}{L}$ predicted with these equations, are

consistent with the trends expected as described in Chapter 5.

6.3.4   Displacement Ductility

The statistics of $\dfrac{\Delta_{spall}}{\Delta_y}$ are summarized in Table 6.9 for the rectangular and spiral-reinforced

columns in the database.

Table 6.9   Statistics of Displacement Ductility at Spalling

	Statistics	Rectangular	Spiral
D_{spall}/D_y	n	102	40
	min	0.391	1.021
	max	4.223	6.140
	mean	1.802	2.307
	COV	0.480	0.464
D_{spall}/D_{mean_m}	min	0.217	0.442
	max	2.344	2.661
	mean	1.000	1.000
	COV	0.480	0.464

The mean value of $\dfrac{\Delta_{spall}}{\Delta_y}$ was 1.80 for rectangular columns and 2.30 for spiral-reinforced

columns. The COV of $\dfrac{\Delta_{spall}}{\Delta_{mean\_D}}$ was 48% for rectangular columns and 46% for spiral-reinforced

columns.

The equations developed in the regression analysis to estimate $\dfrac{\Delta_{spall}}{\Delta_y}$ are provided in

Tables D.19 – D.24. The following can be observed in these tables.

- By including two column properties (L/D and ω) in the estimation of $\dfrac{\Delta_{spall}}{\Delta_y}$ for

  rectangular columns, a COV of 39% was obtained for $\dfrac{\Delta_{spall}}{\Delta_{calc}}$. This COV is significantly

  better than the COV of $\dfrac{\Delta_{spall}}{\Delta_{mean\_D}}$ (48%). The influence of L/D on $\dfrac{\Delta_{spall}}{\Delta_y}$, predicted with

  this regression equation, is consistent with the expected influence from Chapter 5.

78

- When two column properties ($\dfrac{d_b f_y}{D}$ and $\dfrac{P}{A_g f'_c}$) were used to estimate $\dfrac{\Delta_{spall}}{\Delta_y}$ for spiral columns, a COV of 36% was obtained for $\dfrac{\Delta_{spall}}{\Delta_{calc}}$. This COV was significantly better than the COV of $\dfrac{\Delta_{spall}}{\Delta_{mean\_D}}$ (46%). The influences of $\dfrac{d_b f_y}{D}$ and $\dfrac{P}{A_g f'_c}$ on $\dfrac{\Delta_{spall}}{\Delta_y}$, predicted with this regression equation, are consistent with the expected influences from Chapter 5.

6.3.5 Summary of Regression Analysis for Concrete Spalling

Table 6.10 summarizes the key findings of the regression analysis discussed in Sections 6.3.1–6.3.4.

Table 6.10 Summary of Regression Results for Cover Spalling

Deformation Demand	Column Type	Statistics of D_{BB}/D_{mean_DD}		# of Suggested Properties	Properties Used in Estimation of DD			Statistics of D_{BB}/D_{calc}	
		mean	CoV					mean	CoV
ε_{spall}	Rectangular	0.98	42.0%	2	L/D	w		1.06	35.6%
	Spiral	1.01	38.1%	2	dbfy/D	w		1.00	31.4%
θ_{p_spall}	Rectangular	0.99	44.8%	3	L/D	w r eff Cover/D dbfy/D	P/Agfc	1.00	34.0%
	Spiral	1.00	36.2%	2	w Cover/D	P/Agfc		1.00	~30%
$\dfrac{\Delta_{spall}}{L}$	Rectangular	1.00	47.6%	2	L/D	P/Agfc		1.00	35.6%
	Spiral	1.00	44.2%	2	L/D	P/Agfc		1.00	32.1%
$\dfrac{\Delta_{spall}}{\Delta_y}$	Rectangular	1.00	48.0%	2	L/D	w		1.00	39.1%
	Spiral	1.00	46.4%	2	dbfy/D	P/Agfc		1.00	36.3%

6.4   DISCUSSION

There is significant scatter in the ratios of $\dfrac{\Delta_{bb}}{\Delta_{calc}}$ and $\dfrac{\Delta_{spall}}{\Delta_{calc}}$ for all of the regression equations.

This scatter can be partially attributed to the following:

- Most researchers did not use an objective method to identify the onset of bar buckling and cover spalling. The identification of the damage states relied on the subjective opinion of the researcher.

- The columns in the database were deflected to discrete levels of deformation, as illustrated in Figure 6.1. This figure shows a typical force-displacement history for a column from the database. The point at which the onset of bar buckling occurred is shown in this figure as a dot, and the displacement at the onset of bar buckling is also shown. From this figure, the uncertainty and scatter attributed to the discrete deformations are evident. There is no way of knowing if the bar would have buckled if the column displacement had been 1.5 instead of 2.
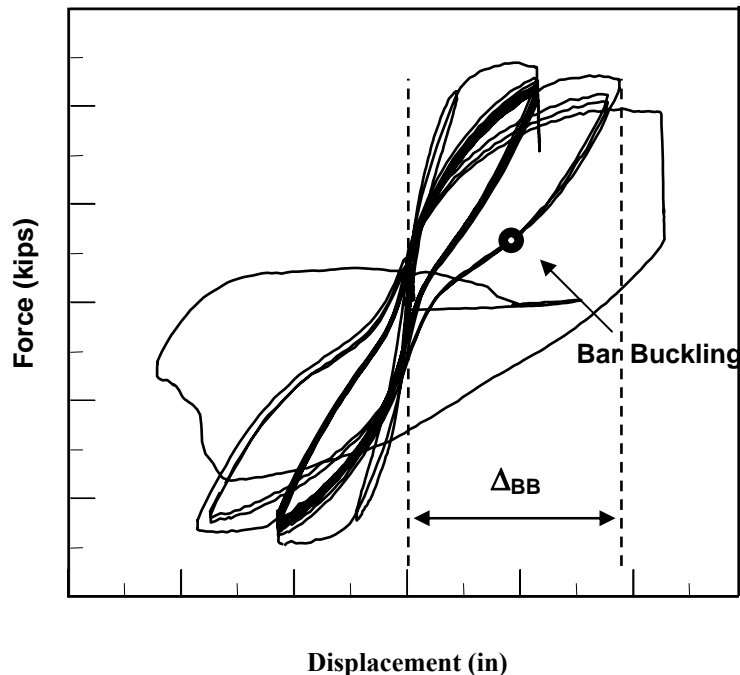
Figure 6.1 Discrete Displacements (Nelson 2000)

- Bar buckling and cover spalling are both complex phenomena, whereas the proposed modeling strategy is simple.

- The effects of cycling and cumulative deformation are ignored.

7 Design Recommendations

In order to implement performance-based earthquake engineering in reinforced concrete structures, it is necessary to quantitatively predict the deformations in reinforced concrete members at the onset of particular damage states. The focus of this chapter is to develop equations that predict the deformations at the onset of longitudinal bar buckling and concrete cover spalling in reinforced concrete columns as functions of key column properties.

In this chapter, two simple equations are proposed to estimate the displacements at the onset of bar buckling and concrete cover spalling in flexure-dominant, reinforced concrete columns. These equations are based on the results of the regression analyses and the discussions in Sections 6.2 and 6.3. The accuracy of these equations is assessed by comparing the measured damage displacements (from the database) with the calculated displacements. In addition, fragility curves are presented that will be helpful in design.

It can be seen in Tables 4.5 and 4.6 that the COVs of the ratios of measured displacements to calculated displacements are similar for all deformation measures. Therefore, for simplicity, the equations that estimate the drift ratios at the onset of bar buckling and concrete cover spalling will be recommended for design. The drift ratio equations are the simplest because no additional analysis is required to estimate the displacements at the onset of the damage states. For example, if the equations based on displacement ductility were used in the estimation, the designer would need to calculate the yield displacement. In addition, the form of the equation will be further simplified wherever possible.

7.1 PROPOSED BAR BUCKLING EQUATION

Based on the results of the regression analysis in Section 6.3, the following equation (Eq. 7.1) was developed to estimate the drift ratio at the onset of bar buckling in both rectangular and spiral-reinforced columns.

$$\frac{\Delta_{bb\_calc}}{L}(\%) \ = 3.25 \ (1 + k_e \rho_{eff}) \ (1 - \frac{P}{A_g \ f'_c}) \ (1 + \frac{L}{10 \ D}) \qquad \text{(Eq. 7.1)}$$

where k_e = 2.84 for rectangular columns and 4.6 for spiral-reinforced columns.

Using Equation 7.1, the COV of $\dfrac{\Delta_{bb}}{\Delta_{bb\_calc}}$ was 29% for the rectangular columns and

26% for the spiral-reinforced columns.

Equation 7.1 does not account for the properties of the longitudinal bars. To address this

issue, ρ_{eff} was multiplied by the normalized bar diameter $(\dfrac{d_b}{D})$. This modification was

performed because the influences of ρ_{eff} and $\dfrac{d_b}{D}$ on the drift ratio at the onset of bar buckling

are similar (drift ratio increases with an increase in ρ_{eff} and $\dfrac{d_b}{D}$). As a result, the transverse and

longitudinal reinforcement properties controlling the onset of bar buckling were captured by this

new parameter $(\rho_{eff} \dfrac{d_b}{D})$. If this new parameter is used, the resulting design equation is

$$\frac{\Delta_{bb\_calc}}{L}(\%) = 3.25 \ (1 + k_e \rho_{eff} \frac{d_b}{D}) \ (1 - \frac{P}{A_g f'_c}) \ (1 + \frac{L}{10 D}) \qquad \text{(Eq. 7.2)}$$

where k_e = 50 for rectangular columns and 150 for spiral-reinforced columns. The k_e values
differ because spiral reinforcement is more effective at confining the longitudinal reinforcement
than the ties found in the rectangular columns.

By using Equation 7.2 to estimate the displacement at the onset of bar buckling, the

resulting COV of $\dfrac{\Delta_{bb}}{\Delta_{bb\_calc}}$ was reduced from 29% (using Eq. 7.1) to 26% for rectangular

columns and from 26% (using Eq. 7.1) to 25% for spiral-reinforced columns. Table 6.1

summarizes the statistics of $\dfrac{\Delta_{bb}}{\Delta_{bb\_calc}}$ that were obtained by using Equation 7.2 and compares

them to the statistics obtained by using the mean value of the measured drift ratios (5.3% for
rectangular columns and 6.6% for spiral-reinforced columns).

Table 7.1 Statistics of $\dfrac{\Delta_{bb}}{\Delta_{bb\_calc}}$ for Design Equation

	Number of Tests	Statistics of D_{BB}/D_{mean_DR}				Statistics of D_{BB}/D_{calc}			
		min	max	mean	CoV	min	max	mean	CoV
Rectangular-Reinforced	62	0.34	1.73	1.00	33.3%	0.42	1.56	1.00	26.3%
Spiral-Reinforced	42	0.34	2.19	1.00	42.0%	0.47	1.50	0.97	24.6%

7.2   EVALUATION OF BAR BUCKLING EQUATION

To determine if the accuracy of the proposed buckling model varies with the key column properties, $\dfrac{\Delta_{bb}}{\Delta_{bb\_calc}}$ is plotted versus the key column properties controlling the onset of bar buckling in Figures 7.1 and 7.2. In these figures, the least-squares best fits are illustrated with dashed lines. The R^2 statistics of the linear fit are also shown in the figures. The R^2 statistic is a measure of the amount of response variability explained by the line (the larger the R^2 value, the larger the effect of the variable).

Figure 7.1 shows that the model accuracy for the rectangular columns did not vary systematically with any of the key column properties. In contrast, the accuracy of the proposed model varied with the aspect ratio (L/D) for the spiral-reinforced columns (Fig, 7.2). If the coefficient multiplying the aspect ratio in Equation 7.2 were increased, this trend could be eliminated, but a trend would then be created in the rectangular columns. To eliminate trends in both sets of columns, separate coefficients would have to be used for the aspect ratio term in Equation 7.2. For example, the aspect ratio was multiplied by 0.2 instead of 0.1 for the spiral columns, the resulting COV of $\dfrac{\Delta_{bb}}{\Delta_{bb\_calc}}$ was 22.6% compared to the 24.6% COV from (Eq. 7.2.

The slight increase in accuracy did not justify the complexity.
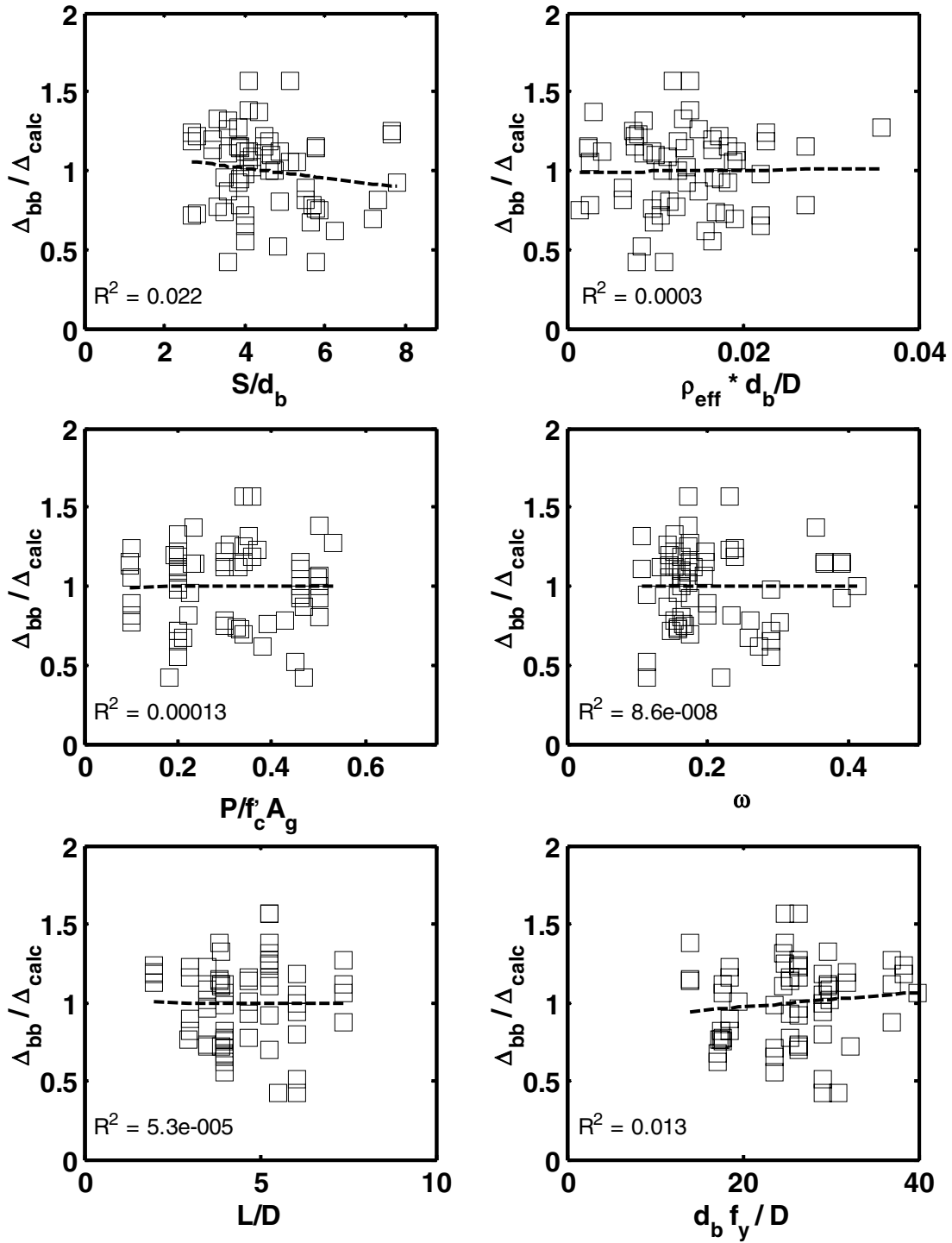
Figure 7.1 $\dfrac{\Delta_{bb}}{\Delta_{bb\_calc}}$ vs. Key Column Properties, Rectangular Columns
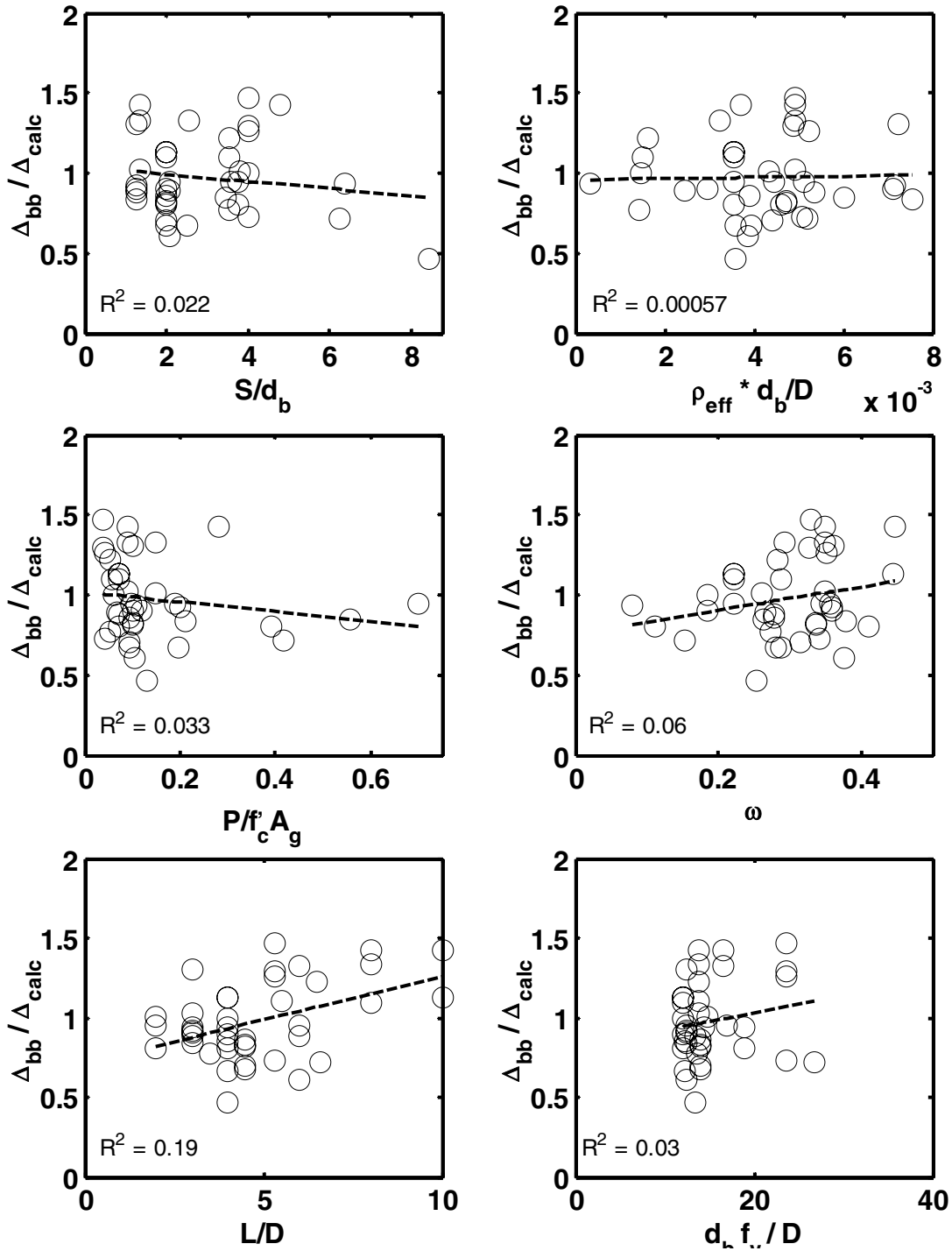
Figure 7.2 $\dfrac{\Delta_{bb}}{\Delta_{bb\_calc}}$ **vs. Key Column Properties, Spiral Columns**

7.3   FRAGILITY CURVES FOR BAR BUCKLING

In this section, fragility curves are presented that could be helpful in design and assessment. The fragility curves help a designer answer the following question:

For a particular level of column deformation, what is the likelihood that the
longitudinal reinforcement will have begun to buckle?

Figures 7.3 and 7.4 show the fragility curves for bar buckling in rectangular and spiral-reinforced columns. In these figures, the Y-axis is the cumulative probability of bar buckling, and the X-axis is the ratio of $\dfrac{\Delta_{bb}}{\Delta_{bb\_calc}}$. If the database is assumed to be representative of the entire population of rectangular and spiral-reinforced columns, this ratio can be interpreted as $\dfrac{\Delta_{demand}}{\Delta_{bb\_calc}}$. These plots also show the normal cumulative distribution functions (CDF) and the lognormal cumulative distribution functions.

The normal CDF fits the data better than the lognormal CDF. However, the lognormal distribution may be more applicable because the quantity of interest ($\dfrac{\Delta_{bb}}{\Delta_{bb\_calc}}$) must always be positive, since the natural log of $\dfrac{\Delta_{bb}}{\Delta_{bb\_calc}}$ exists only when $\dfrac{\Delta_{bb}}{\Delta_{bb\_calc}}$ is positive.   The normal CDF allows negative values of $\dfrac{\Delta_{bb}}{\Delta_{bb\_calc}}$ at low probabilities.

The procedure a designer would follow to use these curves is described below.

- A structural analysis would be performed on a structural system to determine the displacement demand for the columns.
- The displacement at the onset of bar buckling would be calculated with Equation 7.4.
- The probability that a longitudinal bar will have buckled at or before that displacement demand would then be read from the fragility curve.

For example, if it were determined that a rectangular column had a drift ratio demand of 6% , and Equation 7.2 predicted that bar buckling would occur at a drift ratio of 4%, the ratio of

$\dfrac{\Delta_{demand}}{\Delta_{bb\_calc}}$ would equal 1.5. Then, from Figure 7.3, there would be a 97% probability that bar

buckling would occur in that column at or below a drift ratio of 6%.
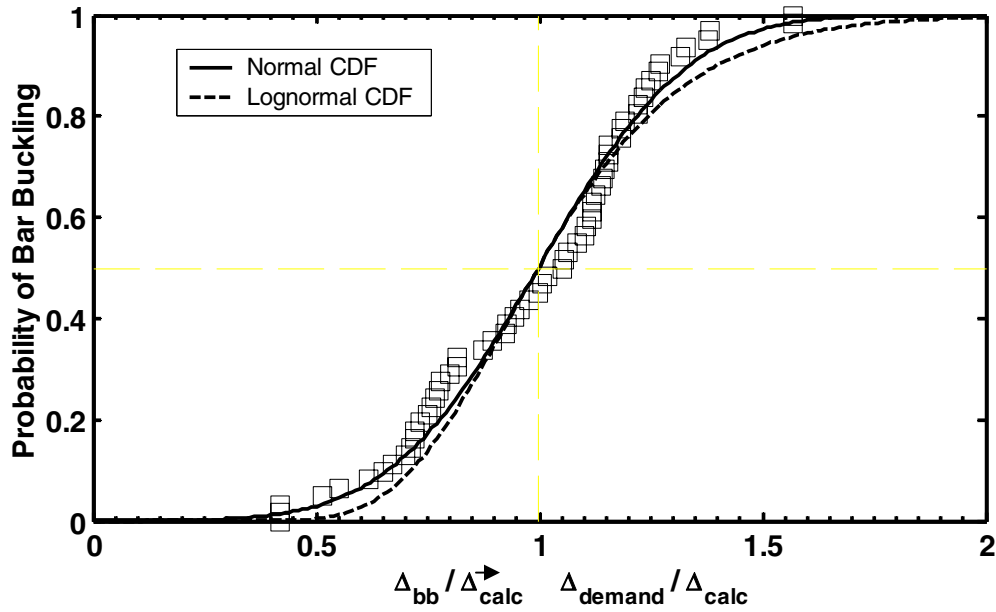
Figure 7.3 Fragility Curves for Bar Buckling, Rectangular Columns
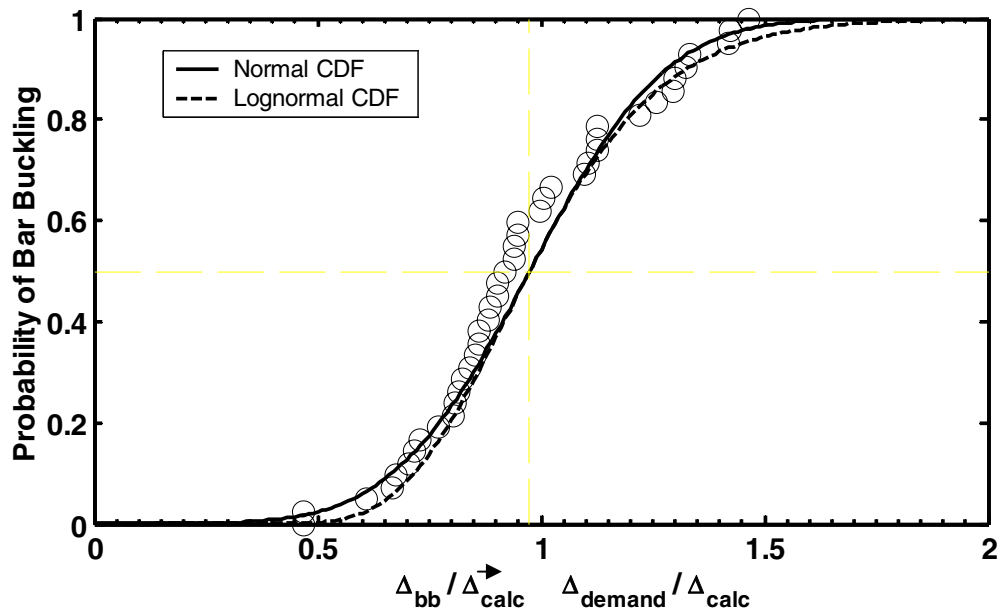
Figure 7.4 Fragility Curves for Bar Buckling, Spiral-Reinforced Columns

7.4 PROPOSED COVER SPALLING EQUATION

A simple equation was developed to estimate the drift ratio at the onset of cover spalling based on the results of Section 6.4. The proposed equation is as follows:

$$\frac{\Delta_{spall\_calc}}{L}(\%) \cong 1.6\,(1 - \frac{P}{A_g f'_c})\,(1 + \frac{L}{10D})$$ (Eq. 7.3)

By using this equation to estimate the drift ratios at the onset of bar buckling, the COV of $\frac{\Delta_{spall}}{\Delta_{spall\_calc}}$ was 43% for rectangular columns and 35% for spiral-reinforced columns.

The following table summarizes the statistics of $\frac{\Delta_{spall}}{\Delta_{spall\_calc}}$ obtained using Equation 7.3 and compares them to the statistics obtained using the mean value of the measured drift ratios (1.5% for rectangular columns and 2.3% for spiral-reinforced columns).

Table 7.2 Statistics of $\dfrac{\Delta_{spall}}{\Delta_{spall\_calc}}$ **for Design Equation**

	Number of Tests	Statistics of D_{spall}/D_{mean_DR}				Statistics of D_{spall}/D_{calc}			
		min	max	mean	CoV	min	max	mean	CoV
Rectangular-Reinforced	102	0.09	1.98	1.00	47.6%	0.17	1.93	0.97	43.3%
Spiral-Reinforced	62	0.27	1.97	1.00	44.2%	0.48	1.93	1.07	35.2%

7.5 EVALUATION OF COVER SPALLING EQUATION

In Figures 7.5 and 7.6, $\frac{\Delta_{spall}}{\Delta_{spall\_calc}}$ is plotted versus key column properties in order to determine if the accuracy of Equation 7.3 varies with key column properties. Provided in these figures are the R^2 statistics, which are measures of how much scatter is accounted for with the linear approximations.

From Figures 7.5 and 7.6, it can be observed that $\dfrac{\Delta_{spall}}{\Delta_{spall\_calc}}$ appears to increase with an increase in ω for both rectangular and spiral-reinforced columns. It should be noted that this trend may be present, because there are only a few columns with $\omega > 0.15$ or $\omega > 0.3$. If this trend is true, it is unclear why ω affects the drift ratio at the onset of concrete spalling in this manner.

Also, it can be observed that $\dfrac{\Delta_{spall}}{\Delta_{spall\_calc}}$ for the spiral-reinforced columns decreases with an increase in $\dfrac{P}{A_g f_c'}$ and increases slightly with an increase in $\dfrac{L}{D}$. These trends could be removed by adjusting the coefficients in Equation 7.5, but adjusting the coefficients would cause the opposite trends to show up in the rectangular data and cause more scatter in the rectangular data. To address this issue, two separate equations would be needed to estimate $\dfrac{\Delta_{spall}}{L}$.
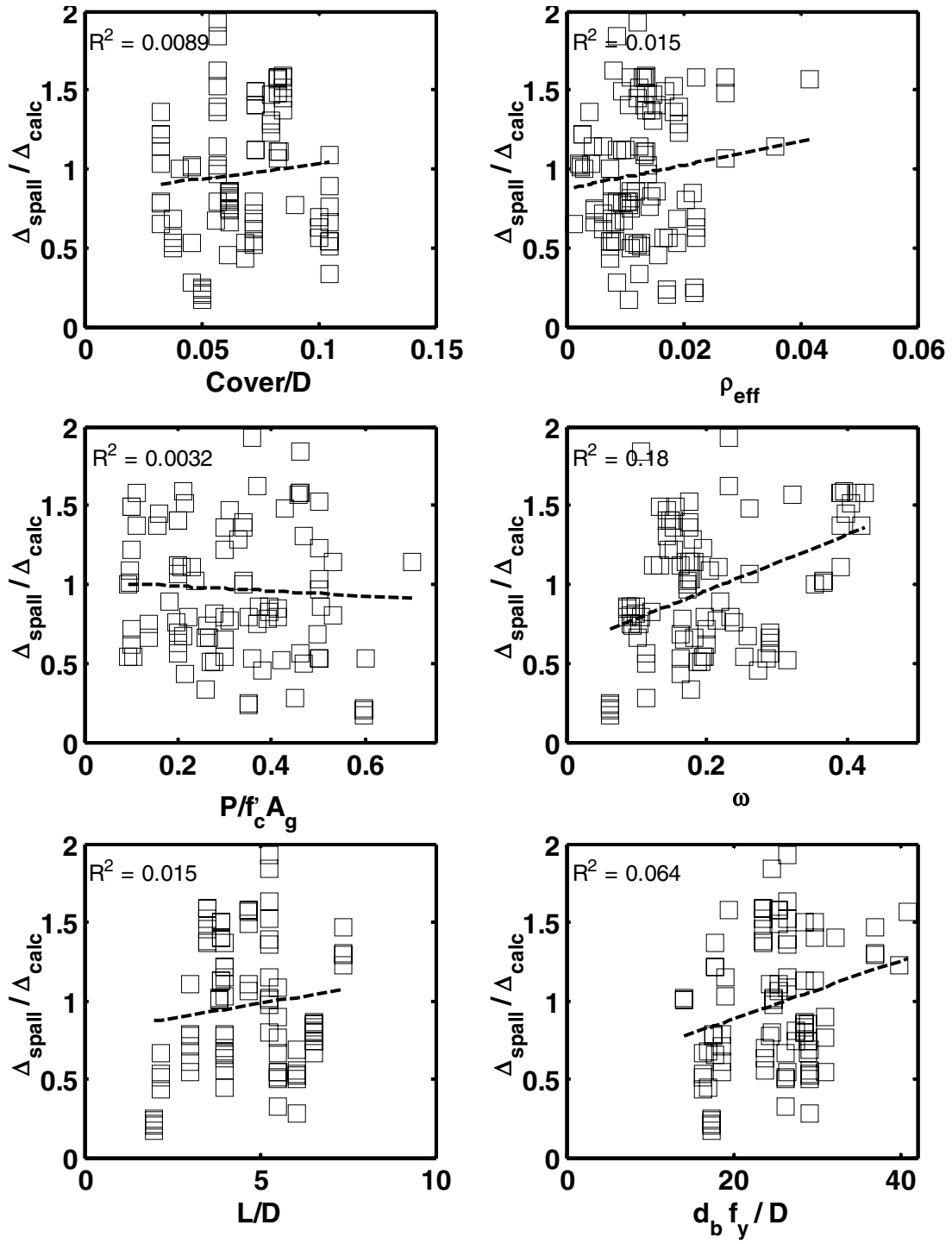
Figure 7.5 $\dfrac{\Delta_{spall}}{\Delta_{spall\_calc}}$ **vs. Key Column Properties, Rectangular Columns**
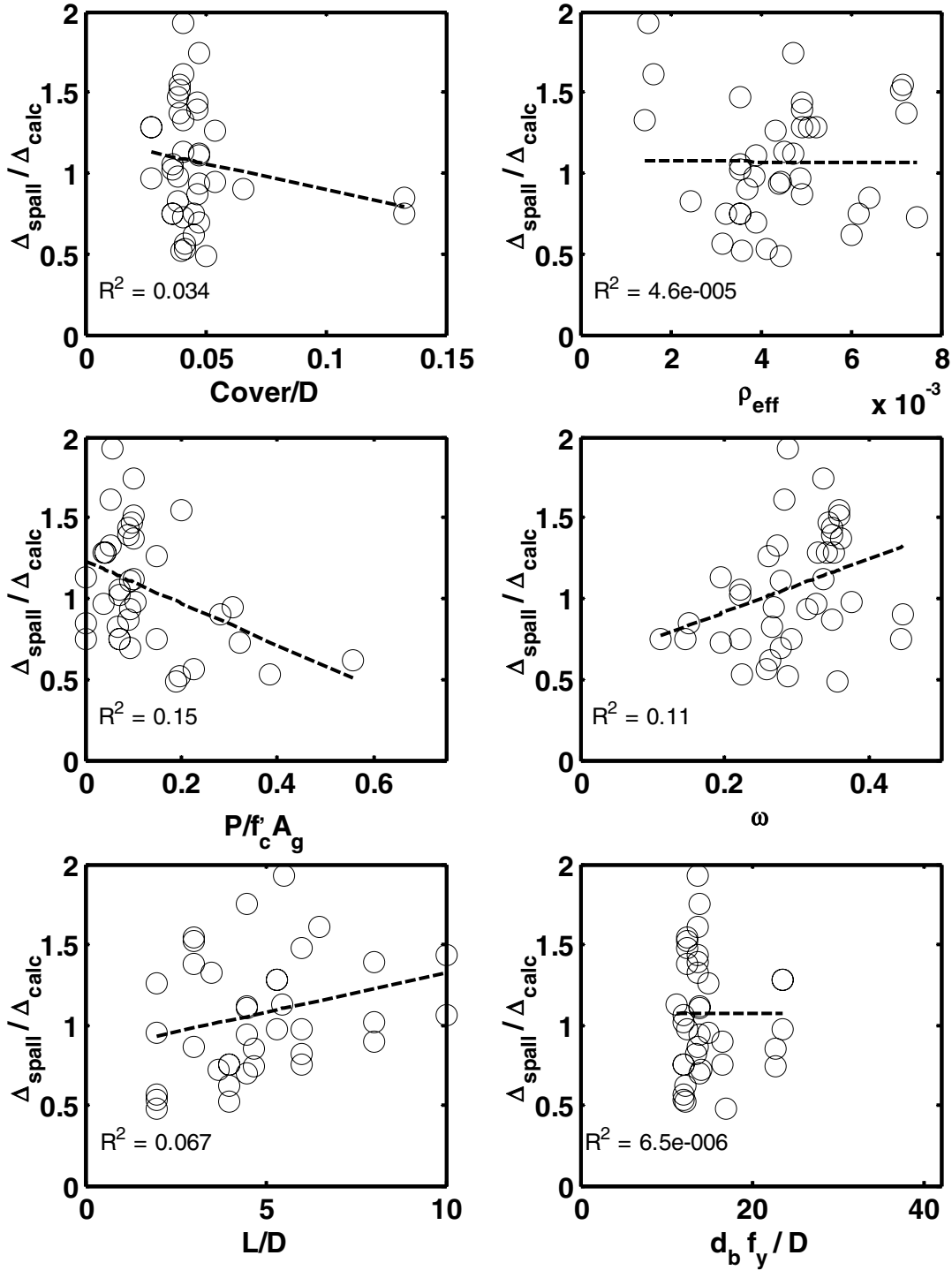
Figure 7.6 $\dfrac{\Delta_{spall}}{\Delta_{spall\_calc}}$ **vs. Key Column Properties, Spiral Columns**

93

7.6   FRAGILITY CURVES FOR COVER SPALLING

The fragility curves shown in Figures 7.7 and 7.8 could be used by a designer to determine the probability that concrete cover spalling will occur in a reinforced concrete column at a given displacement demand. In these figures, the Y-axis is the cumulative probability of cover spalling, and the X-axis is the ratio of $\dfrac{\Delta_{spall}}{\Delta_{spall\_calc}}$. If the database is assumed to be representative of the entire population of rectangular and spiral-reinforced columns, this ratio can be interpreted as $\dfrac{\Delta_{demand}}{\Delta_{spall\_calc}}$. Included in these plots are the normal cumulative distribution functions (CDF) and the lognormal cumulative distribution functions.

The normal CDF fits the data better than the lognormal CDF. However, the normal CDF allows negative values of $\dfrac{\Delta_{spall}}{\Delta_{spall\_calc}}$ at low probabilities.
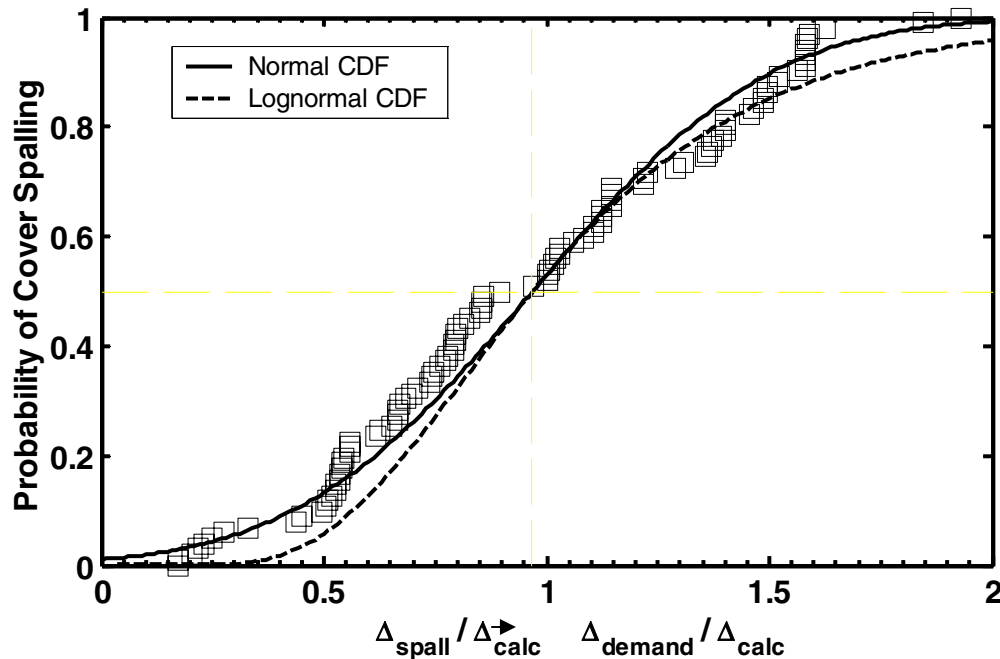
Figure 7.7 Fragility Curves for Cover Spalling, Rectangular Columns
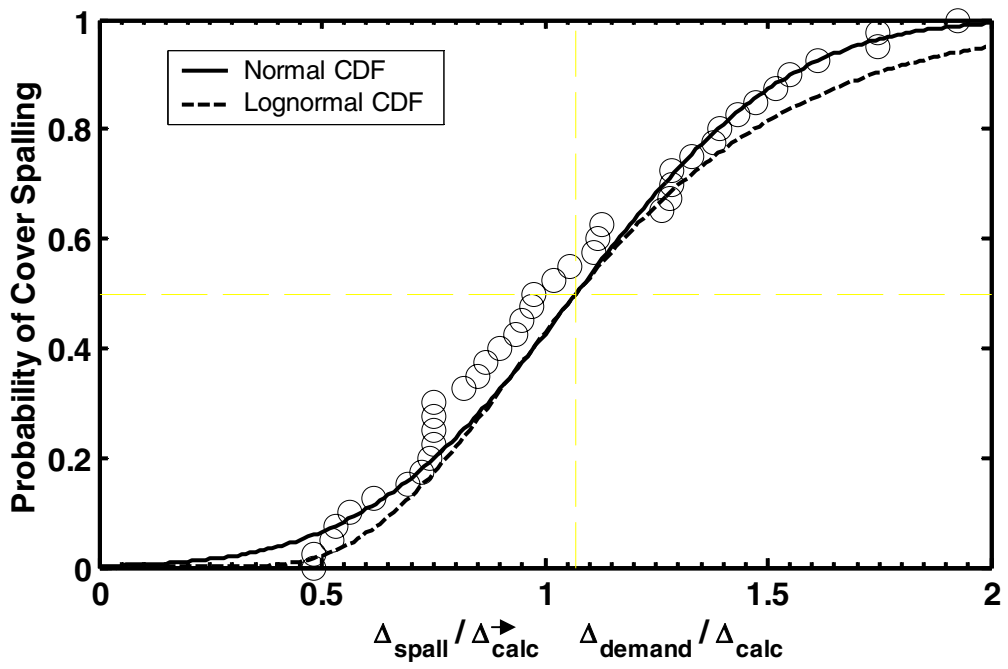
Figure 7.8 Fragility Curves for Cover Spalling, Spiral Columns

8 Summary and Conclusions

8.1 SUMMARY

The goal of performance-based earthquake engineering (PBEE) is to explicitly predict damage and assess the probability of reaching a level of damage in structural and nonstructural elements. The focus of this research was on implementing PBEE in reinforced concrete columns by providing the necessary link between deformation and specific damage states.

A number of key damage states have been identified in reinforced concrete columns as a result of years of research and post-earthquake observations. This report focused on longitudinal bar buckling and concrete cover spalling. Damage in reinforced concrete columns is controlled by a complex series of interrelated mechanisms, so it is difficult to model this behavior in detail. To provide a simple model that will be useful in practice, the proposed modeling strategy is based on the expected trends in deformation measures at the onset of particular damage states as functions of key column properties.

This research used the UW-PEER database, which contains the results of cyclic lateral load tests on approximately 300 rectangular columns and approximately 170 spiral-reinforced columns (Chapter 2). The database provides the column geometry; material, reinforcement, and loading properties; test results; and a reference for each of the column tests. The test results include the digital force-displacement histories (either full or envelope) and the measured maximum displacements before the onset of particular damage states. The displacements at the onset of bar buckling were reported for a total of 62 rectangular columns and 42 spiral-reinforced columns that met the screening criteria (Section 2.2). Similarly, the displacements at the onset of cover spalling were reported for 102 rectangular columns and 40 spiral columns that met the screening criteria. These columns were used to evaluate and assess the accuracies of the proposed bar buckling and cover spalling models.

In this report, plastic-hinge analysis was used to determine the expected influences of key column properties on the flexural response of reinforced concrete columns (Chapter 3). Plastic-hinge analysis was then used to determine the expected influences of key column properties on the deformations (compressive strain, ε_{damage}, plastic rotation, ϑ_{p_damage}, drift ratio, $\frac{\Delta_{damage}}{L}$, and displacement ductility, $\frac{\Delta_{damage}}{\Delta_y}$) at the onset of bar buckling (Chapters 4) and concrete cover spalling (Chapter 5). The expected trends in the deformations were compared to the trends observed in the column data by plotting the deformations versus the key column properties. From this comparison, key column properties were identified to control the onset of bar buckling and cover spalling.

A general form of regression equation was introduced to estimate the deformations at the onset of the particular damage states (Chapter 6). Then, a comprehensive regression analysis was performed using this equation and the UW-PEER database. The equations resulting from this analysis were studied and several key equations were identified. In addition, the influences of key column properties predicted with these equations were compared with the expected and observed trends from Chapters 4 and 5. The equations are presented in table form in Appendices A and B.

Based on the results of the regression analysis, two equations were proposed to estimate the drift ratios at the onset of bar buckling and concrete cover spalling in flexure-dominant reinforced concrete columns. In addition, the accuracies of these equations are evaluated by plotting $\frac{\Delta_{damage}}{\Delta_{calc}}$ versus key column properties. Finally, fragility curves are presented which will be helpful for design.

8.2 CONCLUSIONS

The UW-PEER column database provides the information needed to systematically evaluate the accuracy of force-displacement and damage models. The data made it possible to develop a necessary, quantitative link between deformation and the onset of particular damage states in flexure-dominant reinforced concrete columns.

The magnitudes of the COVs of the measured displacements to calculated displacements obtained by using the maximum compressive strain, plastic rotation, drift ratio, and displacement ductility were similar for both bar buckling and cover spalling. Therefore, for simplicity, the drift ratio is recommended for design.

Equation 8.1 provides a simple, accurate means of estimating the displacement at the onset of bar buckling in flexure-dominant reinforced concrete columns.

$$\frac{\Delta_{bb\_calc}}{L}(\%) = 3.25 \, (1 + k_e \rho_{eff} \, \frac{d_b}{D}) \, (1 - \frac{P}{A_g f'_c}) \, (1 + \frac{L}{10D}) \qquad \text{(Eq. 8.1)}$$

where k_e = 50 for rectangular columns and 150 for spiral-reinforced columns, $\rho_{eff} = \rho_s \frac{f_{ys}}{f'_c}$, ρ_s is the volumetric transverse reinforcement ratio, f_{ys} is the yield stress of the transverse reinforcement, f'_c is the concrete compressive strength, d_b is the diameter of the longitudinal reinforcing, D is the column depth, P is the axial load, A_g is the gross area of the cross section, and L is the distance from the column base to the point of contraflexure.

The mean value of $\frac{\Delta_{bb}}{\Delta_{bb\_calc}}$ obtained with Equation 8.1 was 1.0 with a COV of 26.3% for rectangular columns, and 0.97 with a COV of 24.6% for spiral-reinforced columns. The accuracy would improve if the coefficients multiplying the aspect ratio differed for the rectangular and spiral columns, but the increase in accuracy did not justify the increase in complexity.

Equation 8.2 provides a simple means to estimate the displacement at the onset of cover spalling in flexure-dominant reinforced concrete columns.

$$\frac{\Delta_{spall\_calc}}{L}(\%) \cong 1.6 \, (1 - \frac{P}{A_g f'_c}) \, (1 + \frac{L}{10D}) \qquad \text{(Eq. 8.2)}$$

The COVs of $\frac{\Delta_{spall}}{\Delta_{spall\_calc}}$ were significantly higher than the COVs of $\frac{\Delta_{bb}}{\Delta_{bb\_calc}}$. The mean value of $\frac{\Delta_{spall}}{\Delta_{spall\_calc}}$ obtained by using Equation 8.2 was 0.97 for rectangular columns with a COV of 43%, and 1.07 with a COV 35% for spiral-reinforced columns. The accuracy is improved if two separate equations were recommended for the rectangular columns and spiral-reinforced columns. However, the slight increase in accuracy did not justify the increase in complexity.

The recommended equations provide the capability for predicting reliably two damage states for columns in reinforced concrete buildings and bridges following seismic events. This will be a key factor in the practical implementation of PBEE.

8.3   RECOMMENDATIONS FOR FURTHER RESEARCH

Further investigations in the area of predicting damage progression in reinforced concrete columns should focus on

- Implementing complex bar-buckling models;
- Including the effects of load history and cumulative deformation on damage progression;
- Predicting other key damage states (e.g., 20% reduction in flexural capacity, residual cracking); and
- Developing a variable plastic-hinge model based on different levels of column damage and axial load.

REFERENCES

American Concrete Institute (ACI 318-02), "Building Code Requirements for Structural Concrete," 2002.

Bayrak, O. and Sheikh, S., "Plastic Hinge Analysis," *Journal of Structural Engineering,* ASCE, September 2001.

Bresler, B., and Gilbert, P.H., "Tie Requirements for Reinforced Concrete Columns," *ACI Journal*, November 1961.

Camarillo, Haili R., "Evaluation of Shear Strength Methodologies for Reinforced Concrete Columns," Department of Civil and Environmental Engineering, University of Washington, 2003.

Dhakal R. and Maekawa, K., "Reinforcement Stability and Fracture of Cover Concrete in Reinforced Concrete Members," *Journal of Structural Engineering,* ASCE, October 2002.

Gomes, A. and Appleton, J., "Nonlinear Cyclic Stress-Strain Relationship of Reinforcing Bars Including Buckling," *Engineering Structures,* Vol. 19, No. 10, 1997.

Henry, L., "Study of Buckling of Longitudinal Bars in Reinforced Concrete Bridge Columns," Masters Thesis, University of California, Berkeley, California, September 1998.

Kunnath, Sashi., El-Bahy, A., Taylor, A., and Stone, W., "Cumulative Seismic Damage of Reinforced Concrete Bridge Piers," Technical Report NCEER-97-0006, National Center for Earthquake Engineering Research, September 1997.

Lehman, Dawn E., "Performance-Based Seismic Design of Columns," Chapter 3 Draft, ACI Committee 341-A, May 2003.

Mander, J.B., Priestley, M.J.N. and Park, R. (1988). "Theoretical Stress-Strain Model for Confined Concrete," *Journal of the Structural Division*, ASCE, Vol. 114, No. 8, August, pp. 1804-1826.

Mattock, A. H., Discussion of "Rotational Capacity of Reinforced Concrete Beams," by W.G. Corley, *Journal of Structural Division, ASCE,* Vol. 93, ST2, April 1967.

Monti, G. and Nuti, C., "Nonlinear Cyclic Behavior of Reinforcing Bars Including Buckling," *Journal of Structural Engineering,* ASCE, December 1992.

Moyer, M. and Kowalsky, M., "Influence of Tension Strain on Buckling of Reinforcement in RC Bridge Columns," Department of Civil Engineering, North Carolina State University, Raleigh, North Carolina, May 2001.

Nelson, J., "Damage Accumulation in Lightly Confined Reinforced Bridge Columns,"

Department of Civil and Environmental Engineering, University of Washington, 2000.

Pantazopoulou, S. J., "Detailing for Reinforcement Stability in Reinforced Concrete Members," *Journal of Structural Engineering,* ASCE, June 1998.

Papia, M., Russo, G., and Zingone, G., "Instability of Longitudinal Bars in Reinforced Concrete Columns," *Journal of Structural Engineering,* ASCE, February 1989.

Park, R. and Paulay, T. (1975). *Reinforced Concrete Structures*, John Wiley and Sons, Inc., New York, 769 pp.

Parrish, M., "Accuracy of Seismic Performance Methodologies for Rectangular Reinforced Concrete Columns," Department of Civil and Environmental Engineering, University of Washington, 2001.

Priestley, M.J.N., Seible, F., and Calvi, G.M. (1996). *Seismic Design and Retrofit of Bridges*, John Wiley and Sons, Inc., New York, 686 pp.

Rodriguez, M., Botero, J., and Villa, J., "Cyclic Stress-Strain Behavior of Reinforcing Steel Including Effect of Buckling," *Journal of Structural Engineering,* ASCE, June 1999.

Scribner, C.F., "Reinforcement Buckling in Reinforced Concrete Flexural Members," *ACI Journal,* November-December 1986.

Appendix A: Deformations at Bar Buckling, Cover Spalling, and 20% Loss in Flexural Strength

Table A.1 Deformations at Bar Buckling, Rectangular Columns

Test #	Test Name	D_y	D_{bb}	e_{bb}	θ_{p_bb}	$\dfrac{D_{bb}}{L}$	$\dfrac{D_{bb}}{D_y}$
5	Ang et al. 1981, No. 3	9.6	50.0	0.017	0.028	3.13	5.20
6	Ang et al. 1981, No. 4	12.2	58.0	0.016	0.031	3.63	4.75
7	Soesian. et al. 86, No. 1	10.8	78.4	0.018	0.046	4.90	7.29
8	Soesian. et al. 86, No. 2	9.2	68.4	0.025	0.041	4.28	7.45
9	Soesian. et al. 86, No. 3	8.7	44.9	0.016	0.025	2.81	5.13
10	Soesian. et al. 86, No. 4	9.6	41.0	0.018	0.022	2.56	4.28
11	Zahn et al. 1986, No. 7	11.9	71.0	0.018	0.041	4.44	5.96
12	Zahn et al. 1986, No. 8	10.3	50.0	0.016	0.027	3.13	4.86
18	Tanaka & Park 1990, No. 1	13.8	120.0	0.032	0.074	7.50	8.70
19	Tanaka & Park 1990, No. 2	13.0	87.2	0.023	0.052	5.45	6.69
20	Tanaka & Park 1990, No. 3	11.4	59.0	0.015	0.033	3.69	5.19
21	Tanaka & Park 1990, No. 4	12.3	80.0	0.021	0.047	5.00	6.48
22	Tanaka & Park 1990, No. 5	13.5	73.8	0.016	0.041	4.47	5.45
23	Tanaka & Park 1990, No. 6	12.0	67.2	0.015	0.038	4.07	5.62
24	Tanaka & Park 1990, No. 7	9.7	82.4	0.030	0.049	4.99	8.52
25	Tanaka & Park 1990, No. 8	8.4	78.0	0.028	0.047	4.73	9.30
26	Park & Paulay 1990, No. 9	10.7	84.0	0.020	0.046	4.71	7.84
93	Atalay & Penzien 75, 6S1	19.0	40.7	0.005	0.014	2.43	2.14
132	Wehbe et al. 1998, A1	23.6	122.0	0.027	0.046	5.22	5.17
133	Wehbe et al. 1998, A2	22.0	102.0	0.027	0.037	4.37	4.63
135	Wehbe et al. 1998, B2	26.8	128.0	0.033	0.047	5.48	4.77
144	Xiao & Mar HC48L19T10-0.1P	6.2	47.0	0.027	0.107	9.25	7.56
145	Xiao & Mar HC48L19T10-0.2P	5.3	40.0	0.031	0.091	7.87	7.59
146	Xiao & Mar HC48L16T10-0.1P	5.2	37.0	0.020	0.080	7.28	7.14
147	Xiao & Mar HC48L16T10-0.2P	6.2	35.0	0.027	0.072	6.89	5.62
156	Bayrak & Sheikh 96 ES-1HT	9.5	48.5	0.013	0.023	3.29	5.10
157	Bayrak & Sheikh 96 AS-2HT	11.3	95.1	0.021	0.050	6.45	8.43
158	Bayrak & Sheikh 96 AS-3HT	9.3	62.6	0.016	0.032	4.25	6.73
159	Bayrak & Sheikh 96 AS-4HT	14.0	78.5	0.017	0.039	5.33	5.62
161	Bayrak & Sheikh 96 AS-6HT	14.2	73.3	0.015	0.035	4.98	5.16
162	Bayrak & Sheikh 96 AS-7HT	14.6	31.0	0.006	0.010	2.10	2.12
163	Bayrak & Sheikh 96 ES-8HT	9.6	26.6	0.006	0.010	1.81	2.76
165	Saatcioglu & Grira 99 BG2	9.6	82.3	0.026	0.049	5.00	8.54
167	Saatcioglu & Grira 99 BG4	11.0	65.8	0.022	0.037	4.00	5.98
168	Saatcioglu & Grira 99 BG5	13.8	115.2	0.032	0.068	7.00	8.37
171	Saatcioglu & Grira 99 BG8	20.7	115.2	0.027	0.064	7.00	5.58
172	Saatcioglu & Grira 99 BG9	12.4	65.8	0.023	0.036	4.00	5.30
201	Thomsen & Wallace 1994, A3	3.5	23.9	0.015	0.039	4.00	6.76
208	Thomsen & Wallace 1994, D1	4.6	47.8	0.029	0.083	8.00	10.46
209	Thomsen & Wallace 1994, D2	5.1	35.8	0.023	0.059	6.00	7.00
210	Thomsen & Wallace 1994, D3	5.6	35.8	0.023	0.058	6.00	6.36

Table A.1—*Continued*

Test #	Test Name	D_y	D_{bb}	e_{bb}	θ_{p_bb}	$\dfrac{D_{bb}}{L}$	$\dfrac{D_{bb}}{D_y}$
253	Xaio & Yun 02, No.FHC1-0.2	14.8	142.2	0.035	0.082	8.00	9.64
254	Xaio & Yun 02 No.FHC2-0.34	11.1	71.1	0.021	0.038	4.00	6.40
255	Xaio & Yun 02 No.FHC3-0.22	13.8	106.7	0.027	0.060	6.00	7.72
256	Xaio & Yun 02 No.FHC4-0.33	11.4	71.1	0.021	0.038	4.00	6.26
257	Xaio & Yun 02, No.FHC5-0.2	14.1	106.7	0.026	0.060	6.00	7.59
258	Xaio & Yun 02, No.FHC6-0.2	16.0	106.7	0.025	0.059	6.00	6.69
259	Bayrak & Sheikh 02 RS- 9HT	19.0	128.6	0.030	0.066	8.73	6.77
260	Bayrak & Sheikh 02 RS-10HT	13.4	85.9	0.023	0.043	5.83	6.40
262	Bayrak & Sheikh 02 RS-12HT	15.4	82.9	0.023	0.040	5.63	5.37
263	Bayrak & Sheikh 02 RS-13HT	16.4	89.8	0.024	0.044	6.10	5.48
264	Bayrak & Sheikh 02 RS-14HT	27.8	62.6	0.013	0.021	4.25	2.25
265	Bayrak & Sheikh 02 RS-15HT	29.1	117.9	0.026	0.053	8.00	4.05
266	Bayrak & Sheikh 02 RS-16HT	23.8	79.8	0.018	0.034	5.42	3.35
267	Bayrak & Sheikh 02 RS-17HT	29.5	106.7	0.019	0.046	7.24	3.61
268	Bayrak & Sheikh 02 RS-18HT	16.7	64.5	0.015	0.029	4.38	3.87
269	Bayrak & Sheikh 02 RS-19HT	16.5	121.7	0.028	0.063	8.27	7.39
270	Bayrak & Sheikh 02 RS-20HT	21.1	66.0	0.012	0.027	4.48	3.13
271	Bayrak &Sheikh 02 WRS-21HT	27.6	67.2	0.010	0.024	4.56	2.43
272	Bayrak &Sheikh 02 WRS-22HT	32.4	126.9	0.020	0.057	8.62	3.92
273	Bayrak &Sheikh 02 WRS-23HT	31.7	122.5	0.018	0.055	8.32	3.87
274	Bayrak &Sheikh 02 WRS-24HT	25.6	87.0	0.015	0.037	5.91	3.40
62 Total	Mean	14.5	76.8	0.021	0.046	5.34	5.86
	STD	7.3	31.3	0.007	0.019	1.78	1.93
	COV	0.51	0.4	0.322	0.422	0.33	0.33

Table A.2 Deformations at Bar Buckling, Spiral Columns

Test #	Test Name	D_y	D_{bb}	e_{bb}	θ_{p_bb}	$\frac{D_{bb}}{L}$	$\frac{D_{bb}}{D_y}$
1	Davey 1975, No. 1	25.2	128.9	0.021	0.040	6.45	5.12
2	Davey 1975, No. 2	8.9	78.1	0.024	0.043	3.91	8.82
3	Davey 1975, No. 3	41.5	154.1	0.019	0.036	7.71	3.71
7	Ang '81 No. 1	8.8	60.0	0.023	0.034	3.75	6.79
8	Ang '81 No. 2	8.9	52.0	0.029	0.029	3.25	5.83
39	Zahn '86 No. 5	9.6	45.6	0.014	0.024	2.85	4.74
42	Watson & Park 1989, No 11	6.4	36.3	0.019	0.021	2.27	5.71
43	Wong et al. 1990, No. 1	5.9	40.0	0.036	0.049	5.00	6.81
45	Wong et al. 1990, No. 3	4.3	25.9	0.027	0.032	3.24	5.99
53	NIST Full Scale Flexure	109.4	538.0	0.025	0.049	5.89	4.92
54	NIST Full Scale Shear	41.3	285.0	0.030	0.059	6.24	6.91
55	NIST Model N1	7.4	77.2	0.059	0.102	10.29	10.44
56	NIST Model N2	6.2	44.7	0.037	0.056	5.96	7.23
57	NIST Model N3	16.1	102.4	0.035	0.060	6.83	6.37
58	NIST Model N4	4.9	53.3	0.041	0.071	7.11	10.87
59	NIST Model N5	6.3	48.3	0.040	0.061	6.44	7.67
60	NIST Model N6	14.4	67.2	0.022	0.037	4.48	4.67
93	Kunnath 1997 No. A2	13.9	68.3	0.022	0.043	4.98	4.91
98	Kunnath 1997 No. A7	11.1	80.0	0.027	0.054	5.83	7.22
99	Kunnath 1997 No. A8	15.4	80.0	0.025	0.051	5.83	5.20
100	Kunnath 1997 No. A9	11.9	63.0	0.020	0.040	4.59	5.28
101	Kunnath 1997 No. A10	12.1	82.0	0.028	0.055	5.98	6.78
103	Kunnath 1997 No. A12	11.3	81.0	0.028	0.055	5.90	7.19
106	Hose et al. 1997 No. SRPH1	40.0	320.0	0.042	0.081	8.74	8.01
109	Vu et al. 1998 No. NH3	6.1	50.0	0.041	0.055	5.49	8.16
115	Kowalsky 1996 No. FL3	60.9	340.0	0.052	0.080	9.30	5.58
116	Lehman No.415	17.6	178.0	0.034	0.070	7.30	10.09
117	Lehman No.815	64.9	445.0	0.040	0.081	9.12	6.86
118	Lehman No.1015	109.7	635.0	0.044	0.089	10.42	5.79
119	Lehman No.407	13.6	127.0	0.020	0.050	5.21	9.37
120	Lehman No.430	26.2	178.0	0.040	0.067	7.30	6.81
121	Lehman & Calderone No.328	14.9	125.0	0.038	0.066	6.84	8.42
122	Lehman & Calderone No.828	83.0	600.0	0.057	0.110	12.30	7.23
123	Lehman & Calderone No.1028	95.4	889.0	0.070	0.134	14.58	9.32
131	Saatcioglu No.RC6	11.2	65.8	0.019	0.036	4.00	5.85
136	Nelson & Price 2000 Col2	9.7	56.6	0.030	0.034	3.71	5.81
139	Henry 1998 No. 415p	25.8	127.0	0.025	0.044	5.21	4.91
140	Henry 1998 No. 415s	23.7	127.0	0.024	0.045	5.21	5.37
150	Kowalsky & Moyer 2001 No.1	38.0	149.9	0.015	0.050	6.15	3.94
151	Kowalsky & Moyer 2001 No.2	41.2	261.6	0.030	0.099	10.73	6.36
152	Kowalsky & Moyer 2001 No.3	36.8	261.9	0.031	0.101	10.74	7.11
153	Kowalsky & Moyer 2001 No.4	40.5	297.2	0.035	0.116	12.19	7.34
42 Total	Mean	27.6	179.2	0.032	0.060	6.65	6.70
	STD	28.2	191.2	0.012	0.026	2.80	1.71
	COV	1.02	1.1	0.380	0.442	0.42	0.25

Table A.3 Deformations at Cover Spalling, Rectangular Columns

Test #	Test Name	D_y	D_{crush}	e_{crush}	θ_{p_crush}	$\dfrac{D_{crush}}{L}$	$\dfrac{D_{crush}}{D_y}$
1	Gill et al. 1979, No. 1	7.1	11.5	0.004	0.004	0.96	1.62
2	Gill et al. 1979, No. 2	7.1	8.0	0.002	0.001	0.67	1.12
3	Gill et al. 1979, No. 3	4.9	7.0	0.004	0.002	0.58	1.44
4	Gill et al. 1979, No. 4	4.1	5.0	0.003	0.001	0.42	1.22
5	Ang et al. 1981, No. 3	9.6	10.0	0.002	0.000	0.63	1.04
6	Ang et al. 1981, No. 4	12.2	19.0	0.003	0.005	1.19	1.56
7	Soesian. et al. 86, No. 1	10.8	39.2	0.007	0.020	2.45	3.64
8	Soesian. et al. 86, No. 2	9.2	34.2	0.010	0.017	2.14	3.73
9	Soesian. et al. 86, No. 3	8.7	30.6	0.010	0.015	1.91	3.50
10	Soesian. et al. 86, No. 4	9.6	16.4	0.004	0.005	1.03	1.71
11	Zahn et al. 1986, No. 7	11.9	22.0	0.004	0.007	1.38	1.85
12	Zahn et al. 1986, No. 8	10.3	17.0	0.004	0.005	1.06	1.65
13	Watson & Park 1989, No. 5	8.1	18.5	0.007	0.007	1.15	2.28
14	Watson & Park 1989, No. 6	6.2	18.5	0.008	0.008	1.15	2.98
15	Watson & Park 1989, No. 7	4.0	12.3	0.007	0.006	0.77	3.06
16	Watson & Park 1989, No. 8	4.2	12.3	0.007	0.006	0.77	2.96
17	Watson & Park 1989, No. 9	4.8	12.3	0.006	0.005	0.77	2.58
18	Tanaka & Park 1990, No. 1	13.8	20.0	0.003	0.004	1.25	1.45
19	Tanaka & Park 1990, No. 2	13.0	18.0	0.003	0.003	1.13	1.38
20	Tanaka & Park 1990, No. 3	11.4	16.0	0.003	0.003	1.00	1.41
21	Tanaka & Park 1990, No. 4	12.3	16.0	0.003	0.003	1.00	1.30
22	Tanaka & Park 1990, No. 5	13.5	22.0	0.003	0.006	1.33	1.62
23	Tanaka & Park 1990, No. 6	12.0	19.0	0.003	0.005	1.15	1.59
24	Tanaka & Park 1990, No. 7	9.7	19.0	0.005	0.006	1.15	1.96
25	Tanaka & Park 1990, No. 8	8.4	13.0	0.004	0.003	0.79	1.55
89	Atalay & Penzien 75, 2S1	15.0	20.3	0.002	0.003	1.21	1.35
90	Atalay & Penzien 75, 3S1	15.9	40.7	0.004	0.016	2.43	2.56
91	Atalay & Penzien 75, 4S1	20.1	20.3	0.002	0.000	1.21	1.01
92	Atalay & Penzien 75, 5S1	19.0	25.4	0.003	0.004	1.52	1.34
93	Atalay & Penzien 75, 6S1	19.0	30.5	0.003	0.008	1.82	1.61
94	Atalay & Penzien 75 No. 9	18.1	10.2	0.001	0.000	0.61	0.56
95	Atalay & Penzien 75 No. 10	18.7	20.3	0.002	0.001	1.21	1.09
96	Atalay & Penzien 75 No. 11	15.2	15.3	0.002	0.000	0.91	1.00
97	Atalay & Penzien 75 No. 12	18.8	15.3	0.002	0.000	0.91	0.81
102	Azizina. et al. 88, NC-2	10.6	25.1	0.007	0.012	1.83	2.37
103	Azizina. et al. 88, NC-4	9.3	15.3	0.004	0.005	1.11	1.64
132	Wehbe et al. 1998, A1	23.6	47.0	0.006	0.011	2.01	1.99
133	Wehbe et al. 1998, A2	22.0	40.0	0.007	0.008	1.71	1.82
134	Wehbe et al. 1998, B1	27.3	47.0	0.005	0.009	2.01	1.72
150	Sugano 1996, UC10H	1.3	0.6	0.002	0.000	0.13	0.45
151	Sugano 1996, UC15H	1.4	0.7	0.002	0.000	0.16	0.50
152	Sugano 1996, UC20H	1.5	0.8	0.002	0.000	0.17	0.52

Table A.3—*Continued*

Test #	Test Name	D_y	D_{crush}	e_{crush}	θ_{p_crush}	$\dfrac{D_{crush}}{L}$	$\dfrac{D_{crush}}{D_y}$
154	Sugano 1996, UC20L	1.8	1.4	0.002	0.000	0.31	0.76
156	Bayrak & Sheikh 96 ES-1HT	9.5	10.0	0.002	0.000	0.68	1.05
157	Bayrak & Sheikh 96 AS-2HT	11.3	12.9	0.002	0.001	0.88	1.15
158	Bayrak & Sheikh 96 AS-3HT	9.3	10.0	0.002	0.000	0.68	1.07
159	Bayrak & Sheikh 96 AS-4HT	14.0	12.9	0.002	0.000	0.88	0.92
161	Bayrak & Sheikh 96 AS-6HT	14.2	11.4	0.002	0.000	0.77	0.80
162	Bayrak & Sheikh 96 AS-7HT	14.6	5.7	0.001	0.000	0.39	0.39
163	Bayrak & Sheikh 96 ES-8HT	9.6	9.9	0.002	0.000	0.68	1.03
164	Saatcioglu & Grira 99 BG1	10.0	32.9	0.010	0.015	2.00	3.29
165	Saatcioglu & Grira 99 BG2	9.6	32.9	0.009	0.016	2.00	3.42
166	Saatcioglu & Grira 99 BG3	15.4	32.9	0.006	0.012	2.00	2.13
167	Saatcioglu & Grira 99 BG4	11.0	32.9	0.010	0.015	2.00	2.99
168	Saatcioglu & Grira 99 BG5	13.8	32.9	0.008	0.013	2.00	2.39
169	Saatcioglu & Grira 99 BG6	11.3	32.9	0.007	0.015	2.00	2.91
170	Saatcioglu & Grira 99 BG7	12.0	32.9	0.009	0.014	2.00	2.75
171	Saatcioglu & Grira 99 BG8	20.7	32.9	0.005	0.008	2.00	1.59
172	Saatcioglu & Grira 99 BG9	12.4	32.9	0.010	0.014	2.00	2.65
173	Saatcioglu & Grira 99 BG10	13.6	32.9	0.009	0.013	2.00	2.42
186	Mo & Wang 2000, C1-1	14.9	42.5	0.010	0.022	3.04	2.84
187	Mo & Wang 2000, C1-2	14.8	37.0	0.009	0.018	2.64	2.50
188	Mo & Wang 2000, C1-3	14.9	36.0	0.009	0.017	2.57	2.42
189	Mo & Wang 2000, C2-1	16.7	37.0	0.008	0.016	2.64	2.21
190	Mo & Wang 2000, C2-2	15.6	35.0	0.008	0.016	2.50	2.24
191	Mo & Wang 2000, C2-3	13.5	38.0	0.010	0.020	2.71	2.82
201	Thomsen & Wallace 1994, A3	3.5	14.9	0.009	0.022	2.50	4.22
203	Thomsen & Wallace 1994, B2	4.6	17.9	0.008	0.025	3.00	3.93
204	Thomsen & Wallace 1994, B3	4.0	11.9	0.007	0.015	2.00	3.02
206	Thomsen & Wallace 1994, C2	4.8	17.9	0.007	0.025	3.00	3.75
207	Thomsen & Wallace 1994, C3	5.6	14.9	0.007	0.018	2.50	2.67
208	Thomsen & Wallace 1994, D1	4.6	14.9	0.008	0.020	2.50	3.27
209	Thomsen & Wallace 1994, D2	5.1	11.9	0.006	0.013	2.00	2.33
210	Thomsen & Wallace 1994, D3	5.6	11.9	0.006	0.012	2.00	2.12
214	Paultre et al 00 1006015	27.9	34.0	0.002	0.003	1.70	1.22
215	Paultre et al 00 1006025	20.3	31.1	0.004	0.006	1.56	1.53
216	Paultre et al 00 1006040	21.8	27.4	0.003	0.003	1.37	1.26
217	Paultre et al 00 10013015	28.8	30.4	0.002	0.001	1.52	1.06
218	Paultre et al 00 10013025	18.7	28.8	0.004	0.005	1.44	1.53
219	Paultre et al 00 10013040	16.1	24.8	0.004	0.005	1.24	1.54
220	Paultre et al 01 806040	15.8	26.5	0.004	0.006	1.32	1.68
221	Paultre et al 01 1206040	16.2	24.7	0.004	0.005	1.23	1.53
222	Paultre et al 01 1005540	19.0	26.4	0.004	0.004	1.32	1.39
223	Paultre et al 01 1008040	21.0	28.5	0.004	0.004	1.42	1.35
224	Paultre et al 01 1005552	13.6	19.9	0.004	0.003	1.00	1.47
225	Paultre et al 01 1006052	15.7	22.5	0.004	0.004	1.13	1.43
259	Bayrak & Sheikh 02 RS- 9HT	19.0	24.2	0.003	0.003	1.64	1.27
260	Bayrak & Sheikh 02 RS-10HT	13.4	17.5	0.003	0.002	1.18	1.30

Table A.3—*Continued*

Test #	Test Name	D_y	D_{crush}	e_{crush}	θ_{p_crush}	$\dfrac{D_{crush}}{L}$	$\dfrac{D_{crush}}{D_y}$
262	Bayrak & Sheikh 02 RS-12HT	15.4	23.8	0.004	0.005	1.61	1.54
263	Bayrak & Sheikh 02 RS-13HT	16.4	18.6	0.003	0.001	1.26	1.14
264	Bayrak & Sheikh 02 RS-14HT	27.8	35.8	0.005	0.005	2.43	1.29
265	Bayrak & Sheikh 02 RS-15HT	29.1	44.4	0.006	0.009	3.01	1.53
266	Bayrak & Sheikh 02 RS-16HT	23.8	36.9	0.005	0.008	2.50	1.55
267	Bayrak & Sheikh 02 RS-17HT	29.5	32.2	0.003	0.002	2.19	1.09
268	Bayrak & Sheikh 02 RS-18HT	16.7	27.4	0.005	0.006	1.86	1.64
269	Bayrak & Sheikh 02 RS-19HT	16.5	19.4	0.003	0.002	1.32	1.18
270	Bayrak & Sheikh 02 RS-20HT	21.1	33.1	0.005	0.007	2.25	1.57
271	Bayrak &Sheikh 02 WRS-21HT	27.6	28.3	0.002	0.000	1.92	1.02
272	Bayrak &Sheikh 02 WRS-22HT	32.4	41.4	0.004	0.005	2.81	1.28
273	Bayrak &Sheikh 02 WRS-23HT	31.7	35.3	0.003	0.002	2.40	1.12
274	Bayrak &Sheikh 02 WRS-24HT	25.6	25.1	0.002	0.000	1.70	0.98
102 Total	Mean	13.8	22.8	0.005	0.007	1.53	1.80
	STD	7.4	11.5	0.003	0.007	0.73	0.86
	COV	0.54	0.5	0.551	0.929	0.48	0.48

Table A.4 Deformations at Cover Spalling, Spiral Columns

Test #	Test Name	D_y	D_{crush}	e_{crush}	θ_{p_crush}	$\dfrac{D_{crush}}{L}$	$\dfrac{D_{crush}}{D_y}$
1	Davey 1975, No. 1	25.2	90.3	0.013	0.025	4.51	3.59
2	Davey 1975, No. 2	8.9	54.4	0.015	0.028	2.72	6.14
3	Davey 1975, No. 3	41.5	80.4	0.007	0.013	4.02	1.94
4	Munro '76 No. 1	21.4	76.0	0.009	0.021	2.78	3.56
6	Ng '78 No. 3	7.1	10.0	0.004	0.003	1.08	1.41
7	Ang '81 No. 1	8.8	15.0	0.004	0.004	0.94	1.70
8	Ang '81 No. 2	8.9	9.8	0.003	0.001	0.61	1.09
9	Potangaroa '79 1	5.8	10.0	0.005	0.004	0.83	1.74
11	Potangaroa '79 4	7.2	7.5	0.002	0.000	0.63	1.05
43	Wong et al. 1990, No. 1	5.9	6.0	0.002	0.000	0.75	1.02
53	NIST Full Scale Flexure	109.4	179.0	0.005	0.008	1.96	1.64
55	NIST Model N1	7.4	19.3	0.011	0.017	2.57	2.61
57	NIST Model N3	16.1	51.2	0.014	0.025	3.41	3.19
58	NIST Model N4	4.9	21.3	0.014	0.024	2.84	4.35
59	NIST Model N5	6.3	19.3	0.013	0.019	2.58	3.07
60	NIST Model N6	14.4	33.6	0.009	0.013	2.24	2.33
94	Kunnath 1997 No. A3	12.7	27.0	0.007	0.011	1.97	2.12
98	Kunnath 1997 No. A7	11.1	20.0	0.005	0.007	1.46	1.81
99	Kunnath 1997 No. A8	15.4	32.0	0.007	0.013	2.33	2.08
101	Kunnath 1997 No. A10	12.1	32.0	0.009	0.016	2.33	2.65
102	Kunnath 1997 No. A11	12.7	50.0	0.016	0.029	3.64	3.93
103	Kunnath 1997 No. A12	11.3	50.0	0.016	0.030	3.64	4.44
106	Hose et al. 1997 No. SRPH1	40.0	60.0	0.004	0.006	1.64	1.50
107	Vu et al. 1998 No. NH1	6.5	11.5	0.007	0.006	1.26	1.78
109	Vu et al. 1998 No. NH3	6.1	18.8	0.012	0.016	2.06	3.06
115	Kowalsky 1996 No. FL3	60.9	68.0	0.003	0.002	1.86	1.12
116	Lehman No.415	17.6	38.1	0.005	0.009	1.56	2.16
117	Lehman No.815	64.9	133.0	0.008	0.014	2.73	2.05
118	Lehman No.1015	109.7	191.0	0.008	0.014	3.13	1.74
119	Lehman No.407	13.6	38.0	0.005	0.011	1.56	2.80
120	Lehman No.430	26.2	38.1	0.004	0.005	1.56	1.46
121	Lehman & Calderone No.328	14.9	30.0	0.006	0.009	1.64	2.02
122	Lehman & Calderone No.828	83.0	178.0	0.011	0.020	3.65	2.14
123	Lehman & Calderone No.1028	95.4	254.0	0.014	0.027	4.17	2.66
142	Soderstrom 2001 C1	24.0	39.4	0.003	0.009	2.00	1.64
143	Soderstrom 2001 C2	21.2	34.4	0.003	0.007	1.75	1.62
150	Kowalsky & Moyer 2001 No.1	38.0	73.7	0.006	0.016	3.02	1.94
151	Kowalsky & Moyer 2001 No.2	41.2	55.9	0.003	0.007	2.29	1.36
152	Kowalsky & Moyer 2001 No.3	36.8	73.7	0.006	0.017	3.02	2.00
153	Kowalsky & Moyer 2001 No.4	40.5	73.7	0.005	0.015	3.02	1.82
40 Total	Mean		57.6	0.008	0.013	2.29	2.31
	STD		56.2	0.004	0.008	1.01	1.07
	COV		0.98	0.563	0.650	0.44	0.46

Table A.5 Deformations at 20% Reduction in Flexural Strength, Rectangular Columns

Test #	Test Name	D_y	$D_{20\%}$	$e_{20\%}$	$\theta_{p\_20\%}$	$\dfrac{D_{20\%}}{L}$	$\dfrac{D_{20\%}}{D_y}$
7	Soesian. et al. 86, No. 1	10.76	98.06	0.026	0.060	6.13	9.12
8	Soesian. et al. 86, No. 2	9.18	68.73	0.025	0.041	4.30	7.49
9	Soesian. et al. 86, No. 3	8.75	46.24	0.017	0.026	2.89	5.29
10	Soesian. et al. 86, No. 4	9.59	43.91	0.021	0.024	2.74	4.58
11	Zahn et al. 1986, No. 7	11.91	118.18	0.033	0.073	7.39	9.92
13	Watson & Park 1989, No. 5	8.09	38.91	0.018	0.021	2.43	4.81
14	Watson & Park 1989, No. 6	6.19	26.83	0.014	0.014	1.68	4.33
15	Watson & Park 1989, No. 7	4.02	18.72	0.010	0.010	1.17	4.66
16	Watson & Park 1989, No. 8	4.16	17.17	0.010	0.009	1.07	4.13
17	Watson & Park 1989, No. 9	4.76	43.86	0.021	0.027	2.74	9.22
20	Tanaka & Park 1990, No. 3	11.36	57.20	0.015	0.032	3.58	5.03
32	Ohno & Nishioka 1984, L3	9.84	73.04	0.010	0.043	4.56	7.42
43	Zhou et al. 87, No. 214-08	1.55	6.54	0.021	0.018	2.04	4.22
48	Kanda et al. 1987, 85STC-1	4.38	34.60	0.024	0.045	4.61	7.91
49	Kanda et al. 1987, 85STC-2	3.74	34.60	0.024	0.046	4.61	9.24
50	Kanda et al. 1987, 85STC-3	4.38	34.60	0.024	0.045	4.61	7.91
56	Muguruma et al. 89, AL-1	2.51	21.44	0.037	0.045	4.29	8.55
58	Muguruma et al. 89, AL-2	1.92	10.89	0.020	0.021	2.18	5.67
66	Sakai et al. 1990, B1	2.42	10.17	0.019	0.018	2.03	4.20
67	Sakai et al. 1990, B2	2.28	20.09	0.046	0.042	4.02	8.81
68	Sakai et al. 1990, B3	2.52	10.07	0.035	0.018	2.01	4.00
69	Sakai et al. 1990, B4	2.46	10.07	0.016	0.018	2.01	4.10
70	Sakai et al. 1990, B5	2.24	9.46	0.029	0.017	1.89	4.23
71	Sakai et al. 1990, B6	2.43	10.07	0.040	0.018	2.01	4.13
72	Sakai et al. 1990, B7	1.68	5.06	0.008	0.008	1.01	3.01
94	Atalay & Penzien 75 No. 9	18.15	42.16	0.007	0.016	2.52	2.32
95	Atalay & Penzien 75 No. 10	18.66	40.08	0.007	0.014	2.39	2.15
96	Atalay & Penzien 75 No. 11	15.22	37.65	0.007	0.015	2.25	2.47
97	Atalay & Penzien 75 No. 12	18.80	42.70	0.008	0.016	2.55	2.27
102	Azizina. et al. 88, NC-2	10.61	66.64	0.022	0.047	4.86	6.28
103	Azizina. et al. 88, NC-4	9.27	38.62	0.015	0.025	2.82	4.17
104	Saatcioglu & Ozcebe 89, U3	20.78	51.10	0.015	0.036	5.11	2.46
105	Saatcioglu & Ozcebe 89, U4	13.08	89.90	0.036	0.092	8.99	6.88
106	Saatcioglu & Ozcebe 89, U6	13.56	89.80	0.031	0.091	8.98	6.62
107	Saatcioglu & Ozcebe 89, U7	13.61	88.00	0.030	0.089	8.80	6.47
108	Galeota et al. 1996, AA1	7.54	15.93	0.008	0.008	1.40	2.11
109	Galeota et al. 1996, AA2	8.60	17.17	0.008	0.008	1.51	2.00
110	Galeota et al. 1996, AA3	12.06	20.82	0.006	0.008	1.83	1.73
111	Galeota et al. 1996, AA4	5.41	15.98	0.008	0.010	1.40	2.95
112	Galeota et al. 1996, BA1	5.30	26.71	0.013	0.020	2.34	5.04
113	Galeota et al. 1996, BA2	7.99	36.40	0.024	0.027	3.19	4.56
114	Galeota et al. 1996, BA3	7.69	21.94	0.011	0.014	1.92	2.85
115	Galeota et al. 1996, BA4	9.47	40.97	0.019	0.030	3.59	4.33
116	Galeota et al. 1996, CA1	11.00	67.02	0.027	0.054	5.88	6.09
117	Galeota et al. 1996, CA2	8.00	53.54	0.026	0.043	4.70	6.69
118	Galeota et al. 1996, CA3	6.10	37.06	0.015	0.030	3.25	6.07
119	Galeota et al. 1996, CA4	7.70	40.52	0.019	0.031	3.55	5.26

Table A.5—*Continued*

Test #	Test Name	D_y	$D_{20\%}$	$e_{20\%}$	$\theta_{p\_20\%}$	$\dfrac{D_{20\%}}{L}$	$\dfrac{D_{20\%}}{D_y}$
122	Galeota et al. 1996, AB3	12.58	42.67	0.019	0.030	3.74	3.39
123	Galeota et al. 1996, AB4	10.18	46.30	0.020	0.036	4.06	4.55
124	Galeota et al. 1996, BB	14.97	69.76	0.023	0.055	6.12	4.66
125	Galeota et al. 1996, BB1	9.33	58.03	0.020	0.049	5.09	6.22
126	Galeota et al. 1996, BB4	10.92	71.81	0.033	0.061	6.30	6.58
127	Galeota et al. 1996, BB4B	11.32	75.33	0.035	0.064	6.61	6.65
132	Wehbe et al. 1998, A1	23.58	122.10	0.027	0.046	5.23	5.18
133	Wehbe et al. 1998, A2	22.03	102.26	0.027	0.037	4.38	4.64
134	Wehbe et al. 1998, B1	27.31	160.79	0.036	0.062	6.89	5.89
135	Wehbe et al. 1998, B2	26.84	129.78	0.034	0.048	5.56	4.84
144	Xiao & Mar HC48L19T10-0.1P	6.22	47.76	0.027	0.109	9.40	7.68
145	Xiao & Mar HC48L19T10-0.2P	5.27	40.94	0.032	0.094	8.06	7.77
146	Xiao & Mar HC48L16T10-0.1P	5.18	37.59	0.020	0.081	7.40	7.25
147	Xiao & Mar HC48L16T10-0.2P	6.23	35.01	0.027	0.072	6.89	5.62
150	Sugano 1996, UC10H	1.34	4.09	0.009	0.007	0.91	3.06
151	Sugano 1996, UC15H	1.41	8.24	0.018	0.018	1.83	5.83
152	Sugano 1996, UC20H	1.46	16.30	0.035	0.038	3.62	11.20
153	Sugano 1996, UC15L	1.86	20.40	0.032	0.048	4.53	10.99
154	Sugano 1996, UC20L	1.84	28.30	0.042	0.068	6.29	15.37
156	Bayrak & Sheikh 96 ES-1HT	9.51	42.30	0.011	0.020	2.87	4.45
157	Bayrak & Sheikh 96 AS-2HT	11.28	82.78	0.018	0.043	5.62	7.34
158	Bayrak & Sheikh 96 AS-3HT	9.30	44.77	0.011	0.021	3.04	4.81
159	Bayrak & Sheikh 96 AS-4HT	13.97	67.71	0.014	0.032	4.60	4.85
161	Bayrak & Sheikh 96 AS-6HT	14.21	72.90	0.015	0.035	4.95	5.13
162	Bayrak & Sheikh 96 AS-7HT	14.60	31.07	0.006	0.010	2.11	2.13
163	Bayrak & Sheikh 96 ES-8HT	9.64	33.07	0.008	0.014	2.24	3.43
164	Saatcioglu & Grira 99 BG1	10.00	41.01	0.013	0.021	2.49	4.10
165	Saatcioglu & Grira 99 BG2	9.63	66.52	0.020	0.038	4.04	6.91
166	Saatcioglu & Grira 99 BG3	15.42	116.02	0.024	0.068	7.05	7.52
167	Saatcioglu & Grira 99 BG4	11.01	50.50	0.016	0.027	3.07	4.59
168	Saatcioglu & Grira 99 BG5	13.76	100.03	0.027	0.058	6.08	7.27
169	Saatcioglu & Grira 99 BG6	11.31	100.03	0.021	0.062	6.08	8.84
170	Saatcioglu & Grira 99 BG7	11.97	100.03	0.033	0.059	6.08	8.36
171	Saatcioglu & Grira 99 BG8	20.65	118.00	0.028	0.066	7.17	5.71
172	Saatcioglu & Grira 99 BG9	12.41	116.00	0.045	0.069	7.05	9.35
173	Saatcioglu & Grira 99 BG10	13.60	99.51	0.032	0.057	6.05	7.31
174	Matamoros 1999, C10-05N	10.65	38.61	0.015	0.058	6.33	3.62
175	Matamoros 1999, C10-05S	10.13	38.10	0.015	0.058	6.25	3.76
176	Matamoros 1999, C10-10N	8.95	44.45	0.015	0.073	7.29	4.97
177	Matamoros 1999, C10-10S	9.09	44.70	0.015	0.073	7.33	4.92
178	Matamoros 1999, C10-20N	10.29	38.35	0.017	0.058	6.29	3.73
179	Matamoros 1999, C10-20S	9.27	38.10	0.020	0.059	6.25	4.11
180	Matamoros 1999, C5-00N	11.78	38.86	0.009	0.056	6.37	3.30
181	Matamoros 1999, C5-00S	12.86	38.90	0.008	0.054	6.38	3.03
182	Matamoros 1999, C5-20N	10.56	32.30	0.014	0.045	5.30	3.06
183	Matamoros 1999, C5-20S	10.89	32.00	0.014	0.044	5.25	2.94
184	Matamoros 1999, C5-40N	8.24	26.40	0.015	0.037	4.33	3.21

Table A.5—*Continued*

Test #	Test Name	D_y	$D_{20\%}$	$e_{20\%}$	$\theta_{p\_20\%}$	$\dfrac{D_{20\%}}{L}$	$\dfrac{D_{20\%}}{D_y}$
185	Matamoros 1999, C5-40S	8.09	25.40	0.014	0.036	4.16	3.14
186	Mo & Wang 2000, C1-1	14.95	88.39	0.024	0.059	6.31	5.91
187	Mo & Wang 2000, C1-2	14.80	96.57	0.029	0.066	6.90	6.53
188	Mo & Wang 2000, C1-3	14.87	88.10	0.028	0.059	6.29	5.92
189	Mo & Wang 2000, C2-1	16.71	98.02	0.026	0.066	7.00	5.87
190	Mo & Wang 2000, C2-2	15.63	94.86	0.028	0.064	6.78	6.07
191	Mo & Wang 2000, C2-3	13.46	77.02	0.024	0.051	5.50	5.72
192	Mo & Wang 2000, C3-1	17.91	93.81	0.024	0.061	6.70	5.24
193	Mo & Wang 2000, C3-2	17.92	104.49	0.031	0.070	7.46	5.83
194	Mo & Wang 2000, C3-3	15.43	99.02	0.032	0.067	7.07	6.42
201	Thomsen & Wallace 1994, A3	3.53	20.24	0.012	0.032	3.39	5.73
203	Thomsen & Wallace 1994, B2	4.56	14.63	0.006	0.019	2.45	3.21
204	Thomsen & Wallace 1994, B3	3.96	13.78	0.008	0.019	2.31	3.48
206	Thomsen & Wallace 1994, C2	4.78	29.83	0.012	0.048	5.00	6.24
207	Thomsen & Wallace 1994, C3	5.59	19.05	0.010	0.026	3.19	3.41
208	Thomsen & Wallace 1994, D1	4.57	18.89	0.010	0.027	3.16	4.14
209	Thomsen & Wallace 1994, D2	5.11	11.86	0.006	0.013	1.99	2.32
210	Thomsen & Wallace 1994, D3	5.63	12.06	0.006	0.012	2.02	2.14
214	Paultre et al 00 1006015	27.89	182.76	0.019	0.085	9.14	6.55
215	Paultre et al 00 1006025	20.30	144.46	0.026	0.068	7.22	7.12
216	Paultre et al 00 1006040	21.77	63.20	0.010	0.023	3.16	2.90
217	Paultre et al 00 10013015	28.80	91.05	0.010	0.034	4.55	3.16
218	Paultre et al 00 10013025	18.74	48.27	0.008	0.016	2.41	2.57
219	Paultre et al 00 10013040	16.07	29.90	0.005	0.008	1.50	1.86
220	Paultre et al 01 806040	15.80	174.41	0.038	0.087	8.72	11.04
221	Paultre et al 01 1206040	16.15	122.09	0.032	0.058	6.10	7.56
222	Paultre et al 01 1005540	18.98	97.98	0.016	0.043	4.90	5.16
223	Paultre et al 01 1008040	21.03	52.55	0.008	0.017	2.63	2.50
224	Paultre et al 01 1005552	13.59	66.37	0.014	0.029	3.32	4.88
225	Paultre et al 01 1006052	15.70	66.06	0.014	0.028	3.30	4.21
226	Pujol 2002, 10-2-3N	6.67	21.85	0.008	0.027	3.19	3.27
227	Pujol 2002, 10-2-3S	7.29	20.94	0.007	0.024	3.05	2.87
228	Pujol 2002, 10-3-1.5N	6.82	27.91	0.012	0.037	4.07	4.09
229	Pujol 2002, 10-3-1.5S	6.59	28.76	0.012	0.039	4.19	4.36
230	Pujol 2002, 10-3-3N	7.00	21.49	0.009	0.026	3.13	3.07
231	Pujol 2002, 10-3-3S	6.57	21.59	0.009	0.027	3.15	3.28
232	Pujol 2002, 10-3-2.25N	6.69	20.95	0.009	0.025	3.05	3.13
233	Pujol 2002, 10-3-2.25S	6.84	22.07	0.010	0.027	3.22	3.23
236	Pujol 2002, 20-3-3N	6.52	22.85	0.013	0.029	3.33	3.51
237	Pujol 2002, 20-3-3S	6.85	23.01	0.013	0.029	3.36	3.36
238	Pujol 2002, 10-2-2.25N	6.31	22.01	0.009	0.028	3.21	3.49
239	Pujol 2002, 10-2-2.25S	6.21	21.73	0.009	0.028	3.17	3.50
240	Pujol 2002, 10-1-1.25N	6.28	22.05	0.009	0.028	3.21	3.51
241	Pujol 2002, 10-1-1.25S	6.48	21.53	0.008	0.027	3.14	3.32
242	Bechtoula-Kono 2002 D1N30	3.44	24.75	0.023	0.040	3.96	7.20
243	Bechtoula-Kono 2002 D1N60	2.58	18.73	0.027	0.030	3.00	7.25
245	Bechtoula-Kono 2002 L1N60	3.80	31.27	0.028	0.026	2.61	8.24

Table A.5—*Continued*

Test #	Test Name	D_y	$D_{20\%}$	$e_{20\%}$	$\theta_{p\_20\%}$	$\dfrac{D_{20\%}}{L}$	$\dfrac{D_{20\%}}{D_y}$
247	Takemura-Kawashima 1997 #1	7.85	43.71	0.015	0.031	3.51	5.57
248	Takemura-Kawashima 1997 #2	10.95	48.50	0.016	0.033	3.90	4.43
249	Takemura-Kawashima 1997 #3	8.38	74.18	0.032	0.057	5.96	8.86
250	Takemura-Kawashima 1997 #4	8.47	101.44	0.051	0.081	8.15	11.98
251	Takemura-Kawashima 1997 #5	7.48	84.52	0.038	0.067	6.79	11.31
257	Xaio & Yun 02, No.FHC5-0.2	14.06	105.28	0.026	0.059	5.92	7.49
259	Bayrak & Sheikh 02 RS- 9HT	18.99	111.42	0.025	0.055	7.56	5.87
260	Bayrak & Sheikh 02 RS-10HT	13.44	55.61	0.014	0.025	3.78	4.14
262	Bayrak & Sheikh 02 RS-12HT	15.42	62.18	0.016	0.028	4.22	4.03
263	Bayrak & Sheikh 02 RS-13HT	16.38	74.00	0.018	0.034	5.02	4.52
264	Bayrak & Sheikh 02 RS-14HT	27.80	55.54	0.010	0.017	3.77	2.00
265	Bayrak & Sheikh 02 RS-15HT	29.12	92.74	0.018	0.038	6.30	3.18
266	Bayrak & Sheikh 02 RS-16HT	23.84	55.77	0.011	0.019	3.79	2.34
267	Bayrak & Sheikh 02 RS-17HT	29.52	83.44	0.014	0.032	5.66	2.83
268	Bayrak & Sheikh 02 RS-18HT	16.68	36.25	0.007	0.012	2.46	2.17
269	Bayrak & Sheikh 02 RS-19HT	16.46	67.09	0.015	0.030	4.56	4.08
270	Bayrak & Sheikh 02 RS-20HT	21.10	61.15	0.011	0.024	4.15	2.90
271	Bayrak &Sheikh 02 WRS-21HT	27.63	62.24	0.009	0.021	4.23	2.25
272	Bayrak &Sheikh 02 WRS-22HT	32.39	114.98	0.017	0.050	7.81	3.55
273	Bayrak &Sheikh 02 WRS-23HT	31.66	118.00	0.018	0.052	8.01	3.73
274	Bayrak &Sheikh 02 WRS-24HT	25.58	45.66	0.006	0.012	3.10	1.79
162	Mean	11.3	54.0	0.019	0.039	4.46	5.13
	STD	7.2	36.9	0.010	0.022	2.03	2.37
	COV	0.63	0.68	0.521	0.556	0.46	0.46

Table A.6 Deformations at 20% Reduction in Flexural Strength, Spiral Columns

Test #	Test Name	D_y	$D_{20\%}$	$e_{20\%}$	$\theta_{p\_20\%}$	$\frac{D_{20\%}}{L}$	$\frac{D_{20\%}}{D_y}$
1	Davey 1975, No. 1	25.11	172.93	0.031	0.057	8.65	6.89
3	Davey 1975, No. 3	41.49	157.22	0.020	0.037	7.86	3.79
8	Ang '81 No. 2	8.92	50.09	0.028	0.028	3.13	5.62
22	Ang et. al. 1985 No. 9	14.22	65.58	0.039	0.058	6.56	4.61
39	Zahn '86 No. 5	9.59	68.59	0.023	0.040	4.29	7.15
40	Zahn '86 No. 6	6.45	59.04	0.032	0.035	3.69	9.15
41	Watson & Park 1989, No 10	8.08	32.54	0.015	0.017	2.03	4.03
42	Watson & Park 1989, No 11	6.35	29.00	0.015	0.016	1.81	4.57
43	Wong et al. 1990, No. 1	5.87	41.43	0.037	0.051	5.18	7.05
45	Wong et al. 1990, No. 3	4.32	28.82	0.031	0.036	3.60	6.67
50	McLean 1990 Con1	30.54	89.54	0.019	0.057	7.85	2.93
52	McLean 1990 Con3	10.43	45.59	0.032	0.073	8.00	4.37
53	NIST Full Scale Flexure	109.63	540.99	0.026	0.050	5.92	4.93
54	NIST Full Scale Shear	41.27	355.70	0.039	0.076	7.78	8.62
55	NIST Model N1	7.39	82.50	0.064	0.110	11.00	11.16
56	NIST Model N2	6.16	60.41	0.051	0.079	8.06	9.80
57	NIST Model N3	16.10	110.64	0.038	0.066	7.38	6.87
58	NIST Model N4	4.89	54.69	0.042	0.073	7.29	11.19
59	NIST Model N5	6.31	52.60	0.043	0.068	7.01	8.34
60	NIST Model N6	14.35	123.09	0.045	0.076	8.21	8.58
63	BRI No. 3 (Japan) ws22bs	2.51	24.48	0.052	0.050	4.90	9.75
66	BRI No. 3 (Japan) ws27bs	3.45	39.41	0.060	0.086	7.88	11.43
93	Kunnath 1997 No. A2	13.94	77.20	0.025	0.049	5.63	5.54
95	Kunnath 1997 No. A4	15.29	58.56	0.017	0.034	4.27	3.83
96	Kunnath 1997 No. A5	16.84	76.35	0.023	0.047	5.56	4.53
97	Kunnath 1997 No. A6	13.53	95.49	0.032	0.064	6.96	7.06
100	Kunnath 1997 No. A9	11.87	90.54	0.031	0.062	6.60	7.63
101	Kunnath 1997 No. A10	12.05	90.66	0.032	0.061	6.61	7.52
102	Kunnath 1997 No. A11	12.70	102.16	0.036	0.070	7.45	8.04
103	Kunnath 1997 No. A12	11.24	102.43	0.036	0.071	7.47	9.12
106	Hose et al. 1997 No. SRPH1	39.88	319.79	0.042	0.081	8.74	8.02
107	Vu et al. 1998 No. NH1	6.47	38.13	0.035	0.040	4.19	5.89
109	Vu et al. 1998 No. NH3	6.13	50.33	0.041	0.055	5.53	8.22
112	Vu et al. 1998 No. NH6	7.77	87.47	0.070	0.103	9.61	11.26
115	Kowalsky 1996 No. FL3	60.92	281.60	0.041	0.063	7.70	4.62
116	Lehman No.415	17.60	178.00	0.034	0.070	7.30	10.11
117	Lehman No.815	64.81	446.00	0.040	0.081	9.15	6.88
118	Lehman No.1015	109.46	639.83	0.044	0.089	10.50	5.85
119	Lehman No.407	13.57	128.00	0.021	0.050	5.25	9.43
120	Lehman No.430	26.18	178.00	0.040	0.067	7.30	6.80
121	Lehman & Calderone No.328	14.88	133.00	0.041	0.071	7.27	8.94
123	Lehman & Calderone No.1028	95.47	891.54	NaN	0.135	14.63	9.34
130	Saatcioglu No.RC4	12.67	54.75	0.014	0.028	3.33	4.32
133	Saatcioglu No.RC8	13.47	75.78	0.019	0.041	4.61	5.63
136	Nelson & Price 2000 Col2	9.74	56.59	0.030	0.034	3.71	5.81
139	Henry 1998 No. 415p	25.78	178.84	0.039	0.067	7.33	6.94

Table A.6—*Continued*

Test #	Test Name	D_y	$D_{20\%}$	$e_{20\%}$	$\theta_{p\_20\%}$	$\dfrac{D_{20\%}}{L}$	$\dfrac{D_{20\%}}{D_y}$
140	Henry 1998 No. 415s	23.62	128.93	0.025	0.046	5.29	5.46
141	Chai et al. 1991 TEST 3	29.11	137.64	0.034	0.031	3.76	4.73
142	Soderstrom 2001 C1	23.79	199.01	0.032	0.098	10.11	8.37
143	Soderstrom 2001 C2	21.15	223.70	0.037	0.113	11.36	10.57
150	Kowalsky & Moyer 2001 No.1	37.91	184.02	0.020	0.066	7.55	4.85
151	Kowalsky & Moyer 2001 No.2	41.12	258.09	0.029	0.098	10.58	6.28
152	Kowalsky & Moyer 2001 No.3	36.72	260.51	0.030	0.101	10.68	7.09
153	Kowalsky & Moyer 2001 No.4	40.39	320.58	0.038	0.126	13.15	7.94
154	Coffman et al. 1993 Col1	17.40	109.40	0.022	0.034	3.82	6.29
155	Hamilton 2002 UCI1	16.93	114.30	0.017	0.056	6.16	6.75
156	Hamilton 2002 UCI2	17.93	124.92	0.019	0.062	6.74	6.97
160	Hamilton 2002 UCI6	13.59	205.00	0.035	0.111	11.06	15.08
58	Mean	23.0	154.9	0.033	0.064	6.98	7.23
58	STD	23.6	158.7	0.012	0.027	2.67	2.38
58	COV	1.03	1.02	0.359	0.415	0.38	0.33

Appendix B: Observed Trends in 20% Reduction in Flexural Strength
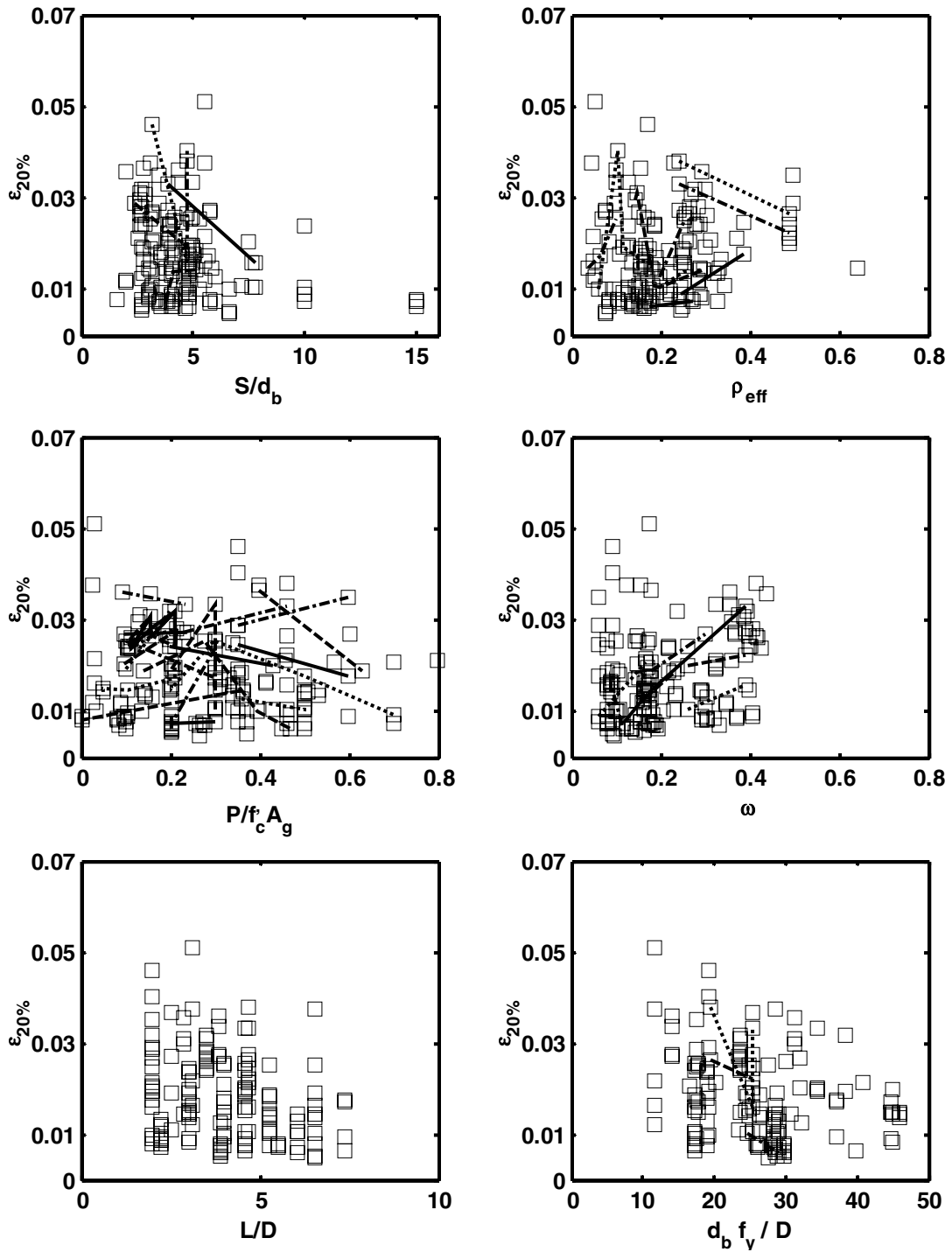
Figure B.1   Trends in Nominal Compressive Strain at 20% Reduction of Flexural Strength, Rectangular Columns
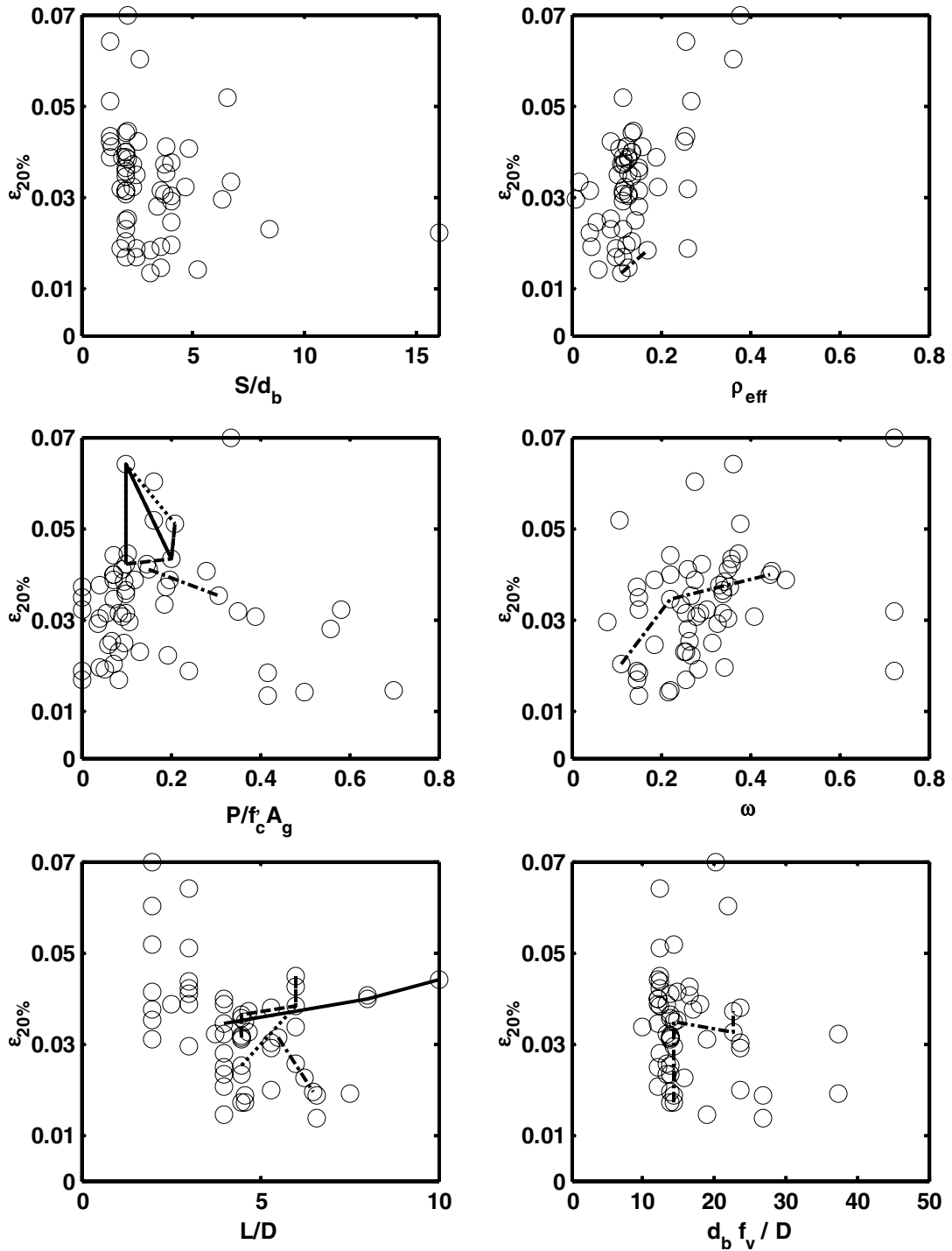
Figure B.2   Trends in Nominal Compressive Strain at 20% Reduction of Flexural Strength, Spiral Columns
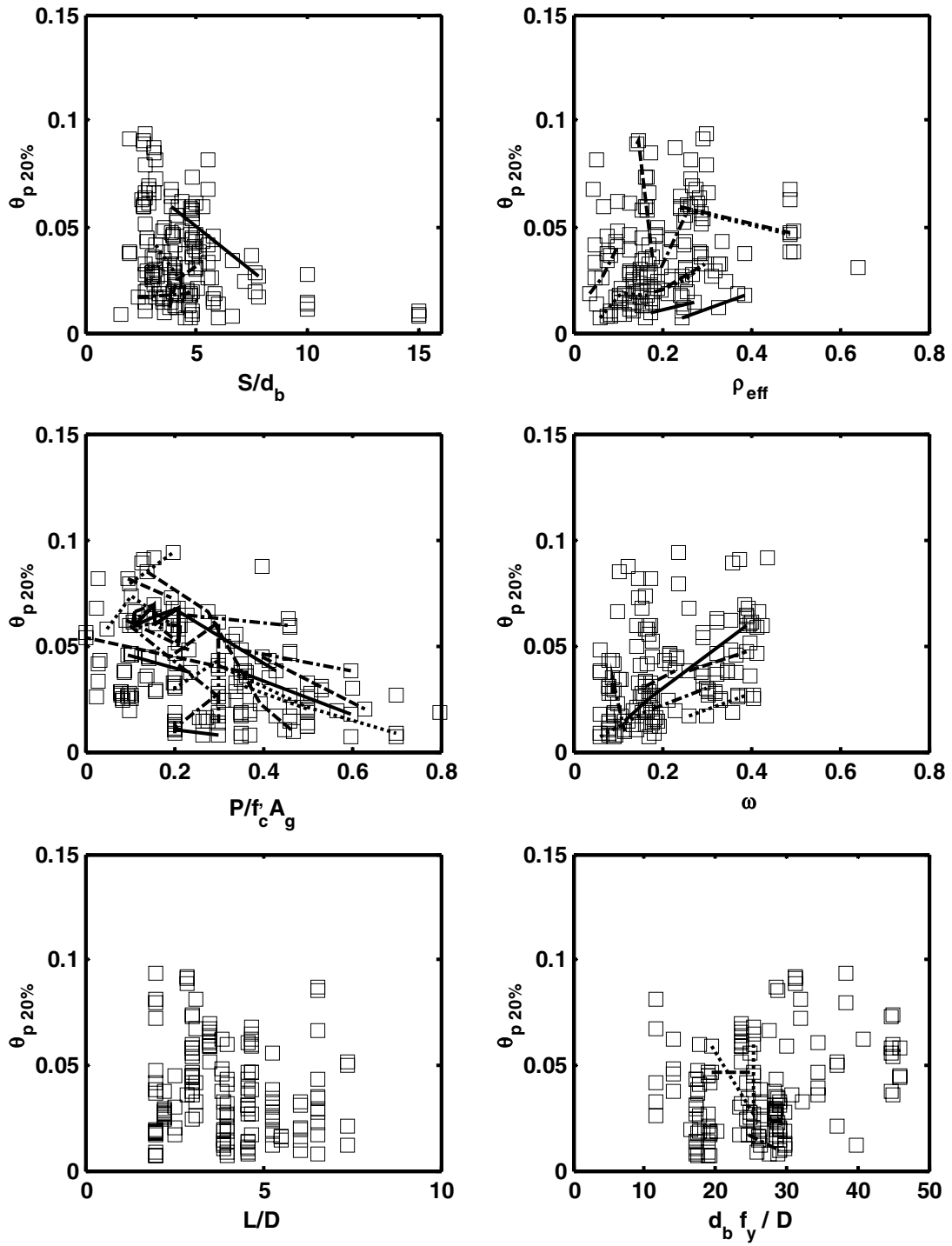
Figure B.3   Trends in Nominal Plastic Rotation at 20% Reduction of Flexural Strength, Rectangular Columns
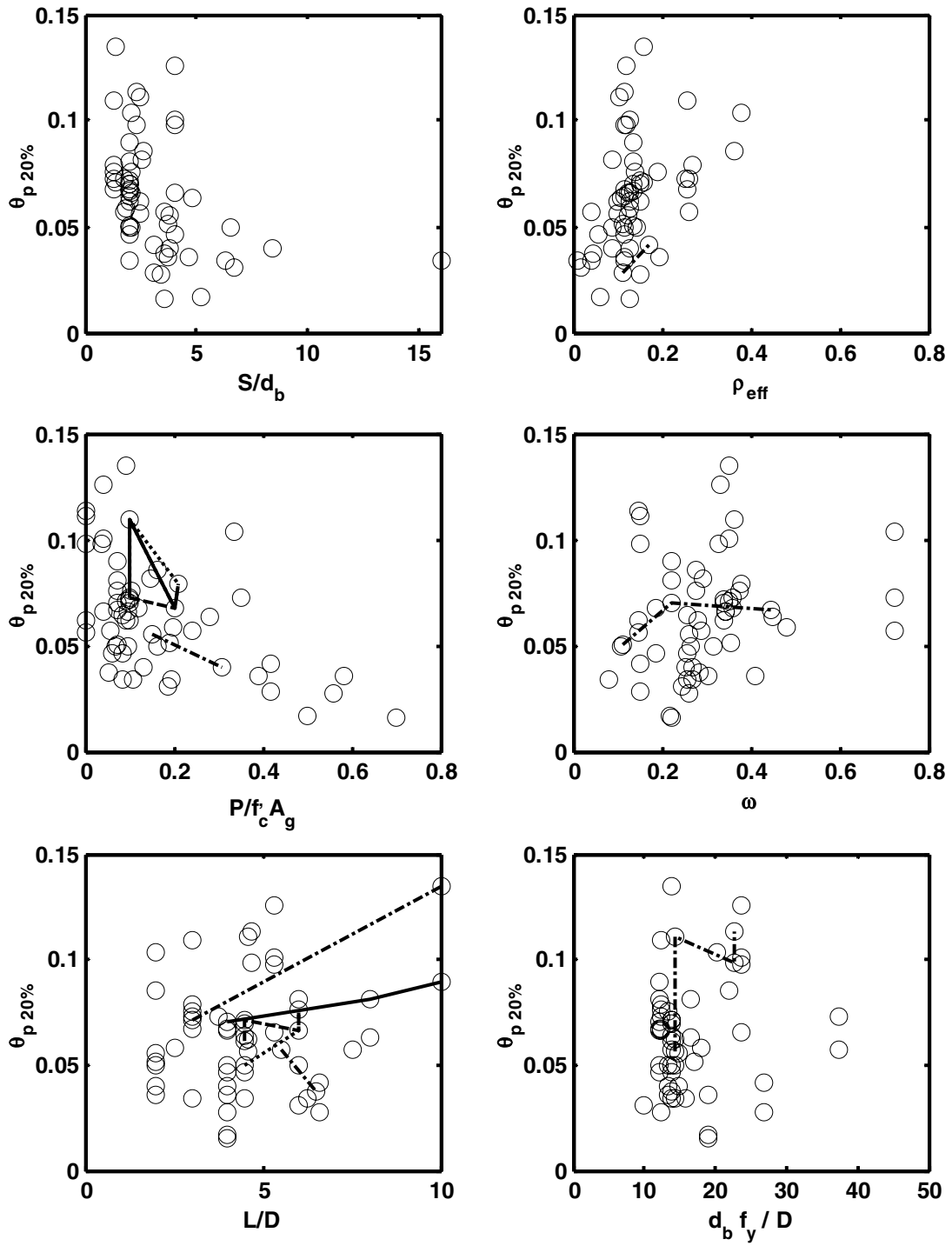
Figure B.4 Trends in Nominal Plastic Rotation at 20% Reduction of Flexural Strength, Spiral Columns
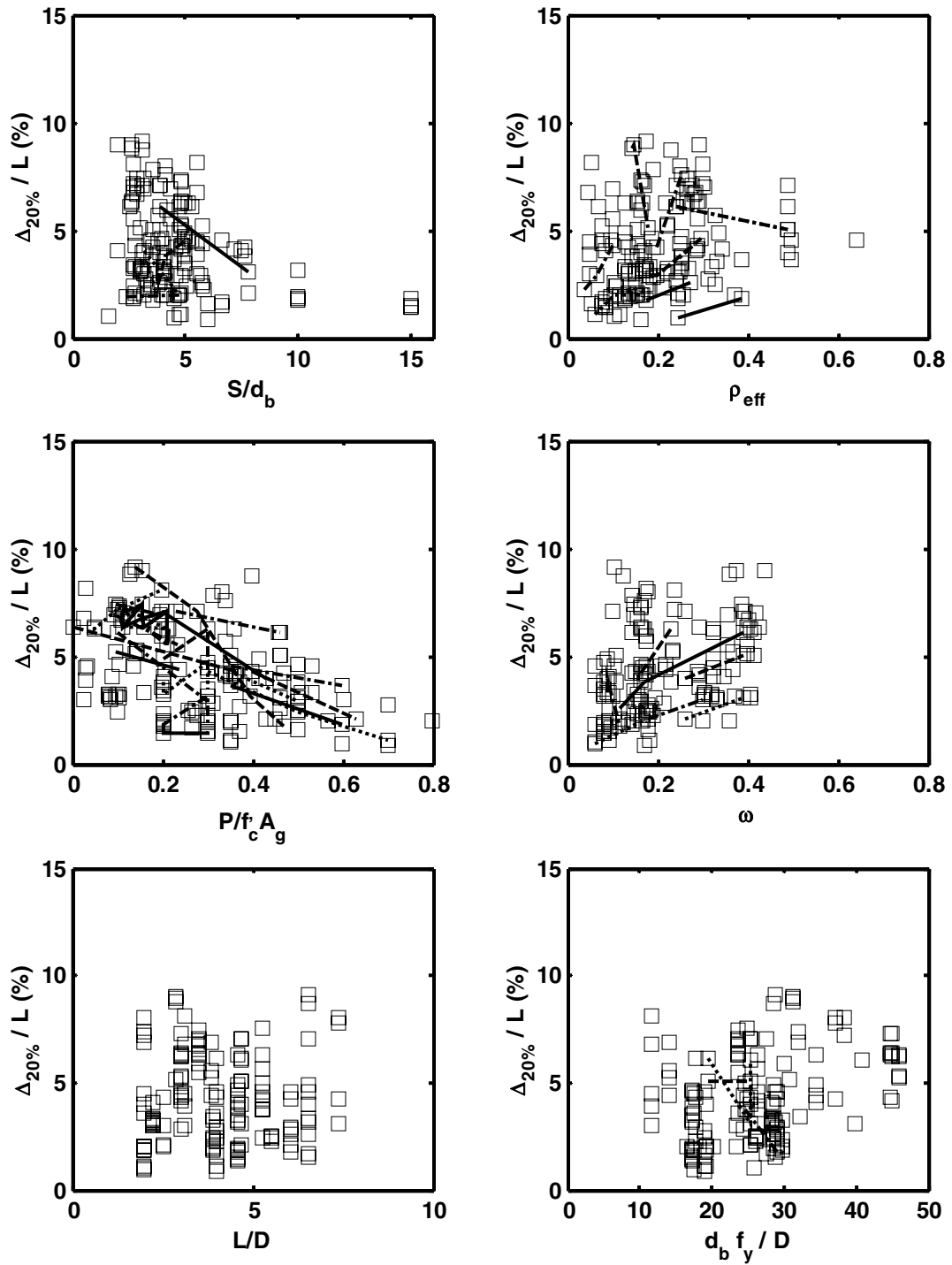
Figure B.5   Trends in Drift Ratio at 20% Reduction of Flexural Strength, Rectangular Columns
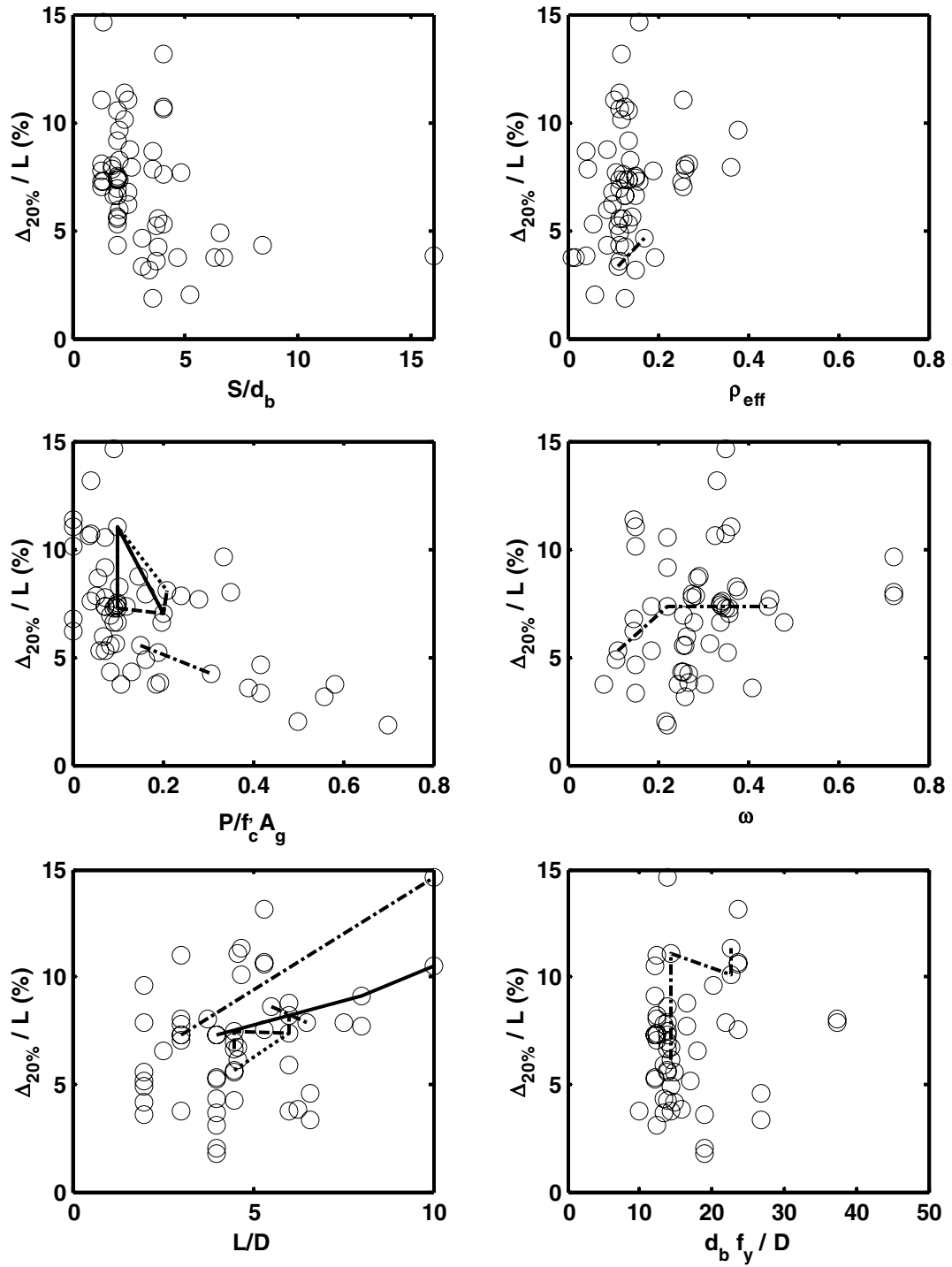
Figure B.6   Trends in Drift Ratio at 20% Reduction of Flexural Strength, Spiral Columns
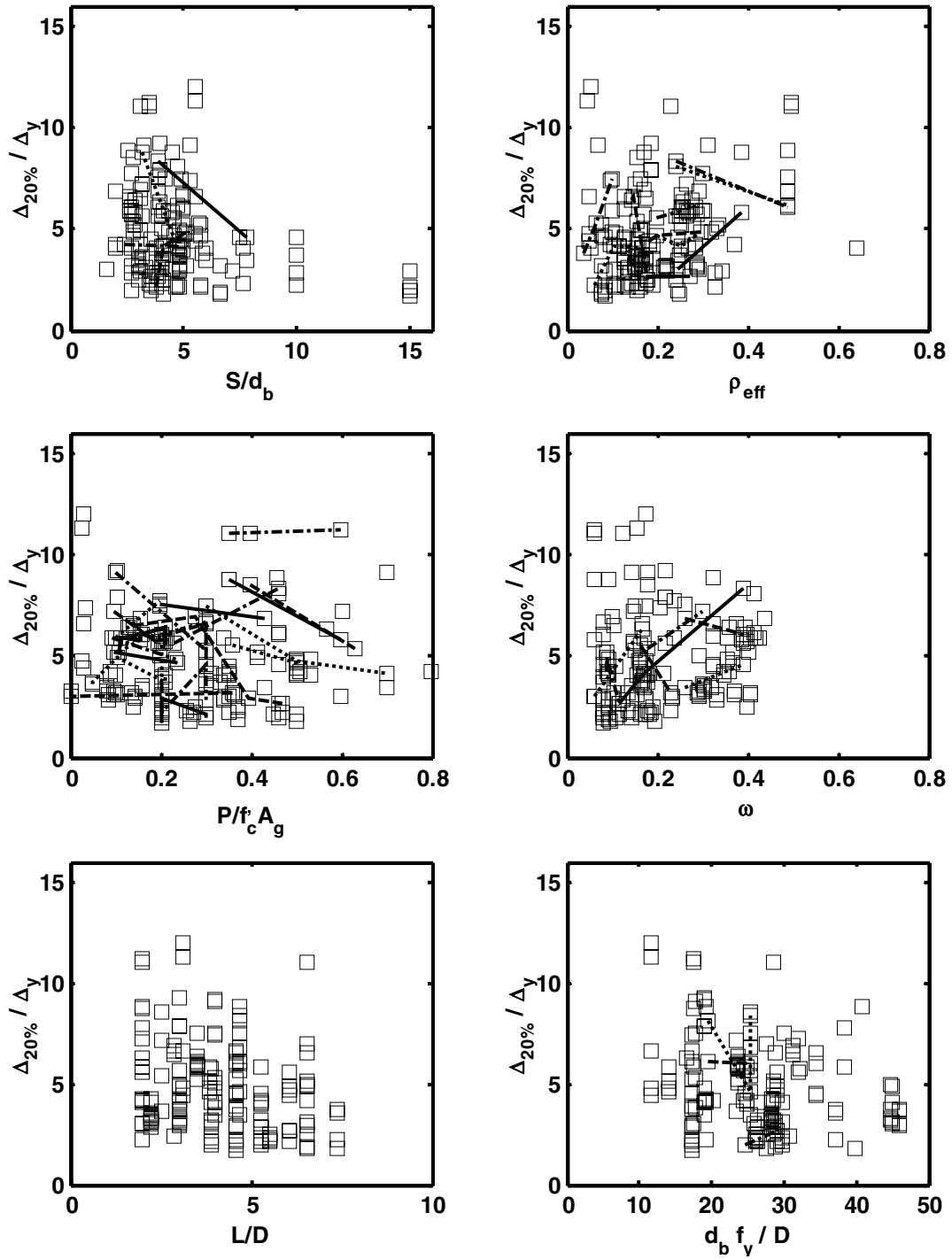
Figure B.7   Trends in Displacement Ductility at 20% Reduction of Flexural Strength, Rectangular Columns
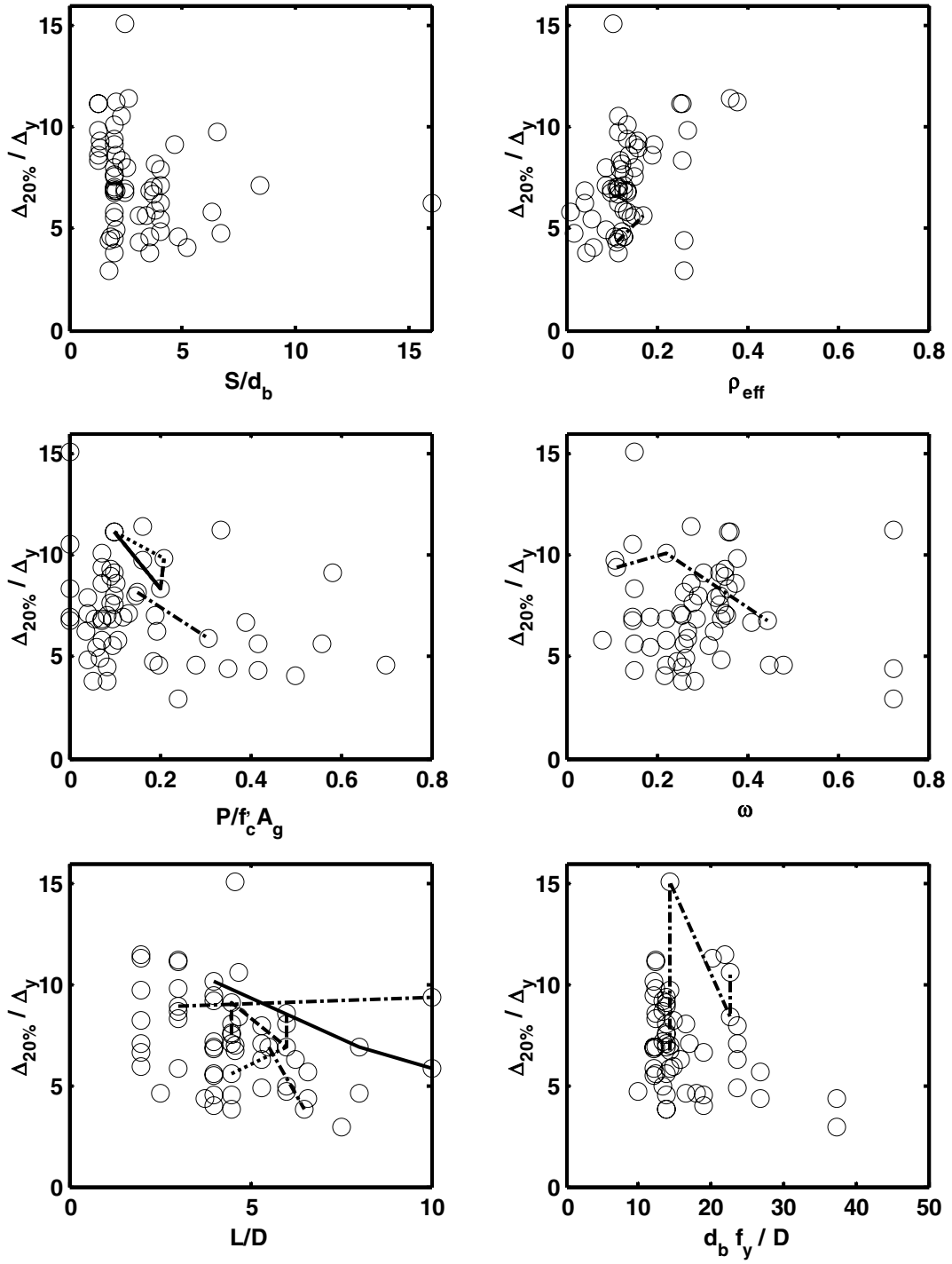
Figure B.8   Trends in Displacement Ductility at 20% Reduction of Flexural Strength, Spiral Columns

Appendix C: Regression Results for Longitudinal Bar Buckling

Table C.1   One-Variable Regression Results for ε_{bb}, Rectangular Columns

	$e_{bb} = A(1 + B * prop1\text{^}C)$				
Property	prop1	r_{eff}	P/fcAg	dbfy/D	S/db
Coefficients	A	0.014	0.013	0.013	0.049
	B	0.921	0.091	0.193	-0.709
	C	4.077	0.098	-0.124	0.000
Statistics of D_{BB}/D_{calc}	Min	0.318	0.316	0.316	0.316
	Max	1.659	1.681	1.690	1.688
	Mean	1.056	1.057	1.058	1.057
	COV	0.262	0.266	0.266	0.267

Table C.2   Two-Variable Regression Results for ε_{bb}, Rectangular Columns

	$e_{bb} = A(1 + B * prop1\text{^}C)(1 + D * prop2\text{^}E)$				
Property	prop1	P/fcAg	r_{eff}	r_{eff}	P/fcAg
	prop2	dbfy/D	dbfy/D	w	w
Coefficients	A	0.011	0.014	0.012	0.003
	B	0.000	7.945	2.349	3.245
	C	-5.943	7.313	5.613	0.058
	D	61.616	-2.411	2.929	4.027
	E	-1.616	-9.360	2.001	2.355
Statistics of D_{BB}/D_{calc}	Min	0.332	0.317	0.318	0.321
	Max	1.721	1.662	1.730	1.725
	Mean	1.059	1.056	1.057	1.057
	COV	0.256	0.259	0.262	0.264

Table C.3   Three-Variable Regression Results for ε_{bb}, Rectangular Columns

	$e_{bb} = A(1 + B * Var1\text{^}C)(1 + D * Var2\text{^}E)(1 + F * Var2\text{^}G)$				
Propertys	Var1	S/db	r_{eff}	r_{eff}	r_{eff}
	Var2	P/fcAg	P/fcAg	P/fcAg	S/db
	Var3	dbfy/D	w	dbfy/D	P/fcAg
Coefficients	A	0.010	0.010	27.564	0.459
	B	0.662	0.183	-1.000	-0.993
	C	-2.227	-0.373	0.000	0.001
	D	0.000	0.000	196.669	3.500
	E	-6.148	-3.657	0.080	-0.158
	F	1.991	15.777	1959.556	0.000
	G	-0.442	3.717	-3.030	-3.100
Statistics of D_{BB}/D_{calc}	Min	0.323	0.308	0.348	0.307
	Max	1.673	1.870	1.673	1.842
	Mean	1.058	1.061	1.056	1.061
	COV	0.255	0.258	0.259	0.261

Table C.4   One-Variable Regression Results for ε_{bb} , Spiral Columns

		e_{bb} = A(1 + B * Var1^C)			
Variable	Var1	S/db	w	L/D	r_{eff}
Coefficients	A	0.022	0.019	0.023	0.018
	B	2.392	10.945	0.000	5.553
	C	-5.239	2.968	5.758	1.313
Statistics of D_{BB}/D_{calc}	Min	0.554	0.512	0.528	0.549
	Max	1.599	1.698	1.834	1.722
	Mean	0.992	0.981	1.002	0.989
	COV	0.241	0.245	0.254	0.260

Table C.5   Two-Variable Regression Results for ε_{bb} , Spiral Columns

		e_{bb} = A(1 + B * prop1^C)(1 + D * prop2^E)			
Properties	prop1	L/D	L/D	L/D	S/db
	prop2	r_{eff}	S/db	w	w
Coefficients	A	0.019	0.021	0.018	0.019
	B	0.000	0.000	0.000	1.750
	C	4.585	4.420	6.034	-4.387
	D	50.937	5.565	12.600	8.266
	E	3.078	-9.652	3.246	3.613
Statistics of D_{BB}/D_{calc}	Min	0.591	0.572	0.540	0.589
	Max	1.427	1.413	1.652	1.493
	Mean	1.000	1.001	0.997	0.989
	COV	0.206	0.207	0.213	0.219

Table C.6   Three-Variable Regression Results for ε_{bb} , Spiral Columns

		e_{bb} = A(1 + B * Var1^C)(1 + D * Var2^E)(1 + F * Var2^G)			
Variables	Var1	L/D	L/D	L/D	L/D
	Var2	S/db	r_{eff}	r_{eff}	S/db
	Var3	w	w	S/db	P/fcAg
Coefficients	A	0.019	0.018	0.019	0.006
	B	0.000	0.000	0.000	0.000
	C	5.289	5.245	4.450	4.034
	D	4.499	32.169	10.115	4.066
	E	-9.761	2.947	2.288	-8.300
	F	7.309	17.311	1.162	2.767
	G	3.405	4.467	-7.215	0.076
Statistics of D_{BB}/D_{calc}	Min	0.589	0.586	0.589	0.569
	Max	1.441	1.467	1.431	1.435
	Mean	0.998	0.999	1.001	1.001
	COV	0.186	0.190	0.205	0.206

Table C.7   One-Variable Regression Results for θ_{p_bb}, Rectangular Columns

	θ_{p_bb} = A(1 + B * prop1^C)			
Property	prop1	S/db	dbfy/D	L/D	r_{eff}
	A	0.026	0.023	0.047	0.000
Coefficients	B	12.854	0.009	9523.660	758.844
	C	-1.864	1.479	-13.671	0.322
	Min	0.320	0.329	0.376	0.384
Statistics of D_{BB}/D_{calc}	Max	1.534	1.569	1.637	1.737
	Mean	1.000	1.000	1.000	1.000
	COV	0.266	0.282	0.291	0.297

Table C.8   Two-Variable Regression Results for θ_{p_bb}, Rectangular Columns

	θ_{p_bb} = A(1 + B * prop1^C)(1 + D * prop2^E)			
Properties	prop1	S/db	r_{eff}	L/D	S/db
	prop2	dbfy/D	S/db	S/db	w
	A	0.004	0.001	0.000	0.056
	B	6.470	58.639	1650.183	13.187
Coefficients	C	-1.325	0.155	-12.289	-1.795
	D	1.321	9.728	1157.044	-0.493
	E	0.438	-1.868	-0.653	-0.087
	Min	0.313	0.336	0.333	0.337
Statistics of D_{BB}/D_{calc}	Max	1.532	1.514	1.541	1.548
	Mean	1.000	1.000	1.000	1.000
	COV	0.259	0.260	0.262	0.265

Table C.9   Three-Variable Regression Results for θ_{p_bb}, Rectangular Columns

	θ_{p_bb} = A(1 + B * prop1^C)(1 + D * prop2^E)(1 + F * prop3^G)			
	prop1	r_{eff}	S/db	r_{eff}	S/db
Properties	prop2	P/fcAg	w	S/db	P/fcAg
	prop3	dbfy/D	dbfy/D	P/fcAg	dbfy/D
	A	0.002	0.003	0.000	0.002
	B	12.322	14.178	41.079	6.162
	C	5.077	-0.834	0.240	-0.767
Coefficients	D	-1.398	0.000	5.305	-0.440
	E	1.759	-3.619	-1.279	0.732
	F	2.369	0.422	116.875	1.267
	G	0.807	0.585	-0.176	0.549
	Min	0.352	0.395	0.380	0.341
Statistics of D_{BB}/D_{calc}	Max	1.615	1.506	1.545	1.574
	Mean	1.000	1.000	1.000	1.000
	COV	0.244	0.248	0.253	0.253

Table C.10   One-Variable Regression Results for θ_{p_bb} , Spiral Columns

			θ_{p_bb} = A(1 + B * prop1^C)		
Property	prop1	L/D	P/fcAg	w	r $_{eff}$
	A	0.050	3.6E-05	0.023	0.004
Coefficients	B	0.001	743.285	5.235	24.952
	C	2.921	-0.347	0.973	0.330
	Min	0.431	0.503	0.453	0.384
Statistics of	Max	1.811	1.926	1.821	1.860
D_{BB}/D_{calc}	Mean	1.000	1.000	1.000	1.000
	COV	0.310	0.316	0.331	0.335

Table C.11   Two-Variable Regression Results for θ_{p_bb} , Spiral Columns

			θ_{p_bb} = A(1 + B * prop1^C)(1 + D * prop2^E)		
Properties	prop1	L/D	L/D	S/db	P/fcAg
	prop2	P/fcAg	r $_{eff}$	P/fcAg	w
	A	0.086	0.024	0.036	0.187
	B	0.000	0.049	2.004	-0.943
Coefficients	C	3.889	1.577	-1.929	0.074
	D	-0.891	6.999	0.000	5.423
	E	0.390	1.260	-4.600	1.830
	Min	0.515	0.438	0.542	0.536
Statistics of	Max	1.702	1.712	1.724	1.733
D_{BB}/D_{calc}	Mean	1.000	1.000	1.000	1.000
	COV	0.256	0.270	0.273	0.273

Table C.12   Three-Variable Regression Results for θ_{p_bb} , Spiral Column

			θ_{p_bb} = A(1 + B * prop1^C)(1 + D * prop2^E)(1 + F * prop3^G)		
	prop1	L/D	L/D	L/D	L/D
Properties	prop2	r $_{eff}$	S/db	P/fcAg	S/db
	prop3	P/fcAg	P/fcAg	w	dbfy/D
	A	0.111	0.032	0.079	0.008
	B	0.003	0.006	2.6E-04	0.001
	C	2.650	2.233	3.595	3.156
Coefficients	D	6.155	1.662	-0.874	5.263
	E	1.081	-2.456	0.190	-0.710
	F	-0.923	0.000	4.995	0.001
	G	0.098	-4.387	1.825	2.421
	Min	0.606	0.568	0.565	0.411
Statistics of	Max	1.483	1.485	1.540	1.516
D_{BB}/D_{calc}	Mean	1.000	1.000	1.000	1.000
	COV	0.206	0.217	0.219	0.238

Table C.13   One-Variable Regression Results for $\dfrac{\Delta_{bb}}{L}$, Rectangular Columns

		D_{bb}/L (%) = A(1 + B * prop1^C)			
Property	prop1	S/db	dbfy/D	L/D	P/fcAg
Coefficients	A	2.753	0.859	4.768	7.109
	B	7.820	0.737	18654.2345	-0.658
	C	-1.605	0.578	-15.128	0.624
Statistics of D_{BB}/D_{calc}	Min	0.261	0.273	0.303	0.345
	Max	1.481	1.583	1.678	1.669
	Mean	1.000	1.000	1.000	1.000
	COV	0.278	0.305	0.306	0.309

Table C.14   Two-Variable Regression Results for $\dfrac{\Delta_{bb}}{L}$, Rectangular Columns

		D_{bb}/L (%) = A(1 + B * prop1^C)(1 + D * prop2^E)			
Properties	prop1	r_{eff}	S/db	S/db	r_{eff}
	prop2	P/fcAg	P/fcAg	w	S/db
Coefficients	A	0.002	1.833	0.001	1.971
	B	5838.930	7.497	9.034	0.717
	C	0.348	-0.971	-1.586	0.248
	D	-1.135	-2.725	4240.202	6.546
	E	1.302	3.872	0.206	-1.593
Statistics of D_{BB}/D_{calc}	Min	0.410	0.291	0.289	0.270
	Max	1.442	1.552	1.449	1.465
	Mean	1.000	1.000	1.000	1.000
	COV	0.262	0.268	0.269	0.275

Table C.15   Three-Variable Regression Results for $\dfrac{\Delta_{bb}}{L}$, Rectangular Columns

		D_{bb}/L (%) = A(1+B*prop1^C)(1 + D * prop2^E)(1 + F * prop3^G)			
Properties	prop1	r_{eff}	r_{eff}	S/db	S/db
	prop2	P/fcAg	S/db	P/fcAg	P/fcAg
	prop3	dbfy/D	P/fcAg	w	dbfy/D
Coefficients	A	1.011	0.348	0.752	0.039
	B	3.168	3.621	7.517	12.741
	C	2.659	0.357	-1.257	-0.516
	D	-1.575	8.766	-0.998	-0.738
	E	1.829	-0.463	2.269	1.379
	F	0.666	-1.249	3.473	7.565
	G	0.597	1.792	0.283	0.302
Statistics of D_{BB}/D_{calc}	Min	0.384	0.356	0.324	0.299
	Max	1.476	1.448	1.546	1.550
	Mean	1.000	1.000	1.000	1.000
	COV	0.247	0.249	0.258	0.260

Table C.16   One-Variable Regression Results for $\dfrac{\Delta_{bb}}{L}$, Spiral Columns

		D_{bb}/L (%) = A(1 + B * prop1^C)			
Property	prop1	L/D	P/fcAg	r $_{eff}$	w
	A	1.793	8.880	0.275	0.257
Coefficients	B	0.904	-0.974	48.911	48.425
	C	0.695	0.641	0.358	0.547
	Min	0.376	0.435	0.338	0.398
Statistics of	Max	1.953	2.076	2.022	2.009
D_{BB}/D_{calc}	Mean	1.000	1.000	1.000	1.000
	COV	0.354	0.371	0.392	0.393

Table C.17   Two-Variable Regression Results for $\dfrac{\Delta_{bb}}{L}$, Spiral Columns

		D_{bb}/L (%) = A(1 + B * prop1^C)(1 + D * prop2^E)			
Properties	prop1	L/D	L/D	L/D	L/D
	prop2	P/fcAg	r $_{eff}$	w	S/db
	A	9.135	1.956	2.907	2.680
	B	0.000	0.119	0.011	0.214
Coefficients	C	3.441	1.297	2.079	1.130
	D	-0.879	5.569	4.351	10.552
	E	0.374	0.988	1.551	-12.883
	Min	0.501	0.390	0.459	0.418
Statistics of	Max	1.763	1.819	1.735	1.878
D_{BB}/D_{calc}	Mean	1.000	1.000	1.000	1.000
	COV	0.285	0.298	0.310	0.315

Table C.18   Three-Variable Regression Results for $\dfrac{\Delta_{bb}}{L}$, Spiral Columns

		D_{bb}/L (%) = A(1+B * prop1^C)(1+D * prop2^E)(1+F * prop3^G)			
	prop1	L/D	L/D	L/D	L/D
Properties	prop2	r $_{eff}$	S/db	P/fcAg	S/db
	prop3	P/fcAg	P/fcAg	w	dbfy/D
	A	7.151	1.660	9.972	0.649
	B	0.006	0.000	0.001	0.001
	C	2.452	3.644	3.201	3.212
Coefficients	D	5.387	3.347	-0.880	8.708
	E	0.909	-0.651	0.147	-0.572
	F	-0.888	0.000	4.669	0.000
	G	0.160	-4.602	1.839	3.413
	Min	0.592	0.527	0.562	0.364
Statistics of	Max	1.521	1.552	1.575	1.553
D_{BB}/D_{calc}	Mean	1.000	1.000	1.000	1.000
	COV	0.227	0.238	0.242	0.254

Table C.19   One-Variable Regression Results for $\dfrac{\Delta_{bb}}{\Delta_y}$, Rectangular Columns

		D_{bb}/D_y = A(1 + B * prop1^C)			
Property	prop1	L/D	S/db	r $_{eff}$	P/fcAg
Coefficients	A	0.001	0.009	0.029	6.784
	B	19874.297	1288.058	250.288	-0.526
	C	-0.465	-0.457	0.150	1.134
Statistics of D_{BB}/D_{calc}	Min	0.418	0.353	0.389	0.343
	Max	1.738	1.619	1.789	1.685
	Mean	1.000	1.000	1.000	1.000
	COV	0.302	0.305	0.319	0.319

Table C.20   Two-Variable Regression Results for $\dfrac{\Delta_{bb}}{\Delta_y}$, Rectangular Columns

		D_{bb}/D_y = A(1 + B * prop1^C)(1 + D * prop2^E)			
Properties	prop1	S/db	L/D	L/D	r $_{eff}$
	prop2	dbfy/D	r $_{eff}$	S/db	P/fcAg
Coefficients	A	0.110	0.002	0.001	5.029
	B	168.490	3734.538	161.566	1.422
	C	-0.714	-0.492	-0.373	0.926
	D	0.000	0.949	163.388	-1.049
	E	3.717	0.582	-0.342	1.720
Statistics of D_{BB}/D_{calc}	Min	0.322	0.457	0.394	0.383
	Max	1.551	1.763	1.686	1.663
	Mean	1.000	1.000	1.000	1.000
	COV	0.288	0.289	0.290	0.298

Table C.21   Three-Variable Regression Results for $\dfrac{\Delta_{bb}}{\Delta_y}$, Rectangular Columns

		D_{bb}/D_y = A(1+B * prop1^C)(1+D * prop2^E)(1+F * prop3^G)			
Properties	prop1	S/db	L/D	S/db	L/D
	prop3	w	r $_{eff}$	P/fcAg	r $_{eff}$
	prop3	dbfy/D	S/db	w	w
Coefficients	A	0.023	0.000	0.016	0.049
	B	61.644	463.604	19.704	22.562
	C	-0.675	-0.425	-0.553	-0.556
	D	0.000	2.374	34.753	1.151
	E	-5.641	3.543	-0.072	1.157
	F	28.146	194.857	0.000	6.038
	G	-0.310	-0.276	-5.367	-0.155
Statistics of D_{BB}/D_{calc}	Min	0.429	0.417	0.394	0.430
	Max	1.601	1.759	1.570	1.754
	Mean	1.000	1.000	1.000	1.000
	COV	0.282	0.282	0.286	0.286

Table C.22   One-Variable Regression Results for $\dfrac{\Delta_{bb}}{\Delta_y}$, Spiral Columns

	D_{bb}/D_y = A(1 + B * prop1^C)				
Property	prop1	S/db	r $_{eff}$	dbfy/D	L/D
Coefficients	A	5.748	5.713	5.861	3.506
	B	0.761	8.323	12146.477	1.478
	C	-2.138	1.974	-4.339	-0.329
Statistics of D_{BB}/D_{calc}	Min	0.614	0.610	0.555	0.589
	Max	1.497	1.523	1.530	1.570
	Mean	1.000	1.000	1.000	1.000
	COV	0.218	0.221	0.244	0.246

Table C.23   Two-Variable Regression Results for $\dfrac{\Delta_{bb}}{\Delta_y}$, Spiral Columns

	D_{bb}/D_y = A(1 + B * prop1^C)(1 + D * prop2^E)				
Properties	prop1	L/D	r $_{eff}$	r $_{eff}$	S/db
	prop2	S/db	S/db	P/fcAg	P/fcAg
Coefficients	A	3.142	2.929	0.012	2.470
	B	1.062	9.787	7.835	0.802
	C	-0.438	2.718	1.898	-2.717
	D	0.847	1.520	393.960	1.175
	E	-1.028	-0.301	-0.075	-0.078
Statistics of D_{BB}/D_{calc}	Min	0.653	0.620	0.568	0.592
	Max	1.437	1.478	1.472	1.491
	Mean	1.000	1.000	1.000	1.000
	COV	0.209	0.215	0.215	0.216

Table C.24   Three-Variable Regression Results for $\dfrac{\Delta_{bb}}{\Delta_y}$, Spiral Columns

	D_{bb}/D_y = A(1+B * prop1^C)(1+D * pro2^E)(1+F * prop3^G)				
Properties	Var1	L/D	L/D	L/D	L/D
	Var2	S/db	S/db	S/db	r $_{eff}$
	Var3	P/fcAg	dbfy/D	w	S/db
Coefficients	A	2.563	1.103	2.124	2.083
	B	0.906	0.893	0.741	0.767
	C	-1.226	-0.940	-0.905	-0.901
	D	0.717	1.360	0.847	0.916
	E	-1.595	-0.748	-1.210	0.021
	F	0.624	0.945	0.819	0.874
	G	-0.138	0.253	-0.143	-0.905
Statistics of D_{BB}/D_{calc}	Min	0.626	0.656	0.656	0.656
	Max	1.439	1.467	1.428	1.441
	Mean	1.000	1.000	1.000	1.000
	COV	0.204	0.206	0.207	0.209

Appendix D: Regression Results for Cover Spalling

Table D.1   One-Variable Regression Results for ε_{spall} , Rectangular Columns

	e_{spall} = A(1 + B * prop1^C)				
Variable	prop1	L/D	w	P/fcAg	dbfy/D
Coefficients	A	0.005	0.000	0.000	0.005
	B	0.000	111269.745	66.069	0.001
	C	7.098	0.487	-0.063	0.001
Statistics of D_{spall}/D_{calc}	Min	0.239	0.295	0.255	0.250
	Max	1.772	2.144	1.897	1.891
	Mean	0.979	1.003	0.984	0.984
	COV	0.386	0.394	0.417	0.418

Table D.2   Two-Variable Regression Results for ε_{spall} , Rectangular Columns

	e_{spall} = A(1 + B * prop1^C)(1 + D * prop2^E)				
Properties	prop1	L/D	L/D	r_{eff}	L/D
	prop2	w	dbfy/D	w	P/fcAg
Coefficients	A	0.001	0.003	0.010	0.001
	B	30.659	-0.007	0.007	-0.017
	C	-0.935	2.333	-1.402	1.883
	D	0.000	0.424	-0.251	10.221
	E	-2.898	0.320	-0.441	0.095
Statistics of D_{spall}/D_{calc}	Min	0.299	0.207	0.289	0.179
	Max	1.700	1.748	2.035	1.683
	Mean	0.977	0.980	0.991	0.980
	COV	0.356	0.372	0.372	0.376

Table D.3   Three-Variable Regression Results for ε_{spall} , Rectangular Columns

	e_{spall} = A(1 + B * prop1^C)(1 + D * prop2^E)(1 + F * prop3^G)				
Properties	prop1	Cover/D	Cover/D	r_{eff}	L/D
	prop2	w	P/fcAg	Cover/D	Cover/D
	prop3	dbfy/D	w	w	w
Coefficients	A	0.000	0.000	0.000	0.006
	B	-96.191	-627.577	-124.751	-0.001
	C	2.158	3.010	12.016	3.012
	D	849.816	832.758	-114940.530	-7.120
	E	0.852	-0.220	5.369	1.465
	F	75.013	4192.905	1178346.9	212.142
	G	0.776	0.742	0.617	6.395
Statistics of D_{spall}/D_{calc}	Min	0.248	0.289	0.276	0.227
	Max	1.973	2.020	2.043	1.875
	Mean	0.999	1.002	1.005	0.994
	COV	0.349	0.351	0.351	0.358

Table D.4   One-Variable Regression Results for ε_{spall}, Spiral Columns

		e_{spall} = A(1 + B * prop1^C)			
Property	prop1	dbfy/D	w	P/fcAg	r_{eff}
Coefficients	A	0.062	0.001	0.008	0.007
	B	-0.601	26.896	-1.872	56.184
	C	0.141	1.031	1.502	3.367
Statistics of D_{spall}/D_{calc}	Min	0.490	0.440	0.520	0.523
	Max	1.750	1.727	1.757	1.828
	Mean	1.007	1.010	1.007	1.009
	COV	0.349	0.350	0.355	0.363

Table D.5   Two-Variable Regression Results for ε_{spall}, Spiral Columns

		e_{spall} = A(1 + B * prop1^C)(1 + D * prop2^E)			
Properties	prop1	w	Cover/D	P/fcAg	P/fcAg
	prop2	dbfy/D	w	w	dbfy/D
Coefficients	A	0.000	0.001	0.004	0.058
	B	459.338	0.000	-2.567	1.100
	C	0.917	-3.563	2.115	0.000
	D	505.949	41.628	3.826	-0.792
	E	-1.357	0.915	1.193	0.062
Statistics of D_{spall}/D_{calc}	Min	0.490	0.403	0.472	0.486
	Max	1.681	1.688	1.686	1.726
	Mean	1.009	1.010	1.010	1.005
	COV	0.314	0.330	0.332	0.341

Table D.6   Three-Variable Regression Results for ε_{spall}, Spiral Columns

		e_{spall} = A(1 + B * prop1^C)(1 + D * prop2^E)(1 + F * prop3^G)			
Properties	prop1	r_{eff}	L/D	Cover/D	r_{eff}
	prop2	P/fcAg	w	w	P/fcAg
	prop3	dbfy/D	dbfy/D	dbfy/D	w
Coefficients	A	0.029	0.000	0.000	0.000
	B	3.171	-2647.702	293.113	43.718
	C	1.558	-6885.660	0.135	3.504
	D	-1.565	2776.201	526.715	-1.422
	E	1.107	0.907	0.977	1.062
	F	-0.266	1716.471	647.293	74.838
	G	0.374	-1.283	-1.375	0.835
Statistics of D_{spall}/D_{calc}	Min	0.582	0.491	0.488	0.493
	Max	1.661	1.679	1.690	1.680
	Mean	1.008	1.010	1.012	1.008
	COV	0.304	0.313	0.314	0.314

Table D.7   One-Variable Regression Results for θ_{p_spall} , Rectangular Columns

		θ_{p_spall} = A(1 + B * prop1^C)			
Variable	prop1	P/fcAg	w	dbfy/D	Cover/D
Coefficients	A	0.065	0.006	0.001	0.005
	B	-0.973	46016.067	0.628	13.324
	C	0.070	12.151	0.830	1.207
Statistics of D_{spall}/D_{calc}	Min	0.207	0.159	0.172	0.159
	Max	1.874	2.281	2.072	2.145
	Mean	1.000	1.000	1.000	1.000
	COV	0.414	0.434	0.440	0.444

Table D.8   Two-Variable Regression Results for θ_{p_spall} , Rectangular Columns

		θ_{p_spall} = A(1 + B * prop1^C)(1 + D * prop2^E)			
Properties	prop1	L/D	L/D	L/D	P/fcAg
	prop2	w	Cover/D	P/fcAg	w
Coefficients	A	0.007	0.001	8.366	0.640
	B	-105.798	-76.143	0.000	-0.999
	C	-6.376	-5.911	4.908	0.001
	D	75.644	24.662	-1.000	8.776
	E	5.333	0.364	0.001	0.554
Statistics of D_{spall}/D_{calc}	Min	0.236	0.236	0.170	0.260
	Max	2.138	1.992	1.752	2.022
	Mean	1.000	1.000	1.000	1.002
	COV	0.365	0.373	0.383	0.401

Table D.9   Three-Variable Regression Results for θ_{p_spall} , Rectangular Columns

		θ_{p_spall} = A(1 + B * prop1^C)(1 + D * prop2^E)(1 + F * prop3^G)			
Properties	prop1	L/D	L/D	L/D	L/D
	prop2	P/fcAg	r_{eff}	P/fcAg	Cover/D
	prop3	w	P/fcAg	dbfy/D	P/fcAg
Coefficients	A	0.011	7.587	0.543	0.171
	B	-101.152	-56.072	-58.257	-75.543
	C	-6.110	-5.450	-5.476	-5.858
	D	-0.993	-0.978	-1.000	69.128
	E	0.009	-0.002	0.000	58.836
	F	74.190	-0.979	10.507	-0.981
	G	0.386	0.028	0.190	0.024
Statistics of D_{spall}/D_{calc}	Min	0.267	0.251	0.246	0.249
	Max	1.890	1.786	1.752	1.777
	Mean	1.000	1.001	1.009	1.000
	COV	0.339	0.349	0.349	0.349

Table D.10   One-Variable Regression Results for θ_{p_spall} , Spiral Columns

	θ_{p_spall} = A(1 + B * prop1^C)			
Variable	prop1	P/fcAg	L/D	w	Cover/D
Coefficients	A	0.019	0.020	0.001	0.014
	B	-1.639	-1.209	24.177	-72.228
	C	0.780	-0.940	0.703	2.355
Statistics of D_{BB}/D_{calc}	Min	0.455	0.340	0.356	0.336
	Max	1.725	1.721	1.825	1.794
	Mean	1.000	1.000	1.000	1.000
	COV	0.327	0.376	0.377	0.383

Table D.11   Two-Variable Regression Results for θ_{p_spall} , Spiral Columns

	θ_{p_spall} = A(1 + B * prop1^C)(1 + D * prop2^E)			
Properties	prop1	P/fcAg	Cover/D	r_{eff}	L/D
	prop2	w	P/fcAg	P/fcAg	P/fcAg
Coefficients	A	0.003	0.027	0.019	0.014
	B	-1.404	-8517.464	128.866	0.163
	C	0.524	4.610	3.857	0.475
	D	27.111	-1.334	-1.523	-1.684
	E	1.046	0.450	0.656	0.826
Statistics of D_{BB}/D_{calc}	Min	0.426	0.468	0.482	0.474
	Max	1.630	1.695	1.743	1.725
	Mean	1.000	1.000	1.000	1.000
	COV	0.299	0.307	0.315	0.326

Table D.12   Three-Variable Regression Results for θ_{p_spall} , Spiral Column

	θ_{p_spall} = A(1 + B * prop1^C)(1 + D * prop2^E)(1 + F * prop3^G)			
Properties	prop1	r_{eff}	L/D	r_{eff}	Cover/D
	prop2	Cover/D	P/fcAg	P/fcAg	P/fcAg
	prop3	P/fcAg	w	w	w
Coefficients	A	0.153	0.034	0.003	0.003
	B	410.164	-0.907	8.483	-6.845
	C	4.518	-0.007	13.100	9.563
	D	-232.312	-1.424	-1.404	-1.404
	E	2.718	0.548	0.524	0.525
	F	-1.036	21.193	27.713	27.125
	G	0.054	1.079	1.042	1.046
Statistics of D_{BB}/D_{calc}	Min	0.530	0.437	0.426	0.426
	Max	1.765	1.622	1.630	1.630
	Mean	1.000	1.000	1.000	1.000
	COV	0.299	0.299	0.299	0.299

Table D.13   One-Variable Regression Results for $\dfrac{\Delta_{spall}}{L}$, Rectangular Columns

		D_{spall}/L (%) = A(1 + B * prop1^C)			
Variable	prop1	P/fcAg	w	Cover/D	L/D
Coefficients	A	1.974	1.371	0.009	0.000
	B	-1.068	8849.989	374.020	20566.624
	C	1.284	10.952	0.319	-0.361
Statistics of D_{spall}/D_{calc}	Min	0.151	0.097	0.099	0.068
	Max	1.715	2.188	2.094	1.938
	Mean	1.000	1.000	1.000	1.000
	COV	0.426	0.452	0.468	0.473

Table D.14   Two-Variable Regression Results for $\dfrac{\Delta_{spall}}{L}$, Rectangular Columns

		D_{spall}/L (%) = A(1 + B * prop1^C)(1 + D * prop2^E)			
Properties	prop1	L/D	P/fcAg	Cover/D	P/fcAg
	prop2	P/fcAg	w	P/fcAg	dbfy/D
Coefficients	A	0.029	0.457	0.359	0.430
	B	-22.173	1.375	11.030	-0.932
	C	-4.704	-0.455	0.307	0.931
	D	32.859	0.000	-0.898	0.976
	E	-0.388	-3.240	0.976	0.441
Statistics of D_{spall}/D_{calc}	Min	0.236	0.258	0.151	0.165
	Max	1.696	1.678	1.799	1.841
	Mean	1.000	1.000	1.000	1.000
	COV	0.356	0.374	0.417	0.418

Table D.15   Three-Variable Regression Results for $\dfrac{\Delta_{spall}}{L}$, Rectangular Columns

		D_{spall}/L (%) = A(1 + B * prop1^C)(1 + D * prop2^E)(1 + F * prop3^G)			
Properties	prop1	L/D	L/D	L/D	P/fcAg
	prop2	P/fcAg	Cover/D	r_{eff}	w
	prop3	w	P/fcAg	P/fcAg	dbfy/D
Coefficients	A	0.123	0.145	0.001	0.384
	B	-8.015	-20.642	-22.343	-0.984
	C	-3.319	-4.620	-4.690	1.195
	D	-0.990	30.263	22.457	-0.002
	E	1.018	0.253	0.175	-2.264
	F	28.711	-0.908	33.926	0.908
	G	0.260	0.937	-0.424	0.532
Statistics of D_{spall}/D_{calc}	Min	0.264	0.254	0.257	0.254
	Max	1.732	1.648	1.687	1.817
	Mean	1.000	1.000	1.000	1.000
	COV	0.324	0.336	0.345	0.349

Table D.16 One-Variable Regression Results for $\frac{\Delta_{spall}}{L}$, Spiral Columns

		D_{spall}/L (%) = A(1 + B * prop1^C)			
Variable	prop1	P/fcAg	L/D	r_{eff}	w
Coefficients	A	3.052	0.001	2.196	0.000
	B	-1.313	963.269	0.000	67236.011
	C	0.760	0.554	-4.579	0.472
Statistics of D_{spall}/D_{calc}	Min	0.391	0.291	0.277	0.278
	Max	1.731	1.806	1.895	1.965
	Mean	1.000	1.000	1.000	1.000
	COV	0.363	0.381	0.419	0.423

Table D.17 Two-Variable Regression Results for $\frac{\Delta_{spall}}{L}$, Spiral Columns

		D_{spall}/L (%) = A(1 + B * prop1^C)(1 + D * prop2^E)			
Properties	prop1	L/D	L/D	P/fcAg	r_{eff}
	prop2	P/fcAg	w	dbfy/D	P/fcAg
Coefficients	A	0.765	0.000	0.004	3.052
	B	1.059	1876.870	-1.288	16.031
	C	0.577	0.567	0.707	3.219
	D	-1.451	5978.205	1779.911	-1.273
	E	1.018	0.484	-0.256	0.695
Statistics of D_{spall}/D_{calc}	Min	0.506	0.304	0.411	0.405
	Max	1.667	1.797	1.708	1.781
	Mean	1.000	1.000	1.000	1.000
	COV	0.321	0.357	0.360	0.360

Table D.18 Three-Variable Regression Results for $\frac{\Delta_{spall}}{L}$, Spiral Columns

		D_{spall}/L (%) = A(1 + B * prop1^C)(1 + D * prop2^E)(1 + F * prop3^G)			
Properties	prop1	L/D	L/D	r_{eff}	P/fcAg
	prop2	P/fcAg	P/fcAg	P/fcAg	w
	prop3	w	dbfy/D	w	dbfy/D
Coefficients	A	0.007	0.759	0.000	0.002
	B	2.654	0.548	82.949	-1.163
	C	0.429	0.665	1107.166	0.531
	D	-1.229	-1.401	-1.164	4550.872
	E	0.720	0.917	0.532	0.691
	F	151.943	1.880	18170.891	371.161
	G	0.618	-0.518	0.691	-1460.999
Statistics of D_{spall}/D_{calc}	Min	0.461	0.502	0.354	0.354
	Max	1.644	1.643	1.704	1.703
	Mean	1.000	1.000	1.000	1.000
	COV	0.285	0.319	0.321	0.321

Table D.19   One-Variable Regression Results for $\dfrac{\Delta_{spall}}{\Delta_y}$, Rectangular Columns

		$D_{spall}/D_y = A(1 + B * prop1^C)$			
Variable	prop1	L/D	P/fcAg	Cover/D	w
Coefficients	A	0.000	1.665	1.722	0.000
	B	4394635.242	0.004	0.000	16571.390
	C	-0.977	-1.961	-4.329	0.172
Statistics of D_{spall}/D_{calc}	Min	0.113	0.231	0.215	0.238
	Max	2.055	2.330	2.434	2.459
	Mean	1.000	1.000	1.000	1.000
	COV	0.444	0.468	0.470	0.474

Table D.20   Two-Variable Regression Results for $\dfrac{\Delta_{spall}}{\Delta_y}$, Rectangular Columns

		$D_{spall}/D_y = A(1 + B * prop1^C)(1 + D * prop2^E)$			
Properties	prop1	L/D	L/D	Cover/D	L/D
	prop2	w	Cover/D	w	P/fcAg
Coefficients	A	0.331	0.046	0.059	0.058
	B	21.145	-0.125	23.520	115.607
	C	-0.975	0.903	-0.162	-0.918
	D	0.000	83.263	-0.008	0.000
	E	-3.768	0.012	-1.639	-5.604
Statistics of D_{spall}/D_{calc}	Min	0.277	0.158	0.233	0.124
	Max	2.004	1.990	2.387	2.127
	Mean	1.000	1.000	1.000	1.000
	COV	0.391	0.418	0.426	0.441

Table D.21   Three-Variable Regression Results for $\dfrac{\Delta_{spall}}{\Delta_y}$, Rectangular Columns

		$D_{spall}/D_y = A(1 + B * prop1^C)(1 + D * prop2^E)(1 + F * prop3^G)$			
Properties	prop1	L/D	L/D	L/D	Cover/D
	prop2	r_{eff}	Cover/D	P/fcAg	w
	prop3	P/fcAg	P/fcAg	dbfy/D	dbfy/D
Coefficients	A	0.268	0.038	0.010	0.001
	B	-0.005	-0.409	-111.105	0.000
	C	2.476	0.371	-7.260	-4.318
	D	-5.493	21.095	119.610	30.861
	E	16.621	-0.012	-0.123	0.489
	F	7.321	6.385	1.043	3.286
	G	-0.058	-0.027	-0.357	1.028
Statistics of D_{spall}/D_{calc}	Min	0.201	0.147	0.220	0.211
	Max	2.009	1.983	2.180	2.417
	Mean	1.000	1.000	1.000	1.000
	COV	0.411	0.422	0.423	0.425

Table D.22 One-Variable Regression Results for $\dfrac{\Delta_{spall}}{\Delta_y}$, Spiral Columns

	prop1	r_{eff}	P/fcAg	dbfy/D	Cover/D
			$D_{spall}/D_y = A(1 + B * prop1\text{\textasciicircum}C)$		
Variable	prop1	r_{eff}	P/fcAg	dbfy/D	Cover/D
Coefficients	A	2.172	2.876	0.000	2.399
	B	0.000	-1.176	394449.943	-233.835
	C	-5.184	0.846	-0.861	3.115
Statistics of D_{spall}/D_{calc}	Min	0.468	0.499	0.391	0.435
	Max	2.042	2.366	2.543	2.587
	Mean	1.004	1.000	1.000	1.000
	COV	0.401	0.414	0.430	0.449

Table D.23 Two-Variable Regression Results for $\dfrac{\Delta_{spall}}{\Delta_y}$, Spiral Columns

$$D_{spall}/D_y = A(1 + B * prop1\text{\textasciicircum}C)(1 + D * prop2\text{\textasciicircum}E)$$

		prop1	prop2		
Properties	prop1	P/fcAg	r_{eff}	Cover/D	L/D
	prop2	dbfy/D	dbfy/D	P/fcAg	P/fcAg
Coefficients	A	0.000	0.887	3.697	0.001
	B	-1.152	0.000	-5823.714	10299.891
	C	0.683	-4.916	4.534	-0.343
	D	306513.664	4.045	-1.030	-1.124
	E	-1.124	-0.388	0.490	0.685
Statistics of D_{spall}/D_{calc}	Min	0.471	0.461	0.465	0.392
	Max	2.187	2.036	2.201	2.148
	Mean	1.000	1.000	1.000	1.000
	COV	0.363	0.386	0.388	0.393

Table D.24 Three-Variable Regression Results for $\dfrac{\Delta_{spall}}{\Delta_y}$, Spiral Columns

$$D_{spall}/D_y = A(1 + B * prop1\text{\textasciicircum}C)(1 + D * prop2\text{\textasciicircum}E)(1 + F * prop2\text{\textasciicircum}G)$$

Properties	prop1	r_{eff}	L/D	Cover/D	r_{eff}
	prop2	w	r_{eff}	P/fcAg	Cover/D
	prop3	dbfy/D	dbfy/D	dbfy/D	dbfy/D
Coefficients	A	0.895	0.010	1.121	0.872
	B	0.000	12.391	-6.882	0.000
	C	-4.710	-0.118	1.307	-4.615
	D	41.490	0.000	-1.051	-24.088
	E	4.781	-4.704	0.536	7.104
	F	75.606	151.029	24.221	54.422
	G	-1.610	-0.803	-0.856	-1.355
D_{BB}/D_{calc}	Min	0.359	0.383	0.496	0.417
	Max	1.923	1.991	2.180	2.009
	Mean	1.000	1.000	1.000	1.000
	COV	0.365	0.368	0.369	0.371

Appendix E: Regression Results for 20% Reduction in Flexural Strength

Table E.1   One-Variable Regression Results for $\varepsilon_{20\%}$, Rectangular Columns

		$e_{20\%}$ = A(1 + B * prop1^C)			
Property	Prop1	dbfy/D	r_l	P/fcAg	S/db
Coefficients	A	0.000	0.018	0.007	0.070
	B	295.887	1321.755	1.757	-0.606
	C	-0.499	9.379	0.000	0.124
Statistics of $D_{20\%}/D_{calc}$	Min	0.382	0.372	0.354	0.319
	Max	1.884	2.146	2.042	2.134
	Mean	1.008	1.001	1.003	0.997
	COV	0.356	0.367	0.373	0.374

Table E.2   Two-Variable Regression Results for $\varepsilon_{20\%}$, Rectangular Columns

		$e_{20\%}$ = A(1 + B * prop1^C)(1 + D * prop2^E)			
Properties	Prop1	S/db	r_l	r_{eff}	P/fcAg
	Prop2	dbfy/D	dbfy/D	dbfy/D	dbfy/D
Coefficients	A	0.000	0.013	2.109	0.007
	B	190.748	38.573	-0.992	1.472
	C	-0.495	5.174	-0.001	0.127
	D	344.038	169.748	142.544	226.116
	E	-2.166	-1.970	-1.862	-2.138
Statistics of $D_{20\%}/D_{calc}$	Min	0.332	0.414	0.397	0.404
	Max	2.008	2.017	1.860	1.849
	Mean	1.004	1.007	1.003	1.009
	COV	0.339	0.341	0.348	0.350

Table E.3   Three-Variable Regression Results for $\varepsilon_{20\%}$, Rectangular Columns

		$e_{20\%}$ = A(1 + B * prop1^C)(1 + D * prop2^E)(1 + F * prop2^ G)			
Properties	Prop1	P/fcAg	L/D	r_{eff}	S/db
	Prop2	r_l	r_l	S/db	r_l
	Prop3	dbfy/D	dbfy/D	dbfy/D	dbfy/D
Coefficients	A	0.007	0.014	15.552	0.000
	B	1.647	883.773	-0.999	235.977
	C	0.226	-10.977	0.000	-0.496
	D	833.836	328.217	-0.131	64.351
	E	8.443	7.051	0.676	0.129
	F	3314.980	1055.162	788.077	364.051
	G	-3.165	-2.810	-2.480	-2.107
Statistics of $D_{20\%}/D_{calc}$	Min	0.444	0.430	0.349	0.347
	Max	1.893	2.130	1.911	1.823
	Mean	1.008	1.011	0.999	1.002
	COV	0.330	0.331	0.333	0.333

Table E.4   One-Variable Regression Results for $\varepsilon_{20\%}$, Spiral Columns

		$e_{20\%}$ = A(1 + B * prop1^C)			
Property	prop1	r_{eff}	L/D	w	S/db
Coefficients	A	0.026	0.028	0.027	0.029
	B	6.160	4.421	1.304	0.791
	C	1.604	-2.672	1.399	-2.152
Statistics of $D_{20\%}/D_{calc}$	Min	0.510	0.517	0.470	0.504
	Max	1.533	1.696	1.761	1.925
	Mean	1.006	1.011	1.009	1.009
	COV	0.248	0.261	0.282	0.286

Table E.5   Two-Variable Regression Results for $\varepsilon_{20\%}$, Spiral Columns

		$e_{20\%}$ = A(1 + B * prop1^C)(1 + D * prop2^E)			
Properties	prop1	r_{eff}	r_{eff}	L/D	L/D
	prop2	P/fcAg	dbfy/D	r_{eff}	S/db
Coefficients	A	0.027	0.010	0.025	0.029
	B	8.772	57.534	2.376	26.225
	C	1.800	3.770	-3.244	-5.515
	D	-1.224	9.102	4.590	30.298
	E	2.253	-0.533	1.501	-17.505
Statistics of $D_{20\%}/D_{calc}$	Min	0.495	0.560	0.525	0.527
	Max	1.510	1.503	1.503	1.442
	Mean	1.007	1.009	1.007	1.009
	COV	0.227	0.232	0.239	0.242

Table E.6   Three-Variable Regression Results for $\varepsilon_{20\%}$, Spiral Columns

		$e_{20\%}$ = A(1 + B * prop1^C)(1 + D * prop2^E)(1 + F * prop2^G)			
Properties	prop1	r_{eff}	L/D	L/D	L/D
	prop2	P/fcAg	r_{eff}	S/db	r_{eff}
	prop3	dbfy/D	P/fcAg	P/fcAg	dbfy/D
Coefficients	A	0.028	0.025	0.026	0.000
	B	7.856	4.235	472.219	9.772
	C	1.567	-3.946	-9.576	-5.011
	D	-1.629	4.913	1.274	4.216
	E	2.925	1.426	-2.333	1.320
	F	-0.001	-1.096	-645.380	150.312
	G	1.893	2.005	20.098	-0.380
Statistics of $D_{20\%}/D_{calc}$	Min	0.582	0.542	0.547	0.564
	Max	1.458	1.480	1.451	1.489
	Mean	1.007	1.008	1.009	1.008
	COV	0.209	0.218	0.224	0.224

Table E.7   One-Variable Regression Results for $\theta_{p\_20\%}$, Rectangular Columns

		$\theta_{p\_20\%}$ = A(1 + B * prop1^C)			
Property	prop1	P/fcAg	S/db	w	r_{eff}
	A	0.048	0.000	0.016	0.031
Coefficients	B	-1.049	1539.514	2.804	1.252
	C	1.520	-0.545	0.374	0.999
	Min	0.295	0.175	0.283	0.236
Statistics of	Max	2.156	2.184	2.177	2.167
$D_{20\%}/D_{calc}$	Mean	1.000	1.000	1.000	1.000
	COV	0.400	0.405	0.418	0.422

Table E.8   Two-Variable Regression Results for $\theta_{p\_20\%}$, Rectangular Columns

		$\theta_{p\_20\%}$ = A(1 + B * prop1^C)(1 + D * prop2^E)			
Properties	prop1	S/db	r_{eff}	S/db	P/fcAg
	prop2	P/fcAg	P/fcAg	w	w
	A	0.079	0.034	0.028	0.040
	B	-0.130	3.509	-0.067	-1.097
Coefficients	C	0.713	0.957	0.943	1.707
	D	-1.076	-1.002	1.606	1.193
	E	1.513	0.848	0.329	1.251
	Min	0.227	0.379	0.268	0.329
Statistics of	Max	2.000	2.208	2.039	2.283
$D_{20\%}/D_{calc}$	Mean	1.000	1.000	1.000	1.000
	COV	0.358	0.367	0.387	0.391

Table E.9   Three-Variable Regression Results for $\theta_{p\_20\%}$, Rectangular Columns

		$\theta_{p\_20\%}$ = A(1 + B * prop1^C)(1 + D * prop2^E)(1 + F * prop2^G)			
Properties	prop1	r_{eff}	S/db	L/D	S/db
	prop2	S/db	P/fcAg	S/db	P/fcAg
	prop3	P/fcAg	w	P/fcAg	dbfy/D
	A	0.051	0.065	0.048	0.076
	B	2.375	-0.162	0.609	-0.107
	C	1.225	0.630	0.320	0.784
Coefficients	D	-0.025	-1.111	-0.188	-1.071
	E	1.297	1.631	0.583	1.500
	F	-1.040	0.685	-0.996	-0.490
	G	1.030	0.604	1.234	-1.310
	Min	0.305	0.248	0.243	0.230
Statistics of	Max	2.047	1.998	2.024	1.987
$D_{20\%}/D_{calc}$	Mean	1.000	1.000	1.000	1.000
	COV	0.340	0.354	0.356	0.358

Table E.10   One-Variable Regression Results for $\theta_{p\_20\%}$, Spiral Columns

	$\theta_{p\_20\%}$ = A(1 + B * prop1^C)				
Property	prop1	P/fcAg	S/db	r $_{eff}$	L/D
Coefficients	A	0.080	0.122	0.000	0.062
	B	-1.120	-0.354	1054.836	0.000
	C	0.950	0.287	0.262	6.317
Statistics of $D_{20\%}/D_{calc}$	Min	0.537	0.311	0.291	0.300
	Max	1.937	1.901	1.794	1.782
	Mean	1.000	1.000	1.000	1.000
	COV	0.290	0.322	0.330	0.340

Table E.11   Two-Variable Regression Results for $\theta_{p\_20\%}$, Spiral Columns

	$q_{p\_20\%}$ = A(1 + B * prop1^C)(1 + D * prop2^E)				
Properties	prop1	r $_{eff}$	P/fcAg	S/db	P/fcAg
	prop2	P/fcAg	w	P/fcAg	dbfy/D
Coefficients	A	0.050	0.063	0.352	0.162
	B	6.560	-0.930	-0.707	-1.139
	C	0.916	0.337	0.081	0.955
	D	-0.999	3.463	-0.971	-1.440
	E	0.485	1.129	0.780	-0.384
Statistics of $D_{20\%}/D_{calc}$	Min	0.581	0.590	0.520	0.542
	Max	1.632	1.631	1.840	1.789
	Mean	1.000	1.000	1.000	1.000

Table E.12   Three-Variable Regression Results for $\theta_{p\_20\%}$, Spiral Column

	$q_{p\_20\%}$ = A(1 + B * prop1^C)(1 + D * prop2^E)(1 + F * prop2^G)				
Properties	prop1	L/D	r $_{eff}$	r $_{eff}$	r $_{eff}$
	prop2	r $_{eff}$	P/fcAg	P/fcAg	S/db
	prop3	P/fcAg	w	dbfy/D	P/fcAg
Coefficients	A	0.053	0.033	0.064	0.053
	B	0.003	3.798	6.024	5.988
	C	2.362	0.775	0.933	0.926
	D	8.633	-0.963	-1.016	-0.003
	E	1.231	0.361	0.519	1.430
	F	-0.966	2.048	-3.776	-0.998
	G	0.435	0.599	-1.104	0.499
Statistics of $D_{20\%}/D_{calc}$	Min	0.611	0.592	0.589	0.576
	Max	1.529	1.591	1.665	1.620
	Mean	1.000	1.000	1.000	1.000
	COV	0.189	0.196	0.207	0.212

Table E.13   One-Variable Regression Results for $\dfrac{\Delta_{20\%}}{L}$, Rectangular Columns

		$D_{20\%}/L$ (%) = A(1 + B * prop1^C)			
Property	prop1	P/fcAg	S/db	w	dbfy/D
Coefficients	A	5.246	0.001	0.166	1.363
	B	-1.061	12108.470	36.378	0.849
	C	1.653	-0.441	0.211	0.303
Statistics of $D_{20\%}/D_{calc}$	Min	0.237	0.149	0.244	0.221
	Max	2.158	2.132	2.330	2.150
	Mean	1.000	1.000	1.000	1.000
	COV	0.419	0.431	0.441	0.449

Table E.14   Two-Variable Regression Results for $\dfrac{\Delta_{20\%}}{L}$, Rectangular Columns

		$D_{20\%}/L$ (%) = A(1 + B * prop1^C)(1 + D * prop2^E)			
Properties	prop1	r_{eff}	S/db	P/fcAg	P/fcAg
	prop2	P/fcAg	P/fcAg	w	dbfy/D
Coefficients	A	2.907	0.000	2.374	1.962
	B	3.037	1.213E+05	-1.138	-1.010
	C	0.618	-0.450	1.918	1.565
	D	-1.029	-1.066	1.893	0.540
	E	1.077	1.678	0.310	0.351
Statistics of $D_{20\%}/D_{calc}$	Min	0.297	0.154	0.279	0.238
	Max	2.182	2.026	2.293	2.115
	Mean	1.000	1.000	1.000	1.000
	COV	0.388	0.393	0.409	0.412

Table E.15   Three-Variable Regression Results for $\dfrac{\Delta_{20\%}}{L}$, Rectangular Columns

		$D_{20\%}/L$ (%) = A(1 + B * prop1^C)(1 + D * prop2^E)(1 + F * prop2^G)			
Properties	prop1	r_{eff}	L/D	L/D	r_{eff}
	prop2	S/db	r_{eff}	S/db	P/fcAg
	prop3	P/fcAg	P/fcAg	P/fcAg	w
Coefficients	A	-7.271	2.595	0.000	2.201
	B	-2.451	0.149	70.255	2.404
	C	0.097	0.924	0.314	0.697
	D	-0.063	3.257	12839.666	-1.060
	E	0.906	0.760	-0.518	1.217
	F	-1.031	-0.949	-0.890	0.891
	G	1.194	0.617	0.977	0.357
Statistics of $D_{20\%}/D_{calc}$	Min	0.225	0.346	0.184	0.327
	Max	1.967	1.939	2.048	2.288
	Mean	1.000	1.000	1.000	1.000
	COV	0.366	0.372	0.380	0.383

Table E.16 One-Variable Regression Results for $\dfrac{\Delta_{20\%}}{L}$, Spiral Columns

		D$_{20\%}$/L (%) = A(1 + B * prop1^C)			
Property	prop1	P/fcAg	L/D	S/db	r$_{eff}$
Coefficients	A	8.479	2.206	0.001	0.001
	B	-1.154	1.176	9497.052	9576.323
	C	1.043	0.412	-0.272	0.197
Statistic of D$_{20\%}$/D$_{calc}$	Min	0.494	0.267	0.285	0.259
	Max	1.905	1.781	2.130	2.004
	Mean	1.000	1.000	1.000	1.000
	COV	0.310	0.359	0.360	0.368

Table E.17 Two-Variable Regression Results for $\dfrac{\Delta_{20\%}}{L}$, Spiral Columns

		D$_{20\%}$/L (%) = A(1 + B * prop1^C)(1 + D * prop2^E)			
Properties	prop1	P/fcAg	r$_{eff}$	S/db	P/fcAg
	prop2	w	P/fcAg	P/fcAg	dbfy/D
Coefficients	A	5.185	4.225	3.154	2.047
	B	-0.927	4.973	2.626	-1.127
	C	0.380	0.615	-0.399	0.949
	D	3.658	-1.024	-0.985	1.082
	E	0.826	0.596	0.802	0.397
Statistic of D$_{20\%}$/D$_{calc}$	Min	0.591	0.571	0.525	0.511
	Max	1.772	1.768	1.794	1.985
	Mean	1.000	1.000	1.000	1.000
	COV	0.249	0.251	0.287	0.294

Table E.18 Three-Variable Regression Results for $\dfrac{\Delta_{20\%}}{L}$, Spiral Columns

		D$_{20\%}$/L (%) = A(1 + B * prop1^C)(1 + D * prop2^E)(1 + F * prop2^G)			
Properties	prop1	L/D	L/D	r$_{eff}$	S/db
	prop2	r$_{eff}$	P/fcAg	P/fcAg	P/fcAg
	prop3	P/fcAg	w	w	w
Coefficients	A	5.083	6.614	2.544	0.014
	B	0.014	0.000	2.832	509.350
	C	1.845	4.917	0.437	-0.174
	D	6.819	-0.898	-0.960	-0.898
	E	1.177	0.332	0.408	0.384
	F	-0.967	2.993	2.480	2.616
	G	0.508	1.094	0.605	0.877
Statistic of D$_{20\%}$/D$_{calc}$	Min	0.616	0.630	0.589	0.568
	Max	1.566	1.473	1.718	1.614
	Mean	1.000	1.000	1.000	1.000
	COV	0.203	0.215	0.224	0.237

Table E.19   One-Variable Regression Results for $\dfrac{\Delta_{20\%}}{\Delta_y}$, Rectangular Columns

		$D_{20\%}/D_y$ = A(1 + B * prop1^C)			
Property	prop1	dbfy/D	r_{eff}	L/D	S/db
Coefficients	A	2.897	4.771	0.635	0.000
	B	32.614	10.190	10.488	1.809E+05
	C	-1.186	3.772	-0.305	-0.243
Statistics of $D_{20\%}/D_{calc}$	Min	0.281	0.293	0.357	0.347
	Max	2.529	2.511	2.550	2.879
	Mean	1.000	1.000	1.000	1.000
	COV	0.422	0.435	0.449	0.455

Table E.20   Two-Variable Regression Results for $\dfrac{\Delta_{20\%}}{\Delta_y}$, Rectangular Columns

		$D_{20\%}/D_y$ = A(1 + B * prop1^C)(1 + D * prop2^E)			
Properties	prop1	S/db	r_{eff}	w	L/D
	prop2	dbfy/D	dbfy/D	dbfy/D	dbfy/D
Coefficients	A	0.014	2.238	3.342	3.509
	B	530.385	6.344	0.000	49.275
	C	-0.554	2.854	-6.100	-7.798
	D	338.762	17.336	22.844	78.002
	E	-2.071	-0.885	-1.217	-1.673
Statistics of $D_{20\%}/D_{calc}$	Min	0.373	0.320	0.277	0.295
	Max	2.179	2.387	2.366	2.448
	Mean	1.000	1.000	1.000	1.000
	COV	0.383	0.394	0.413	0.414

Table E.21   Three-Variable Regression Results for $\dfrac{\Delta_{20\%}}{\Delta_y}$, Rectangular Columns

		$D_{20\%}/D_y$ = A(1 + B * prop1^C)(1 + D * prop2^E)(1 + F * prop2^G)			
Properties	prop1	r_{eff}	L/D	S/db	S/db
	prop2	S/db	S/db	w	P/fcAg
	prop3	dbfy/D	dbfy/D	dbfy/D	dbfy/D
Coefficients	A	0.298	0.112	0.145	0.229
	B	118.502	126.255	51.359	33.114
	C	7.612	-28.480	-0.576	-0.591
	D	20.384	66.779	0.685	-8.579
	E	-0.505	-0.571	18.652	63.502
	F	165.866	428.542	445.720	580.599
	G	-1.845	-2.167	-2.182	-2.289
Statistics of $D_{20\%}/D_{calc}$	Min	0.171	0.373	0.373	0.373
	Max	2.191	2.180	2.180	2.181
	Mean	1.000	1.000	1.000	1.000
	COV	0.373	0.383	0.384	0.384

Table E.22 One-Variable Regression Results for $\dfrac{\Delta_{20\%}}{\Delta_y}$, Spiral Columns

		$D_{20\%}/D_y = A(1 + B * prop1^C)$			
Property	prop1	r_{eff}	P/fcAg	S/db	L/D
Coefficients	A	4.124	9.574	5.554	0.184
	B	2.553	-0.356	0.706	54.351
	C	0.604	0.142	-0.976	-0.246
Statistics of $D_{20\%}/D_{calc}$	Min	0.333	0.432	0.374	0.467
	Max	2.220	1.692	2.107	2.135
	Mean	1.000	1.000	1.000	1.000
	COV	0.296	0.310	0.311	0.312

Table E.23 Two-Variable Regression Results for $\dfrac{\Delta_{20\%}}{\Delta_y}$, Spiral Columns

		$D_{20\%}/D_y = A(1 + B * prop1^C)(1 + D * prop2^E)$			
Properties	prop1	r_{eff}	r_{eff}	L/D	r_{eff}
	prop2	P/fcAg	w	P/fcAg	dbfy/D
Coefficients	A	7.363	0.000	5.197	0.013
	B	4.525	5.121	2.544	2.766
	C	1.162	0.855	-0.696	0.586
	D	-0.545	10776.581	-0.510	701.622
	E	0.217	-0.326	0.243	-0.295
Statistics of $D_{20\%}/D_{calc}$	Min	0.340	0.409	0.541	0.429
	Max	1.549	1.912	1.661	2.174
	Mean	1.000	1.000	1.000	1.000
	COV	0.247	0.268	0.276	0.288

Table E.24 Three-Variable Regression Results for $\dfrac{\Delta_{20\%}}{\Delta_y}$, Spiral Columns

		$D_{20\%}/D_y = A(1 + B * prop1^C)(1 + D * prop2^E)(1 + F * prop2^G)$			
Properties	prop1	r_{eff}	L/D	r_{eff}	r_{eff}
	prop2	P/fcAg	r_{eff}	P/fcAg	S/db
	prop3	dbfy/D	P/fcAg	ong Reinf Rati	P/fcAg
Coefficients	A	-0.026	3.630	1.406	3.644
	B	4.913	1.665	5.834	7.061
	C	1.217	-0.335	1.171	1.094
	D	-0.528	3.235	-0.509	0.493
	E	0.144	0.972	0.286	0.352
	F	-981.778	-0.573	2.596	-0.638
	G	-0.422	0.232	-0.216	0.267
Statistics of $D_{20\%}/D_{calc}$	Min	0.486	0.396	0.377	0.339
	Max	1.486	1.532	1.554	1.551
	Mean	1.000	1.000	1.000	1.000
	COV	0.227	0.238	0.239	0.241